Net Acid Production, Acid Neutralizing Capacity, and Associated Mineralogical and Geochemical Characteristics of Animas River Watershed Igneous Rocks Near Silverton, Colorado

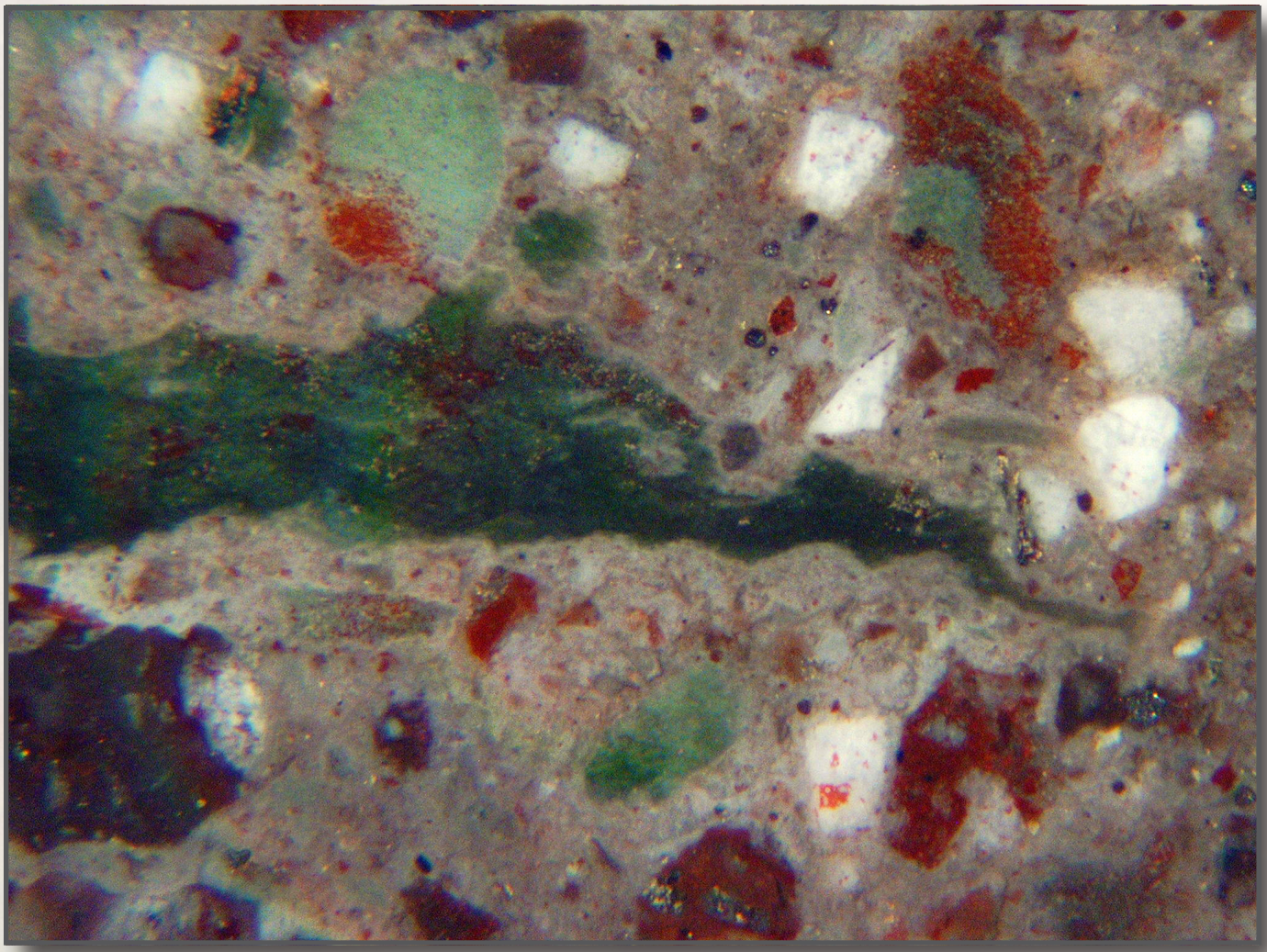

Scientific Investigations Report 2008–5063

U.S. Department of the Interior
U.S. Geological Survey

Cover. Photograph of Eureka Member of Sapinero Mesa Tuff with high acid neutralizing capacity. Green chlorite (after pumice fiamme) in center of photograph; calcite stained with alizarin red (after phenocrysts and groundmass). Sample is 3 cm across.

Net Acid Production, Acid Neutralizing Capacity, and Associated Mineralogical and Geochemical Characteristics of Animas River Watershed Igneous Rocks Near Silverton, Colorado

By Douglas B. Yager, LaDonna Choate, and Mark R. Stanton

Prepared in cooperation with the U.S. Bureau of Land Management

Scientific Investigations Report 2008–5063

U.S. Department of the Interior
U.S. Geological Survey

U.S. Department of the Interior
DIRK KEMPTHORNE, Secretary

U.S. Geological Survey
Mark D. Myers, Director

U.S. Geological Survey, Reston, Virginia: 2008

About USGS Products

For product and ordering information:
World Wide Web: http://www.usgs.gov/pubprod
Telephone: 1-888-ASK-USGS

For more information on the USGS—the Federal source for science about the Earth, its natural and living resources, natural hazards, and the environment:
World Wide Web: http://www.usgs.gov
Telephone: 1-888-ASK-USGS

About this Product

For more information concerning this publication, contact:
Team Chief Scientist, USGS Central Region Minerals Resources Team
Box 25046
Denver Federal Center
MS 973
Denver, CO 80225-0046
(303) 236-1800

Or visit the Central Region Minerals Resources Team Website at:
http://minerals.usgs.gov/

This publication is available online at:
http://pubs.usgs.gov/

Suggested citation:
Yager, D.B., Choate, LaDonna, and Stanton, M.R., 2008, Net acid production, acid neutralizing capacity, and associated mineralogical and geochemical characteristics of Animas River watershed igneous rocks near Silverton, Colorado: U.S. Geological Survey Scientific Investigations Report 2008–5063, 63 p.

Any use of trade, product, or firm names is for descriptive purposes only and does not imply endorsement by the U.S. Government.

Although this report is in the public domain, permission must be secured from the individual copyright owners to reproduce any copyrighted materials contained within this report.

Contents

Abstract 1
Introduction 2
Previous Work 2
New Work for this Study 2
Study Area 3
Geologic Setting 4
    Mid-Tertiary Volcanism 4
    Mineralization and Subsequent Erosion Events 4
Rock Types of Interest for Potential Acid Neutralization Capacity 5
    Precambrian Rocks 5
    Paleozoic Sedimentary Rocks 6
    Mesozoic Sedimentary Rocks 6
    Tertiary Sedimentary Rocks 6
    Tertiary Igneous Rocks 6
    Regional Propylitic Alteration 6
    Quaternary Surficial Deposits 7
    Acid-Generating and Acid-Neutralizing Minerals 7
    Acid-Generating Mineral Reactions 7
    Acid-Neutralizing Minerals 7
Methods 7
    Sample Preparation and Analyses 7
    Net Acid Production Test 18
    Acid Neutralization Capacity Test (Acid Titration) 18
    Sequential Extraction Procedure 19
    Rock Physical Properties (Magnetic Susceptibility) 20
Results 20
    Net Acid Production 20
    Sulfide-Bearing Samples 23
    Nonsulfide-Bearing(?) Samples 23
    Acid Neutralizing Capacity 23
    Eureka (Unit Tse) and Picayune Megabreccia (Unit Tsemb) Members 24
    San Juan Formation (Unit Tsj) 24
    Burns Member (Unit Tb) 25
    ANC and NAP Unit Comparisons 25
Sequential Leachate Results (Whole Rocks) 27
    Magnesium 27
    Aluminum 27
    Potassium 29
    Calcium 29
    Titanium 31
    Iron 31
    Manganese 31
    Nickel 33
    Copper 33

Zinc 33
Arsenic 35
Strontium 35
Molybdenum 35
Cadmium 35
Barium 37
Lead 37
Sequential Leachate Results (Grand Mogul Mine Waste) 37
Magnesium 37
Aluminum 37
Calcium 39
Titanium 39
Iron 39
Manganese 39
Nickel 41
Copper 41
Zinc 41
Arsenic 41
Strontium 41
Molybdenum 41
Cadmium 41
Barium 41
Lead 41
Rock Physical Properties (Magnetic Susceptibility) 41
Summary 41
ANC and NAP 41
Burns Member (Unit Tb) and Picayune Megabreccia Member (Unit Tsemb) 41
San Juan Formation (Unit Tsj) 43
Sultan Mountain Stock (Unit Tig) 43
Sequential Leachate Studies (Whole Rocks) 43
Major Elements 43
Mineralogic Control on Leachate Compositions 44
Trace-Element Leachate Abundances 44
San Juan Formation (Unit Tsj) 44
Burns Member (Unit Tb) 44
Pyroxene Andesite Member (Unit Tpa) 44
Mine-Waste-Leachate Compositions 44
Magnetic Susceptibility and Corresponding ANC, NAP, and Leachate Rock Properties 44
Pyroxene Andesite Member (Unit Tpa) 44
Burns Member (Unit Tb) 44
Eureka Member (Unit Tse) 44
Sultan Mountain Stock (Unit Tig) 44
San Juan Formation (Unit Tsj) 45
Conclusions 45
Acknowledgments 45
References Cited 45

Plate

[in pocket]

1. Map showing acid neutralizing capacity and net acid production of Animas River watershed rocks near Silverton, Colorado.

Figures

1. Location map and geographic features 3
2. Generalized geology 5
3. Generalized map of alteration types in the Animas River watershed 8
4. Boxplots of NAP results 23
5–7. Acid titration curves for:
5. Unit Tsemb sample HWDY090543 26
6. Unit Tsj samples ODY090552, ODY090553, and IDY090537 26
7. Unit Tsj sample SDY090535A 26
8. Boxplots of ANC results for unit Tsj 27
9. Acid titration curves for unit Tb 28
10. Boxplots of ANC results for unit Tb 28
11. Boxplots of ANC and NAP for units Pz(?), Tb, Tig, Tse, Tsemb, and Tsj 29
12–27. Histogram of whole-rock leachate results for:
12. Mg 30
13. Al 30
14. K 31
15. Ca 32
16. Ti 32
17. Fe 33
18. Mn 34
19. Ni 34
20. Cu 35
21. Zn 36
22. As 36
23. Sr 37
24. Mo 38
25. Cd 38
26. Ba 39
27. Pb 40
28–30. Histogram of Grand Mogul mine waste leachate results for:
28. Ca, Cu, Mg, Mn, P, and Ti 40
29. Al, Fe, Pb, and Zn 42
30. As, Ba, Cd, Mo, Ni, and Sr 42
31. Boxplots of volume magnetic susceptibility 43

Tables

1. Geologic unit and locality information for samples studied 9
2. Major element oxide wavelength dispersive X-ray fluorescence (WDXRF) analyses 11
3. Mineralogy determined by X-ray diffractometry (XRD) analysis 12
4. Weight percent CO_2, carbon from carbonate, total carbon, and total sulfur analyses 13
5. Inductively coupled plasma–mass spectroscopy analyses 14
6. Procedure used to determine NAP 18
7. Procedure used to determine ANC 19
8. Major- and trace-element abundances for whole rocks selected for sequential leachate analysis 20
9. Seven-step sequential extraction procedure 21
10. Nine-step sequential extraction procedure 21
11. Volume magnetic susceptibility 22
12. Net acid production results 24
13. Acid neutralizing capacity 25

Appendixes—Sequential Leachate Results

A. Magnesium 48
B. Aluminum 49
C. Potassium 50
D. Calcium 51
E. Titanium 52
F. Iron 53
G. Manganese 54
H. Nickel 55
I. Copper 56
J. Zinc 57
K. Arsenic 58
L. Strontium 59
M. Molybdenum 60
N. Cadmium 61
O. Barium 62
P. Lead 63

Net Acid Production, Acid Neutralizing Capacity, and Associated Mineralogical and Geochemical Characteristics of Animas River Watershed Igneous Rocks Near Silverton, Colorado

By Douglas B. Yager, LaDonna Choate, and Mark R. Stanton

Abstract

This report presents results from laboratory and field studies involving the net acid production (NAP), acid neutralizing capacity (ANC), and magnetic mineralogy of 27 samples collected in altered volcanic terrain in the upper Animas River watershed near Silverton, Colo., during the summer of 2005. Sampling focused mainly on the volumetrically important, Tertiary-age volcanic and plutonic rocks that host base- and precious-metal mineralization in the study area. These rocks were analyzed to determine their potential for neutralization of acid-rock drainage.

Rocks in the study area have been subjected to a regional propylitic alteration event, which introduced calcite, chlorite (clinochlore), and epidote that have varying amounts and rates of acid neutralizing capacity (ANC). Locally, hydrothermal alteration has consumed any ANC and introduced minerals, mainly pyrite, that have a high net acid production (NAP). Laboratory studies included hydrogen peroxide (H_2O_2) acid digestion and subsequent sodium hydroxide (NaOH) titration to determine NAP, and sulfuric acid (H_2SO_4) acid titration experiments to determine ANC. In addition to these environmental rock-property determinations, mineralogical, chemical, and petrographic characteristics of each sample were determined through semiquantitative X-ray diffractometry (Rietveld method), optical mineralogy, wavelength dispersive X-ray fluorescence, total carbon-carbonate, and inductively coupled plasma–mass spectrometric analysis.

An ANC ranking was assigned to rock samples based on calculated ANC quantity in kilograms/ton (kg/t) calcium carbonate equivalent and ratios of ANC to NAP. Results show that talus near the southeast Silverton caldera margin, composed of andesite clasts of the Burns Member of the Silverton Volcanics, has the highest ANC (>100 kg/t calcium carbonate equivalent) with little to no NAP. The other units found to have moderate to high ANC include (a) andesite lavas and volcaniclastic rocks of the San Juan Formation, west and northwest of the Silverton caldera, and (b) the Picayune Megabreccia Member of Sapinero Mesa Tuff along the western San Juan caldera margin. Sultan Mountain stock, composed of granitoid intrusive rocks, was shown to have low ANC and moderate NAP.

Sequential leachate analyses on a suite of whole-rock samples from the current and a previous study indicate that host rock composition and mineralogy control leachate compositions. The most mafic volcanic samples had high leachate concentrations for Mg, Fe, and Ca, whereas silicic volcanic samples had lower ferromagnesiun compositions. Samples with high chlorite abundance also had high leachable Mg concentrations. Trace-element substitution, such as Sr for Ca in plagioclase, controls high Sr concentrations in those samples with high plagioclase abundance. High Ti abundance in leachate was observed in those samples with high magnetite concentrations. This is likely due to samples containing intergrown magnetite-ilmenite. Whole rocks having high trace-element concentrations have relatively high leachate trace-element abundances. Some lavas of the San Juan Formation and Burns Member of the Silverton Volcanics had elevated Zn-, Cd-, and Pb-leachate concentrations. Manganese was also elevated in one San Juan Formation sample. Other San Juan Formation and Burns Member lavas had low to moderate trace-element abundances. One sample of the pyroxene andesite member of the Silverton Volcanics had elevated concentrations for As and Mo. Most other pyroxene andesite member samples had low leachate trace-element abundances.

Mine-waste-leachate analyses indicated that one mine-waste sample had elevated concentrations of Cu (1.5 orders of magnitude), Zn (1 order of magnitude), As (1 order of magnitude), Mo (1.5 to 2 orders of magnitude), Cd (1 to 2 orders of magnitude), and Pb (2 to 3 orders of magnitude) compared to whole rocks. These data indicate the importance of whole-rock geochemistry or leachate analyses prior to using igneous outcrops or talus for mine-waste remediation projects. Also, if ANC units have modest trace contaminant abundances compared with mine waste targeted for cleanup, then these ANC materials could still be useful to consider for remediation projects.

New magnetic susceptibility measurements indicate that the high ANC pyroxene andesite member of the Silverton Volcanics (previous study) also has the highest median volume magnetic susceptibility. Other units with representative high ANC outcrops or talus (Burns Member lavas, tuffs of Eureka Member of Sapinero Mesa Tuff, Picayune Megabreccia Member, and San Juan Formation) have variable but generally moderate to low magnetic susceptibility. Sultan Mountain stock has a moderate, mean magnetic susceptibility.

Introduction

Land management agencies, in partnership with mine owners, and other local, State, and Federal stakeholders in several watersheds located in the western United States are involved in the cleanup of abandoned hard-rock metal mines and mine-related features such as waste piles or tailings ponds. These cleanup efforts are necessary because many abandoned mine sites have acid-generating minerals, predominantly pyrite, that in the presence of oxygen and water produce sulfuric acid that is toxic to aquatic life. In addition, acidic water leaches major and trace elements from rocks in concentrations that can also be toxic to aquatic life.

Mine-site remediation project managers must consider multiple variables in order to achieve the goal of reducing the impact that acid-mine drainage has on surface and ground water (Hutchison and Ellison, 1992). Mine-site configuration in relation to topography, hydrology, possible attenuation of metals and acidity by surficial deposits and bedrock, geologic structures and hazards, and transportation logistics are but a few examples of issues that need consideration when designing and implementing a mine-site remediation project.

A little studied but potentially important part of mine-waste remediation is the environmental rock properties of net acid production (NAP) and acid neutralizing capacity (ANC) of local bedrock. This study addresses the NAP and ANC of igneous rocks that are host to base- and precious-metal mineralization in areas adjacent to the historic mining town of Silverton, Colo. The area has more than a 100-year legacy of hard-rock mining. Federal land management agencies and the Animas River Stakeholders Group are involved in current mine-waste remediation efforts near Silverton. In addition to NAP and ANC, we examine magnetic susceptibility, geochemistry, and mineralogy of samples that were analyzed for NAP and ANC. Our data are useful to land managers and stakeholders interested in locally available acid-neutralizing materials for use in mine-cleanup operations.

Previous Work

This report is a continuation of ongoing research on the environmental rock properties NAP and ANC, and magnetic susceptibility of Silverton Volcanics. In a previous study (Yager and others, 2005), we focused on igneous rocks near Silverton, Colo., and identified several igneous units that have high, instantaneous ANC in laboratory tests. We also measured magnetic susceptibility of rocks for which NAP and ANC were determined. The magnetic susceptibility measurements were used to ground-truth airborne magnetic survey data and to test if rocks with corresponding NAP and ANC properties could be mapped by airborne geophysical methods. The pyroxene andesite member of the Silverton Volcanics was shown to have the highest overall ANC and also has, on average, a high magnetic susceptibility. Other units that had one or more samples with a moderate to high ANC include the San Juan Formation (unit Tsj), Eureka Member of the Sapinero Mesa Tuff (unit Tse), Burns Member of the Silverton Volcanics (unit Tb), and Sultan Mountain stock (unit Tig).

New Work for this Study

Our current research is based on supplemental samples collected on units that were sparsely sampled in our previous study. Additional sampling of these units was warranted because at least one or more samples from these units had a high ANC, and we needed a more statistically representative sample to determine the ANC rock properties of the units. In September 2005, 27 samples were collected from the following units: Tsj, Tig, Tse, and Silverton caldera wall sediments. In addition, sampling focused on unit Tb lava outcrop and adjacent talus clasts that are logistically accessible to land management agencies for use in mine-waste remediation projects. The talus, located in Minnie Gulch (fig. 1), is composed of both unit Tb and subordinate lava clasts of the pyroxene andesite member of the Silverton Volcanics (unit Tpa).

The emphasis of this report is three-fold. First, we address the environmental rock properties net acid production (NAP) and acid neutralizing capacity (ANC) of igneous rocks that are host to most of the base-metal and precious-metal mineralization in the study area. Net acid production and acid neutralizing capacity data can be used to understand the relative acid generating and neutralizing capacity of waste rock that is commingled in mine-waste piles. Net acid production data can be used to identify subbasins that are likely to generate acidity. Conversely, acid neutralizing capacity data can be used to identify subbasins that might attenuate acidity and metals, and delineate local bedrock that could be used in mine-waste remediation projects.

A second focus of this research involves measuring geophysical properties, specifically, magnetic susceptibility for rocks in which NAP and ANC were also determined. We use these data to identify correlations between geophysical properties, NAP, and ANC. These data are also used in ground-truth verification of airborne electromagnetic (EM) and magnetic survey data, which can be used to regionally map rocks with varying NAP and ANC properties. In research subsequent to the Yager and others (2005) study, resistivity studies by McCafferty and others (2006) have shown a trend

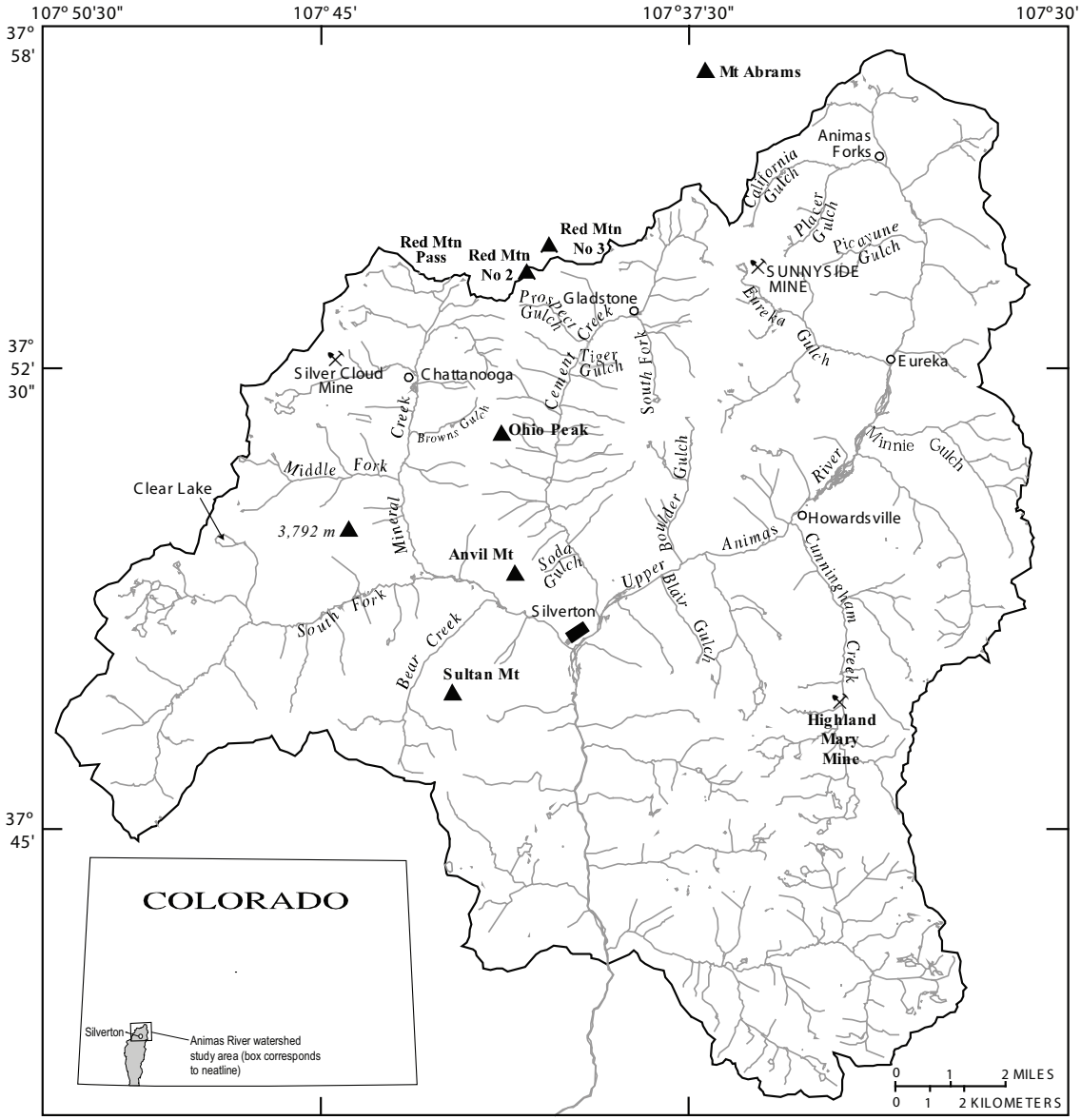

Figure 1. Location map and geographic features referred to in this and previous ANC studies.

between the magnetic susceptibility of a rock unit, its resistivity, and ANC. For example, unit Tpa has, on average, a high ANC, high magnetic susceptibility, and in some areas a low resistivity. These ANC and geophysical rock property data on unit Tpa, for example, enable regional EM survey information to be used in combination with regional maps that have unit Tpa delineated, to help predict where this unit is likely to have a high ANC.

Finally, a third focus of this study is to investigate the major and trace elements that can be leached from ANC rocks and from a mine-waste site that is targeted for remediation in the study area. These studies involve sequential extractions of leachate derived as the ANC rocks and mine waste are reacted with solutions of varying and buffered pH. Geochemical analyses of leachate are used to test (in controlled lab experiments) potential contaminants that may go into solution when mine water reacts with ANC rocks and mine waste in a field scenario. This information is important to land managers who might use ANC rocks in mine-waste remediation projects.

Study Area

The Animas River watershed near the historic mining town of Silverton, Colo. (fig. 1), is an excellent area in which to study the ANC of local rocks. A more than 100-year history of mining, primarily for silver, gold, and base metals (copper-lead-zinc), has left behind hundreds of abandoned mine-waste piles and associated mining-related features and deposits. Many mining-related features are located on lands managed by the U.S. Forest Service and U.S. Bureau of Land

Management, which require Federal involvement in any cleanup efforts. The Animas River Stakeholders Group that is based in Silverton, Colo., is also currently involved in several mine-cleanup efforts that could benefit from detailed information on the ANC of local rocks for application in remediation projects. If it can be demonstrated that nearby geologic units have significant ANC, then more local source materials could be used in remediation projects, thereby reducing the amount of limestone that would need to be hauled from long distances. The town of Silverton, Colo., is relatively remote, nestled between two mountain passes, and located 50 miles from Durango, Colo., the nearest large town. Elevations in the area are generally greater than 9,000 ft (2,743 m). Thus, utilization of local source materials could help reduce remediation costs associated with transportation of ANC rocks from other areas.

Geologic Setting

A brief discussion of the geology of the study area is important because it provides context for the various rock types that were studied in our ANC experiments. The western San Juan Mountains record a relatively complete geologic record from Precambrian to Cenozoic time. However within the upper Animas River watershed near Silverton, multiple Tertiary volcano-tectonic and intrusive events have obliterated much of the geologic record and have left thick accumulations of silicic igneous rocks. The stratigraphy of the Animas River watershed study area consists of Precambrian crystalline basement overlain by Paleozoic-, Mesozoic-, and Eocene-age sedimentary rocks, and a 1- to 2-km-thick Oligocene- to Miocene-age volcanic cover (fig. 2) (Yager and Bove, 2002; Yager and Bove, 2007).

Mid-Tertiary Volcanism

Rocks related to the episode of mid-Tertiary volcanism and later alteration is of principal interest in this study. Tertiary volcanic rocks in the San Juan Mountains blanketed more than 25,000 km^2, forming one of the great epicontinental volcanic piles of intermediate- to silicic-composition volcanic rocks. Onset of mid-Tertiary volcanism records the construction of stratovolcanoes and volcanic shields built up by thick accumulations of andesite to rhyolite flows and breccias that were followed by several eruption cycles of silicic ash flows. The eruption of ash flows led to caldera formation and localized subsidence.

Mid-Tertiary volcanism in the San Juan Mountains began between 35 and 30 Ma with the eruption and deposition of voluminous intermediate-composition (52–63 percent SiO_2) lava flows, flow breccias, volcaniclastics, minor mafic tuffs, and abundant mudflows of the San Juan Formation (Lipman and others, 1973; Steven and Lipman, 1976). From 30 to 23 Ma, multiple calderas formed and related volcanic units were deposited throughout the San Juan volcanic field (Lanphere, 1988; Lipman and others, 1997; Bove and others, 2001). Two caldera-forming events took place in the upper Animas River watershed: the 28.2-Ma San Juan-Uncompahgre caldera complex and the younger, nested, 27.6-Ma Silverton caldera (Bove and others, 2001). The San Juan caldera in the study area is within the southwest half of the roughly dumbbell shaped San Juan-Uncompahgre caldera complex. San Juan caldera eruptives include the outflow units of the Sapinero Mesa Tuff and the intracaldera Eureka and Picayune Megabreccia Members.

San Juan caldera activity culminated with ring-fracture volcanism, the products of which constitute the Silverton Volcanics. These rocks, which are primarily intermediate composition lava flows and volcaniclastic sedimentary rocks, fill the caldera depression to a thickness exceeding 1 km and are perhaps the most important rocks in this study area as they can have a high ANC in some places and are host to the majority of mineral deposits mined (Bejnar, 1957).

Beginning approximately 1 million years after Silverton caldera formation, numerous stocks, dikes, and other silicic intrusions formed along the Silverton caldera ring-fracture zone and are known as the Sultan Mountain stock. The oldest postcaldera granitic stocks (monzonite, monzodiorite, granodiorite, and monzogranite) are about 26.6 Ma and intrude along the southern part of the Silverton caldera ring fracture (Lipman, 1976; Ringrose, 1982; Bove and others, 2001).

Mineralization and Subsequent Erosion Events

The Tertiary volcano-tectonic activity was followed by multiple silicic igneous intrusion and mineralization events that span more than 20 million years and have resulted in five major alteration types in the study area (Bove, Yager, and others, 2007; Bove, Mast, and others, 2007). The multiple alteration and coincident mineralization events postdate caldera collapse, taking place between 26 and 10 Ma (Bove and others, 2001). For a detailed discussion of the alteration types, see Bove, Mast, and others (2007).

Neogene erosion denuded much of the San Juan Mountains volcanic cover. The high potential for erosion developed during this time due to differential displacement of the San Juan Mountains relative to the incipient, adjacent Rio Grande rift basin to the east and post-middle Tertiary extensional tectonic activity. Chapin and Cather (1994) estimated Precambrian bedrock offset in adjacent mountain ranges and basins in order to approximate the amount of late Tertiary relative displacement. Using this technique, they determined an average relative displacement of Precambrian rocks of 5 km. They further estimated from basin stratigraphy that 7–30 times more sediment was supplied to the Rio Grande rift basin during the Miocene and Pliocene than in the Pleistocene. Clearly, late Tertiary erosion was important in exposing large surface areas of mineralized terrain and also exposing large areas of igneous bedrock that may have a high ANC. Steven and others (1995) suggested that regional uplift and tilting from 5 to 2 Ma, concurrent with continued active rifting in the Rio Grande rift to the east, further accelerated erosion and canyon cutting throughout the uplifted area.

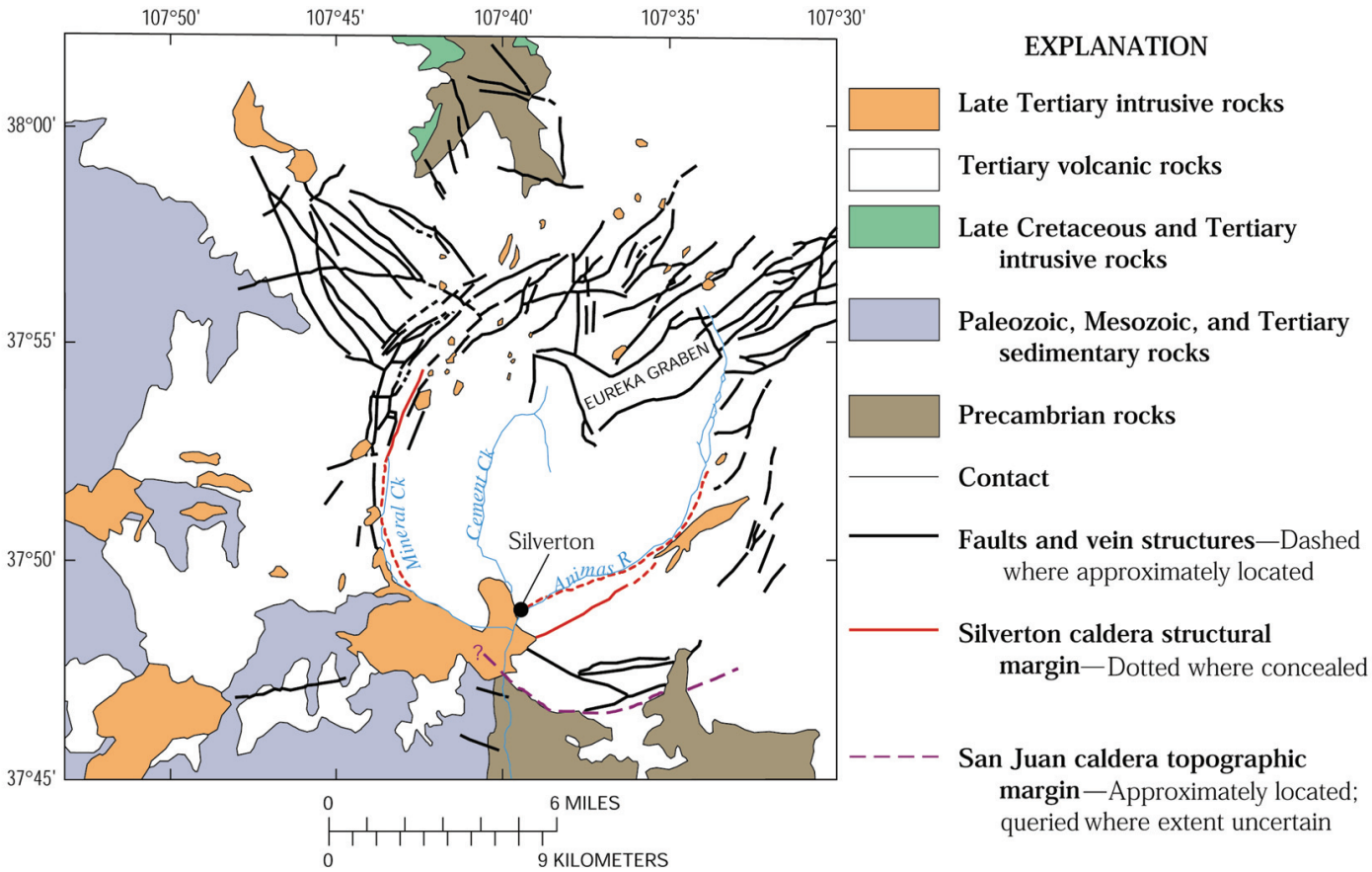

Figure 2. Generalized geology of study area and surrounding regions near Silverton, Colo. Major tributaries to Animas River are shown in addition to major Tertiary volcano-tectonic structures related to Silverton and San Juan calderas. Modified from Casadevall and Ohmoto (1977).

Weathering processes in glaciated cirque basins and subalpine to alpine mountain valleys have resulted in accumulation of large volumes of talus, debris-cone, and landslide deposits. The mineral constituents present in these unstable surficial deposits may influence their acid generating or acid neutralizing capacities.

Numerous surficial deposits in the upper Animas River watershed serve as porous and permeable pathways for surface-water infiltration and ground-water flow (Blair and others, 2002). From GIS analysis of geology coverage (Yager and Bove, 2007), we estimate that 27 percent of the bedrock in the watershed is covered by 1 to ≥5 m of porous Pleistocene to Holocene sedimentary deposits (Yager and Bove, 2007).

Rock Types of Interest for Potential Acid Neutralization Capacity

Multiple lithologic units throughout the stratigraphic section in or near the study area, from Precambrian basement rocks to Quaternary surficial deposits, have a potentially moderate to high ANC. These rock types are discussed below.[1]

Precambrian Rocks

Precambrian rocks crop out near the periphery of the Animas River watershed study area—principally along the Animas River below Silverton, near Cunningham Creek, near the eastern margin of the watershed, east of the historical Animas Forks townsite, and north of Mount Abrams. Precambrian rocks along the Animas River below Silverton and at the headwaters of Cunningham Creek (sampled in this study) are equivalent to the Irving Formation (Barker, 1969; Luedke and Burbank, 2000). Irving Formation rocks consist of interlayered fine-grained, dark-gray to greenish-gray banded amphibolite with various fine-grained, gray to green, plagioclase-, quartz-, and biotite-bearing gneisses and minor sericite-biotite-chlorite schists (Barker, 1969). Amphibolite is the predominant rock type in the Irving Formation and consists of blue-green hornblende, calcic plagioclase, and epidote; varieties with

[1] Paleozoic, Mesozoic, and Eocene sedimentary rocks were not investigated for ANC as part of this study.

biotite, chlorite, and quartz are not uncommon (Barker, 1969). In many places, plagioclase-, quartz-, and biotite-bearing gneisses contain one or more of the following phases: chlorite, epidote, microcline, garnet, calcite, magnetite, and pyrite. Regional uplift, tilting to the west, and subsequent retrograde metamorphism (Steven and others, 1969) resulted in formation and concentration of the possible acid-neutralizing mineral assemblage of chlorite-epidote-calcite (Desborough and Driscoll, 1998; Desborough and Yager, 2000).

Paleozoic Sedimentary Rocks

Paleozoic sedimentary units are primarily exposed south and west of Silverton along the Animas River and in the South Fork Mineral Creek subbasin (Luedke and Burbank, 2000; Yager and Bove, 2007). Several of the Paleozoic sedimentary units likely have a high ANC due to the presence of limestone ($CaCO_3$) interbeds, calcareous units such as mudstone, and the presence of either limestone clasts or calcite-cemented matrix. Calcareous-bearing units include the Upper Devonian Elbert Formation and Ouray Limestone, Mississippian Leadville Limestone, Pennsylvanian Molas Formation, Pennsylvanian Hermosa Formation, and Permian Cutler Formation. The thickest section of Paleozoic strata is preserved along the Animas River below Silverton and in the subbasins that drain South Fork Mineral Creek.

Mesozoic Sedimentary Rocks

Mesozoic-age rocks are best exposed near the Animas River watershed margins, outside the Tertiary calderas in the headwater subbasins of South Fork Mineral Creek (Luedke and Burbank, 2000; Yager and Bove, 2007). As with the Paleozoic section, several units in the Mesozoic sedimentary section contain calcareous-bearing units such as the Triassic Dolores Formation and Jurassic Wanakah and Morrison Formations.

Tertiary Sedimentary Rocks

Tertiary sedimentary rocks in the Animas River watershed crop out in the western and southern part of the study area and are composed of the Eocene Telluride Conglomerate. Lower layers within the Telluride Conglomerate contain rounded to subangular cobbles of Mesozoic and Paleozoic red sandstone and limestone. The Telluride Conglomerate is an important unit because of its high ANC potential.

Tertiary Igneous Rocks

Rocks of the San Juan Formation represent the oldest Tertiary units sampled and are exposed outward from the Silverton caldera structural margin in the Mineral Creek basin and near the San Juan caldera margin south of Silverton in the vicinity of Cunningham Creek and Deer Park Creek, as well as within other Animas River subbasins. The San Juan Formation is primarily composed of intermediate composition volcaniclastic sedimentary rocks; however, minor intercalated andesitic lavas are typically porphyritic and consist of plagioclase, clinopyroxene, hornblende, and opaque oxide primary phases. This unit along with all other igneous units studied is altered to a secondary propylitic mineral assemblage (see below).

Subsequent to deposition of the San Juan Formation, ash flows were deposited in response to collapse of both the San Juan and younger nested Silverton calderas and are sources of the Eureka Member of the Sapinero Mesa Tuff and the Crystal Lake Tuff, respectively. The Eureka Member of the Sapinero Mesa Tuff is the intracaldera component of the Sapinero Mesa Tuff, is dacitic to rhyolitic in composition, and contains phenocrysts of plagioclase, with lesser amounts of sanidine, biotite, and trace augite. The Crystal Lake Tuff is volumetrically minor in comparison to the Sapinero Mesa Tuff and thus was not sampled.

During formation of the San Juan caldera, limestone units of the Leadville and Ouray Limestones caved inward toward the central core of the caldera forming megabreccia. One such megabreccia block crops out near the Highland Mary mine in the Cunningham Creek subbasin.

San Juan caldera activity culminated with ring fracture volcanism, the products of which constitute the Silverton Volcanics. The Burns Member of the Silverton Volcanics is characterized by propylitically altered lavas. The pyroxene andesite member, which generally overlies the Burns Member, is mainly composed of intermediate composition lava flows with a trend toward more mafic compositions (Yager and Bove, 2007) and tends to be somewhat less altered than the Burns Member. The volcaniclastic sedimentary rocks of the Henson Member of the Silverton Volcanics interfinger with both the Burns and the pyroxene andesite (Lipman, 1976). In general, lavas of the Silverton Volcanics are porphyritic and typically contain phenocrysts of plagioclase, amphibole, pyroxene, opaque oxides, and minor biotite in a fine-grained to aphanitic groundmass.

Late-stage (23–10 Ma) dacitic to rhyolitic intrusions emplaced along the north and northwest structural margin of the Silverton caldera were concomitant with hydrothermal alteration and related mineralization (Bove, Yager, and others, 2007; Bove, Mast, and others, 2007). Dacitic intrusions dated at 23 Ma in the Red Mountain mining district are coarsely porphyritic, containing large (1 cm) phenocrysts of potassium feldspar, plagioclase, quartz, and biotite in a fine-grained groundmass.

Regional Propylitic Alteration

Regional propylitic alteration identified by Burbank (1960) and described further in Bove and others (2007) as a “pre-ore propylitization” event has affected most igneous rocks in the vicinity of the San Juan-Uncompahgre and Silverton caldera complex (fig. 3). The mineralogy of this assemblage, although variable, consists of quartz, chlorite,

epidote, calcite, secondary potassium feldspar, albite, pyrite, and opaque Fe-oxides in the presence of unaltered to slightly altered primary feldspar crystals. This alteration type is thought to have formed from 28.2 Ma to about 27.6 Ma as the nearly 1-km-thick sequence of lavas of Silverton Volcanics that infilled the San Juan caldera cooled and degassed volatile constituents. Large quantities of carbon dioxide (CO_2), perhaps the primary rock-altering volatile component (among others are water (H_2O) and sulfur dioxide (SO_2)), were released during cooling, altering the original minerals and matrix of the country rock (Burbank, 1960; Bove, Yager, and others, 2007; Bove, Mast, and others, 2007). Rocks that have undergone this type of alteration commonly have a greenish hue in outcrop owing to the presence of chlorite and epidote. Where pyrite is either sparse or absent, the propylitic assemblage can supply some ANC. The subsequent, more intense alteration and mineralization events that were commonly focused along vein structures related to San Juan and Silverton caldera formation in several places overprint the regionally pervasive propylitic alteration assemblage and locally eliminate any ANC of the propylitic assemblage (fig. 3).

Quaternary Surficial Deposits

Weathering of mineralized bedrock and subsequent deposition of weathered material in downslope surficial deposits will result in acid generation as water infiltrates and reacts with pyrite and other acid-generating sulfide minerals. In contrast, water infiltrating surficial deposits containing abundant propylitic rocks with the mineral assemblage chlorite-epidote-calcite will probably undergo some reduction in acidity (Desborough and Yager, 2000; Yager and others, 2002).

Acid-Generating and Acid-Neutralizing Minerals

Complex weathering reactions of geochemical constituents of minerals in rocks determine if a sample will produce or consume acid. Reactions at the water-mineral interface involving oxidation, adsorption, desorption, ion exchange, dissolution, and surface area control the processes that ultimately result in the elements that are released into solution or are chemically bound or sequestered (Davis and Kent, 1990). The kinetic rates at which these reactions occur in place are variable and are thus difficult to reproduce or simulate in a laboratory setting. It is, therefore, important to emphasize that our laboratory data provide an estimate of readily available neutralizing or acid-generating capacity.

Important oxidation-weathering reactions that contribute to acid generation in some samples studied include pyrite, the principal acid-generating phase (Salmon and Malmström, 2004), chalcopyrite and sphalerite (Salmon and Malmström, 2004), and galena (Blowes and others, 2003). Weathering reactions are given below.

Acid-Generating Mineral Reactions

- Pyrite oxidation (FeS_2) (ferric iron reaction path)

  $$FeS_2(s) + 14Fe^{3+} + 8H_2O \rightarrow 15Fe^{2+} + 2SO_4^{2-} + 16H^+$$

- Chalcopyrite oxidation ($CuFeS_2$) (ferric iron reaction path; trace abundances in some samples)

  $$CuFeS_2(s) + 16Fe^{3+} + 8H_2O \rightarrow 17Fe^{2+} + Cu^{2+} + 2SO_4^{2-} + 16H +$$

- Spahalerite oxidation (ZnFeS) (ferric iron reaction path; trace abundances) in some samples)

  $$ZnS(s) + 8Fe^{3+} + 4H_2O \rightarrow Zn^{2+} + SO_4^{2-} + 8Fe^{2+} + 8H^+$$

- Galena (PbS) (ferric iron reaction path; trace abundances in some samples)

  $$PbS(s) + 8Fe^{3+} + 4H_2O \rightarrow + Pb^{2+} + SO_4^{2-} + 8Fe^{2+} + 8H^+$$

Weathering reactions for the high ANC minerals with relatively fast dissolution rates for calcite (Jambor, 2003), and moderate ANC and intermediate dissolution rates for chlorite (Salmon and Malmström, 2004), are given below.

Acid-Neutralizing Minerals

- Calcite ($CaCO_3$)

  $$2CaCO_3(s) + 4H^+ \rightarrow 2Ca^{2+} + 2H_2CO_3^-$$

- Chlorite ($(MgFeAl)AlSi_3O_{10}(OH)_2$)

  $$(Mg_{4.5}Fe^{II}_{0.2}Fe^{III}_{0.2}A1)A1Si_3O_{10}(OH)_8(s) + 16H^+ \rightarrow 4.5Mg^{2+} + 0.2Fe^{2+} + 0.2Fe^{3+} + 2Al^{3+} + 3SiO_2(s) + 12H_2O$$

Additional phases locally present in Animas River watershed rocks that were shown in other studies to have some ANC are epidote ($Ca_2(Fe^{3+},Al)_3(SiO_4)_3(OH)$) and hornblende ($Ca_2(Mg,Fe)_4Al(Si_7Al)O_{22}(OH,F)_2$) (Jambor and others, 2002). Other silicate phases that are thought to have low reactivity and minimal ANC include the sodic feldspars, potassium feldspar, and sericite (Jambor, 2003; Jambor and others, 2002).

Methods

Sample Preparation and Analyses

Twenty-seven composite rock samples were collected in September 2005 for NAP, ANC, and geochemical, mineralogical, and rock physical property studies (table 1). Splits of all samples were first jaw-crushed to pebble-size using steel plates, then pulverized to approximately <200 mesh (70 μm) in an agate shatterbox for wavelength dispersive X-ray fluorescence (WDXRF) analyses (table 2), x-ray diffractometry (XRD) semi-quantitative mineralogy using the Rietveld method (Young, 1993; Raudsepp and Pani, 2003) (table 3),

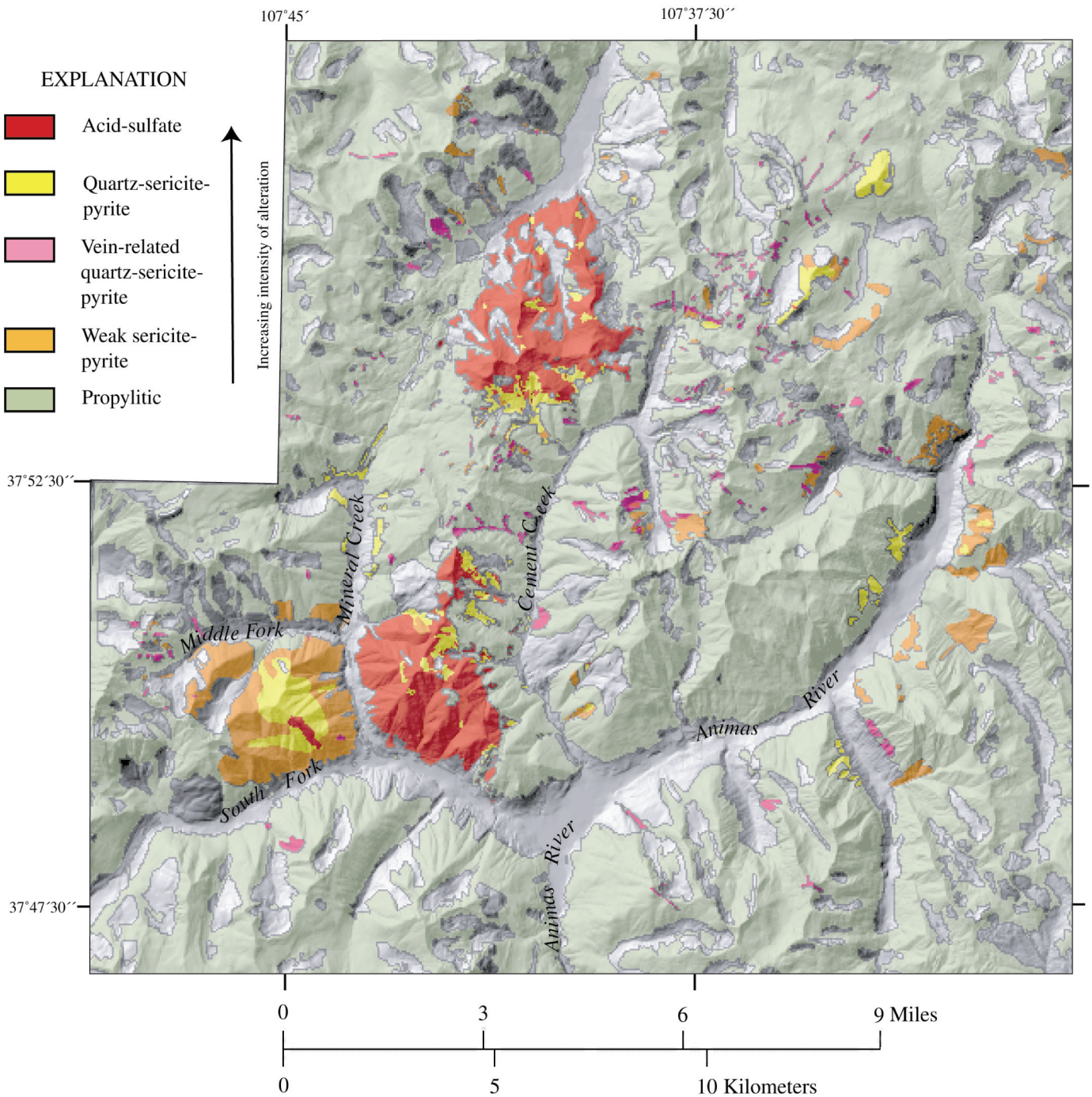

Figure 3. Generalized map of alteration types in the Animas River watershed study area. Data in Bove , Yager and others (2007) and Yager and others (2007).

total carbon-carbonate analyses (table 4), inductively coupled plasma–mass spectrometric analyses (ICP–MS) (table 5), and net acid production (Lapakko and Lawrence, 1993). Additional splits were crushed and sieved to less than 2 mm for ANC acid titration experiments. None of the samples was subjected to grinding during any preparation process. Grinding could lead to surface exposure and water–mineral reactions on layered chlorite surfaces not commonly found in natural weathering processes. Such surfaces may not be exposed during normal weathering processes involving freeze–thaw cycles, rainfall precipitation events, and grain-to-grain abrasion that occurs during fluvial transport.

Table 1. Geologic unit and locality information for samples studied.

[Geologic unit abbreviations for tables 1, 3, 8, 11, 12, and 13 are as follows: p€, Precambrian Irving Formation; Pz(?), Paleozoic(?) rocks; Tsj, San Juan Formation; Tig, Sultan Mountain stock; Tsemb, Picauyune Megabreccia Member of the Sapinero Mesa Tuff; Tse, Eureka Member of the Sapinero Mesa Tuff; Tb, Burns Member of the Silverton Volcanics; Tpa, pyroxene andesite member of the Silverton Volcanics]

Field sample number	Unit	Rock type	Longitude	Latitude	Locality description
SDY090532	Tig	Propylitically altered granitic intrusion	–107.74424	37.81690	West of highway 550 along Bear Creek
SDY090533	Tig	Weakly sericitized lava	–107.70367	37.80735	West of highway 550 along Bear Creek
SDY090534A	Tig	Propylitically altered granitic intrusion (clast in colluvium)	–107.70413	37.80832	West of highway 550 along Bear Creek
SDY090534B	Tig	Propylitically altered granitic intrusion (clast in colluvium)	–107.70413	37.80832	West of highway 550 along Bear Creek
SDY090535A	Tsj	Propylitically altered andesite	–107.72785	37.86369	West of highway 550 below Imogene mine
SDY090535B	Tsj	Propylitically altered, dacite	–107.72785	37.86369	West of highway 550 below Imogene mine
SDY090536	Tsj	Propylitically altered weakly sericitized, dacite	–107.73027	37.86173	West of highway 550 above and south of Imogene mine
IDY090537A	Tsj	Propylitically altered dacite	–107.73569	37.87625	West of Chattanooga adjacent to Silver Cloud mine portal
IDY090537B	Tsj	Propylitically altered basalt	–107.73569	37.87625	West of Chattanooga adjacent to Silver Cloud mine portal
IDY090537C	Tsj	Propylitically altered dacite	–107.73569	37.87625	West of Chattanooga adjacent to Silver Cloud mine portal
IDY090538E	Tsj	Quartz-sericite-pyrite altered lava	–107.74138	37.87210	West of Chattanooga east of Silver Cloud mine
IDY090538G	Tsj	Propylitically altered dacite	–107.74138	37.87210	West of Chattanooga east of Silver Cloud mine
SDY090539	Tig	Propylitically altered granitic intrusion	–107.80741	37.68138	Northwest of Highway 550
HWDY090540	Unknown	Propylitically altered pre-caldera sedimentary rocks	–107.56105	37.86170	Minnie Gulch
HWDY090541A	Tb	Propylitically altered andesite	–107.53239	37.85848	Minnie Gulch
HWDY090541B	Tb	Propylitically altered andesite	–107.53239	37.85848	Minnie Gulch

Table 1. Geologic unit and locality information for samples studied—Continued.

Field sample number	Unit	Rock type	Longitude	Latitude	Locality description
HWDY090542A	Tb	Propylitically altered andesite	–107.53812	37.85436	Minnie Gulch
HWDY090542B	Tb	Propylitically altered andesite	–107.53812	37.85436	Minnie Gulch
HWDY090543	Tsemb	Propylitically altered dacitic megabreccia	–107.53295	37.84766	Minnie Gulch
SDY090545	Tb	Propylitically altered basaltic andesite	–107.72210	37.85645	Near mouth of Browns Gulch
SDY090548	Tse	Propylitically altered rhyolite ash-flow tuff	–107.66163	37.79294	Deer Park trail
SDY090549	Tse	Propylitically altered trachydacitic ash-flow tuff	–107.56049	37.88902	Near Eureka townsite west of Animas River in roadcut
HPDY090550	Tse	Propylitically altered trachydacitic ash-flow tuff	–107.55782	37.90268	Along Picayune Gulch road
ODY090552A	Tsj	Propylitically altered dacitic lahar outcrop	–107.77485	37.82190	Clearlake road, south of lake
ODY090552B	Tsj	Propylitically altered basaltic lahar (float)	–107.77485	37.82190	Clearlake road, south of lake
ODY090552C	Tsj	Propylitically altered basalt (float)	–107.77485	37.82190	Clearlake road, south of lake
ODY090553	Tsj	Propylitically altered dacite (float)	–107.76957	37.81340	Clearlake road, south of lake

Table 2. Major element oxide wavelength dispersive X-ray fluorescence (WDXRF) analyses.[1]

Field sample no.	SiO_2	Al_2O_3	$FeTO_3$	MgO	CaO	Na_2O	K_2O	TiO_2	P_2O_5	MnO	LOI
SDY090532	64.3	16.8	2.86	0.66	2.63	4.39	5.84	0.28	0.24	0.07	0.81
SDY090533	57.3	16.1	8.30	3.52	2.73	2.70	2.18	0.96	0.71	0.25	5.57
SDY090534A	61.7	15.8	6.48	2.38	4.71	3.46	3.99	0.79	0.42	0.12	0.36
SDY090534B	64.5	15.2	5.37	1.93	3.97	3.25	4.02	0.64	0.32	0.10	0.52
SDY090535A	58.7	15.3	6.87	2.78	7.87	1.84	1.36	0.69	0.39	0.39	3.76
SDY090535B	62.4	15.8	5.73	2.06	4.84	2.52	1.80	0.76	0.39	0.19	2.59
SDY090536	65.4	14.5	5.82	1.97	2.75	2.80	1.16	0.64	0.36	0.10	3.76
IDY090537A	62.4	15.3	5.25	0.79	4.20	3.05	3.00	0.60	0.32	0.06	4.69
IDY090537B	44.4	18.4	9.54	4.67	7.10	4.69	1.15	1.15	0.57	0.20	7.73
IDY090537C	60.4	15.3	5.19	1.22	4.78	2.31	2.86	0.69	0.37	0.13	5.46
IDY090538E	69.1	16.1	3.29	0.85	0.49	<0.15	4.71	0.87	0.35	0.07	3.79
IDY090538G	59.9	16.8	7.56	2.44	4.97	2.26	2.52	0.82	0.38	0.15	1.65
SDY090539	72.1	13.4	2.41	0.45	0.91	2.59	6.40	0.28	0.17	0.03	1.11
HWDY090540	65.1	17.7	3.08	1.48	0.33	1.76	6.68	0.47	0.25	0.11	2.16
HWDY090541A	58.3	15.7	6.50	2.50	3.67	3.99	3.97	0.78	0.37	0.11	3.52
HWDY090541B	56.9	15.6	6.32	2.31	5.21	3.11	3.40	0.78	0.37	0.16	5.78
HWDY090542A	58.6	15.7	6.64	2.51	5.28	3.28	3.45	0.79	0.39	0.13	2.97
HWDY090542B	56.9	15.4	6.40	2.65	3.71	3.00	4.42	0.80	0.38	0.18	5.77
HWDY090543	65.7	13.0	2.99	0.89	4.45	1.29	4.90	0.39	0.17	0.14	5.20
SDY090545	54.2	16.4	10.1	3.27	6.35	2.90	1.85	0.99	0.54	0.21	2.59
SDY090548	69.2	15.0	2.06	0.65	1.72	2.36	6.48	0.33	0.16	0.05	1.20
SDY090549	67.9	15.2	3.05	1.06	2.65	2.81	5.09	0.45	0.22	0.09	1.29
HPDY090550	65.3	15.5	3.49	1.23	1.72	2.64	5.72	0.49	0.23	0.12	2.27
ODY090552A	59.1	14.5	5.61	2.65	5.31	2.43	2.73	0.63	0.28	0.18	6.13
ODY090552B	46.7	18.6	9.96	3.75	10.6	3.06	0.56	1.01	0.44	0.21	4.43
ODY090552C	53.7	15.5	10.0	3.65	7.12	2.05	2.42	1.13	0.52	0.18	2.71
ODY090553	64.6	14.9	4.96	1.97	3.65	2.94	2.40	0.56	0.30	0.09	3.48

[1]WDXRF analyses provided by Peter M. Theodorakos, U.S. Geological Survey.

Table 3. Mineralogy determined by X-ray diffractometry (XRD) analysis (values reported in weight percent).

[Rietveld XRD analyses provided by Stephen J. Sutley, USGS. Accuracy and precision using the Rietveld method were shown to vary based on phase abundance. In another study (Raudsepp, and others, 1999), it was demonstrated that in complex mixtures of varying proportions of skarn minerals that included wollastonite as the major phase, the accuracy ranged from 1.3 to 6 percent containing wollastonite in mixtures of 30 to 90 weight percent and 6 weight percent respectively. See table 1 for unit abbreviations]

Field sample no.	Unit	Calcite	Clinochlore	Epidote	Hematite	Hornblende	Magnetite	Plagioclase	Quartz	Mica (sericite[1])	Potassium feldspar	Pyrite
SDY090532	Tig		3			8	2	36	10	2	40	
SDY090533	Tsj		20				0.5	34	24	4	13	5
SDY090534A	Tig		2			1	4	30	31	20	12	
SDY090534B	Tig		2			8	3	30	24	20	13	
SDY090535A	Tsj	7	15	11				32	30	5		
SDY090535B	Tsj		12	11				36	35	5		
SDY090536	Tsj		23	5				22	39	10		
IDY090537A	Tsj	10	4		6			29	32	18		
IDY090537B	Tsj	20	17		6			42	10	4		
IDY090537C	Tsj	9	14		3			25	37	12		
IDY090538E	Tsj		2						52	42	2	2
IDY090538G	Tsj		21					21	42	3	12	0.5
SDY090539	Tig		5		0.5			23	39	4	28	
HWDY090540	Pz(?)		9					20	32	20	18	
HWDY090541A	Tb	7	10				3	45	16	2	17	
HWDY090541B	Tb	11	12		tr.		2	38	21	8	9	tr.
HWDY090542A	Tb	4	12		2		4	40	19		18	
HWDY090542B	Tb	9	15		2		2	36	17	5	15	
HWDY090543	Tsemb	12	5		3			17	42	11	10	
SDY090545	Tb					15		28	22	tr.	10	3
SDY090548	Tse		4				2	29	31	3	30	
SDY090549	Tse		5				2	30	32	4	27	
HPDY090550	Tse		6		1		4	29	28	7	25	
ODY090552A	Tsj	13	6		6			31	31	13		
ODY090552B	Tsj	10	15	18				42	8	6		
ODY090552C	Tsj	5	16		4	3	6	32	18	3	13	
ODY090553	Tsj	5	4		6			27	42	7	8	

[1]Sericite is used throughout this report. The term sericite is a field and petrographic term used to describe samples containing micaceous minerals that are not definitively identified by x-ray diffractometry or by another analytical method. Samples containing sericite in this study are most similar to fine-grained muscovite but could contain illite.

Table 4. Weight percent CO_2, carbon from carbonate, total carbon, and total sulfur analyses.[1]

Field sample no.	CO_2 (%)	C (%)	Total carbon (%)	Total sulfur
SDY090532	0.05	0.01	0.02	<0.05
SDY090533	<0.01	<0.003	<0.01	2.83
SDY090534A	<0.01	<0.003	<0.01	<0.05
SDY090534B	<0.01	<0.003	<0.01	<0.05
SDY090535A	1.83	0.5	0.61	0.37
SDY090535B	0.02	0.01	0.06	0.98
SDY090536	0.06	0.02	0.1	1.05
IDY090537A	2.82	0.77	0.8	<0.05
IDY090537B	4.25	1.16	1.25	<0.05
IDY090537C	3.44	0.94	0.97	<0.05
IDY090538E	<0.01	<0.003	<0.01	1.77
IDY090538G	0.07	0.02	0.09	<0.05
SDY090539	0.12	0.03	0.03	0.32
HWDY090540	<0.01	<0.003	<0.01	0.14
HWDY090541A	1.59	0.43	0.45	<0.05
HWDY090541B	3.56	0.97	1	<0.05
HWDY090542A	0.85	0.23	0.26	<0.05
HWDY090542B	2.32	0.63	0.67	0.06
HWDY090543	3.58	0.98	1.03	<0.05
SDY090545	0.12	0.03	0.06	0.29
SDY090548	0.18	0.05	0.06	<0.05
SDY090549	0.15	0.04	0.04	<0.05
HPDY090550	0.84	0.23	0.26	<0.05
ODY090552A	3.71	1.01	1.04	<0.05
ODY090552B	1.59	0.43	0.47	<0.05
ODY090552C	1.17	0.32	0.37	<0.05
ODY090553	1.38	0.38	0.41	<0.05

[1]Total carbon, carbonate carbon, and total sulfur analyses provided by Zoe Ann Brown, USGS.

Table 5. Inductively coupled plasma–mass spectroscopy analyses (ICP–MS).

[ICP-MS analyses provided by Monique Adams, USGS]

Field sample no.	Al (wt. %)	Ca (wt. %)	Fe (wt. %)	K (wt. %)	Mg (wt. %)	Na (wt. %)	P (wt. %)	Ti (wt. %)	Ag (ppm)	As (ppm)
SDY090532	11.1	2.07	2.18	5.37	0.494	4.05	0.0814	0.236	< 2	2.6
SDY090533	8.98	1.98	6.13	1.84	2.25	2.21	0.319	0.643	< 2	11.9
SDY090534A	9.83	3.6	4.89	3.59	1.67	3.12	0.17	0.681	< 2	1.1
SDY090534B	9.57	2.94	4.19	3.56	1.37	2.97	0.13	0.551	< 2	1.7
SDY090535A	9.52	6.19	5.13	1.19	1.88	1.68	0.15	0.4	< 2	16.8
SDY090535B	9.43	3.63	4.44	1.56	1.4	2.2	0.156	0.546	< 2	13
SDY090536	8.31	2.05	4.59	1.02	1.37	2.35	0.148	0.391	< 2	4.2
IDY090537A	9.54	3.17	3.62	2.7	0.524	2.74	0.132	0.35	< 2	1.3
IDY090537B	Nr	5.39	6.38	1.09	3.29	4.12	0.269	0.299	< 2	1.6
IDY090537C	10.3	3.74	4.08	2.76	0.888	2.32	0.175	0.226	< 2	1.4
IDY090538E	< 50	< 100	< 50	< 20	< 6	< 20	< 5	< 40	< 2	< 1
IDY090538G	11.2	4	6.3	2.5	1.87	2.26	0.175	0.747	< 2	3.5
SDY090539	9.27	0.666	2.09	6.36	0.35	2.7	0.0455	0.142	< 2	4.6
HWDY090540	13.3	0.264	2.66	6.96	1.26	1.94	0.101	0.275	< 2	2.6
HWDY090541A	11.6	3.03	5.55	4.11	2.11	4.13	0.193	0.731	< 2	2.4
HWDY090541B	11.6	4.09	5.19	3.4	1.88	3.33	0.186	0.402	< 2	< 1
HWDY090542A	11.8	4.24	5.55	3.56	2.16	3.47	0.192	0.764	< 2	3.5
HWDY090542B	9.12	2.76	4.81	4	1.85	2.69	0.163	0.467	< 2	1
HWDY090543	9.81	3.47	2.44	4.97	0.775	1.56	0.0591	0.172	< 2	1.2
SDY090545	10.3	5.02	8.13	1.76	2.41	2.68	0.275	0.856	< 2	12.9
SDY090548	11.2	1.37	1.71	6.68	0.539	2.63	0.0508	0.25	< 2	3.2
SDY090549	11.7	2.08	2.54	5.35	0.93	3.14	0.0807	0.35	< 2	3.3
HPDY090550	12.3	1.44	2.96	6.03	1.18	3.07	0.101	0.269	< 2	4.6
ODY090552A	7.8	3.92	3.41	2.32	1.63	1.92	0.104	0.249	< 2	2.6
ODY090552B	9.96	8.02	7.4	0.489	2.28	2.47	0.179	0.584	< 2	4
ODY090552C	8.18	5.29	7.19	2.08	2.26	1.67	0.216	1	< 2	8.2
ODY090553	8.07	2.68	3.31	2.08	1.22	2.37	0.0981	0.413	< 2	3

Table 5. Inductively coupled plasma–mass spectroscopy analyses (ICP–MS)—Continued.

Field sample no.	Ba (ppm)	Be (ppm)	Bi (ppm)	Cd (ppm)	Ce (ppm)	Co (ppm)	Cr (ppm)	Cu (ppm)	Ga (ppm)
SDY090532	1,810	1.8	0.36	0.34	91.8	3.6	2.4	39.5	23.6
SDY090533	870	1.8	0.1	0.05	95	18.5	26.1	144	20.5
SDY090534A	1,010	2.1	< 0.06	0.18	101	17.3	12.8	66.2	21.2
SDY090534B	865	2.1	< 0.06	0.12	96.6	14	9.9	39.4	19.3
SDY090535A	440	1.3	< 0.06	0.26	99	11.4	20	33	20.6
SDY090535B	498	1.6	< 0.06	0.18	95.6	14.9	22.8	64	20.9
SDY090536	393	1.1	1.54	0.06	83.4	6.6	3.7	84.8	18.7
IDY090537A	850	1.2	< 0.06	0.05	78.9	8.2	5.7	5.2	17.6
IDY090537B	544	1.3	< 0.06	0.14	121	24.1	1.4	7.2	22.4
IDY090537C	1,240	1.3	< 0.06	0.2	102	7.4	1.8	6	19.6
IDY090538E	< 0.2	< 0.03	< 0.06	< 0.007	< 0.1	< 0.03	< 0.5	< 2	< 0.02
IDY090538G	1,090	1.2	< 0.06	0.17	91.6	16.6	3	6.8	20.3
SDY090539	1,090	1.8	0.48	0.12	272	4.6	5	69.4	18
HWDY090540	2,750	3	0.15	0.03	167	7.1	5.3	71.3	26.7
HWDY090541A	1,290	1.6	< 0.06	0.08	97.4	19.2	16.6	53.2	20.9
HWDY090541B	847	2.1	< 0.06	0.09	93.8	17.2	15	50	21.5
HWDY090542A	1,050	1.7	0.19	0.09	96.7	20	15.6	67.8	20.5
HWDY090542B	1,340	2	< 0.06	0.05	88.9	17.3	13.8	50.4	19.4
HWDY090543	1,860	1.4	0.06	0.1	104	6.5	5.5	11.4	14.2
SDY090545	1,480	1.6	1.21	0.12	99.4	10.5	4.3	51.6	22
SDY090548	1,580	2.1	0.06	0.16	120	4.1	4.7	7.4	19.4
SDY090549	1,280	2.2	0.14	0.12	103	6.2	9.1	20.2	18.6
HPDY090550	1,500	2.4	0.19	0.27	120	9.3	10.6	23.2	19.8
ODY090552A	917	1.4	0.06	0.08	69.7	13	15.6	4.9	17.1
ODY090552B	272	1.1	< 0.06	0.1	83.7	26.6	14.8	17.8	22.3
ODY090552C	872	1.4	0.06	0.1	90.6	26.6	41.2	31.2	18.9
ODY090553	1,310	1.6	0.07	0.11	76.2	11.7	12.7	18.6	18

Table 5. Inductively coupled plasma–mass spectroscopy analyses (ICP–MS)—Continued.

Field sample no.	La (ppm)	Li (ppm)	Mn (ppm)	Mo (ppm)	Nb (ppm)	Ni (ppm)	Pb (ppm)	Rb (ppm)	Sb (ppm)	Sc (ppm)
SDY090532	63.3	5	595	1.8	43	1.7	57.3	129	1	2.7
SDY090533	51.5	6.6	1,960	2.8	20	17.4	36.8	41.3	0.96	21.1
SDY090534A	56.1	17.3	979	1.8	25	11.2	26	118	0.08	14.9
SDY090534B	53.2	20.6	847	1.1	29	9.5	24.7	132	0.2	11.9
SDY090535A	56.4	26.7	3,310	0.32	19	10.8	9.14	46.7	0.75	15.7
SDY090535B	53	21.1	1,620	0.2	22	10.4	11	63.1	0.53	16.4
SDY090536	43.9	18.1	832	0.2	21	3.9	15.9	45	0.67	12.6
IDY090537A	41.5	16.4	439	0.27	14	2.8	10.3	94.2	0.38	10.6
IDY090537B	66.2	71.9	1,640	0.2	14	2.5	11.9	42.2	0.33	25.7
IDY090537C	55.3	28.3	1,170	0.1	13	2	8.03	91.8	0.26	12
IDY090538E	< 0.05	< 0.3	<0.7	< 0.05	< 0.1	<0.3	<0.4	0.02	<0.04	< 0.04
IDY090538G	50	34.7	1,360	0.1	21	3	19.4	65.5	0.75	20.1
SDY090539	151	10.7	271	3.6	16	3.7	37.6	183	0.37	3.1
HWDY090540	94.5	36.9	1,010	0.38	20	4.9	53.2	241	0.34	8.1
HWDY090541A	54.3	56.5	993	0.39	26	13.4	9.92	151	0.68	15.8
HWDY090541B	52.2	56.2	1,460	1.1	12	12.8	13	155	0.34	13.3
HWDY090542A	53.7	69.2	1,200	0.32	28	13.2	20.1	118	1.6	15.7
HWDY090542B	51	65.9	1,450	1.5	18	11.8	15	192	0.45	13.5
HWDY090543	58.5	23	1,260	0.37	17	3.6	16.9	269	0.66	6.8
SDY090545	54.2	20.8	1,800	1.1	40	7.3	10.5	50.9	2.5	32
SDY090548	73	11.2	412	0.74	36	6.9	21.6	182	0.88	4.5
SDY090549	61	22.9	809	0.36	30	8.4	25.6	204	0.88	7.5
HPDY090550	70.8	24.5	1,130	0.2	26	8.6	35.6	262	1.4	8.4
ODY090552A	37.1	27.2	1,430	0.25	12	8.5	14.7	72.4	0.68	11.4
ODY090552B	47.8	41	1,660	0.28	16	8.2	17.2	16.3	0.42	24.9
ODY090552C	50.4	20.6	1,450	1.3	28	12.8	11.9	39.6	0.1	29.3
ODY090553	40.9	16	683	0.46	24	6.8	18.1	59.1	0.2	10.4

Table 5. Inductively coupled plasma–mass spectroscopy analyses (ICP–MS)—Continued.

Field sample no.	Sr (ppm)	Th (ppm)	Tl (ppm)	U (ppm)	V (ppm)	Y (ppm)	Zn (ppm)
SDY090532	1,100	22.9	1.01	7.01	88	16.9	65.9
SDY090533	761	13.4	0.83	4.01	213	26.2	156
SDY090534A	832	21.1	0.59	4	150	28.8	97.7
SDY090534B	622	24.6	0.73	3.76	116	27.8	89.2
SDY090535A	657	13.3	0.68	3.82	149	29.7	133
SDY090535B	548	13.6	0.78	3.89	168	25.3	96.6
SDY090536	765	5.8	1.24	0.86	95.7	23.8	85.7
IDY090537A	498	7.14	0.81	0.76	67.4	20.8	70.2
IDY090537B	1,090	5.22	0.47	1.11	135	32.2	166
IDY090537C	498	5.04	0.96	1.19	82.3	24.5	88.6
IDY090538E	< 0.8	< 0.1	<0.08	< 0.02	<0.2	< 0.05	< 3
IDY090538G	763	8.62	1.05	0.94	176	34.6	136
SDY090539	224	80	1.19	11.7	27.1	22.4	47.7
HWDY090540	290	28.6	1.83	4.88	48.3	30.1	95.4
HWDY090541A	627	10.8	1.98	3.52	152	23.5	93
HWDY090541B	343	7.85	2.14	2.56	152	20.8	83.4
HWDY090542A	690	12.3	1.09	3.52	154	24.2	90.5
HWDY090542B	277	10.8	3.03	3.44	146	21.6	88.6
HWDY090543	195	20.2	3.99	4.17	56.6	20.8	47.3
SDY090545	1,020	5.8	1.59	1.56	263	38.1	85.4
SDY090548	521	25.4	1.35	6.83	31	24.7	43.5
SDY090549	566	19	2.71	5.99	56.6	21	83
HPDY090550	376	20.1	4.26	6.93	67.9	23.8	102
ODY090552A	485	5.45	0.67	1.46	92.1	19.4	119
ODY090552B	1,040	5.38	0.17	1.21	209	29	122
ODY090552C	719	6.63	0.26	1.8	273	35.8	121
ODY090553	808	6.11	0.5	1.53	102	21.3	90

Net Acid Production Test

The net acid production (NAP) test was developed as a screening tool to determine the acid-generating potential of mine-waste materials (Lapakko and Lawrence, 1993). This method is a static laboratory bench test that utilizes hydrogen peroxide (H_2O_2) to oxidize sulfide minerals in a sample, creating sulfuric acid that subsequently reacts with other phases present. Because enhanced sulfide oxidation is achieved, this test provides an upper limit for acid-generating potential. A modified version of the Lapakko and Lawrence (1993) NAP method was used for this study. The steps used for this procedure are listed in table 6.

Net acid production is calculated in calcium carbonate equivalent units (kg/t) that would be necessary to neutralize a sample to the final pH of 7.00. This calculation is based on the following formula:

Net acid production in kg/t $CaCO_3 = 50 \times ml_b \times N_b$/ sample weight,

where ml_b = total volume of NaOH used during titration to pH 7.00 from step nine (table 6), and N_b = normality of NaOH used.

Thus, progressively higher NAP values would require more calcite to neutralize a solution to pH 7.00.

Acid Neutralization Capacity Test (Acid Titration)

The ANC method used in this study is similar to that described in Shaw and others (2002) and initially described by Robertson Geoconsultants (written commun., 2000) and provides an estimate of the instantaneous and readily available ANC of rock and mineral particles. The procedure used to determine ANC is listed in table 7.

Acid neutralization capacity is calculated in calcium carbonate equivalent mass units (kg/t) with the following formula, where total acid added in this example is 50 ml, N is the normality of acid used, grams (g) of sample = 50, mol = moles, formula weight for calcite ($CaCO_3$) is 100 g:

H_2SO_4 (0.05 liters) × 0.1 N H_2SO_4 = 0.005 equivalents $CaCO_3$ (0.005 mol $CaCO_3$)

$$0.005 \text{ mol } CaCO_3 \times \frac{100 \text{ g } CaCO_3}{1 \text{ mol } CaCO_3} = 0.50 \text{ g } CaCO_3$$

$$\frac{0.50 \text{ g } CaCO_3}{30 \text{ g sample}} \times \frac{1{,}000 \text{ g}}{1 \text{ kg}} \times \frac{1{,}000 \text{ kg}}{1 \text{ t}} CaCO_3 \times \frac{1 \text{ kg } CaCO_3}{1{,}000 \text{ g}} \approx 17 \text{ kg/t } CaCO_3$$

Table 6. Procedure used to determine NAP. Steps are listed in sequential order.

Step	Procedure
1	Powder rock in shatterbox to less than 200 mesh.
2	Place 1 g representative split of rock powder from step 1 in 250 ml beaker
3	Incrementally add 100 ml 30 percent H_2O_2. Watch for energetic reaction with sulfides and record relative fizz response (low-moderate-high).
4	After reactions have subsided and all 100 ml of H_2O_2 is added, place beaker on hot plate and heat to 94°C (near boiling) for 1 hour. Remove from hot plate and cool for 5 minutes. Initial pH is recorded prior to titration to pH 7. Note that some samples have no NAP and will have a neutral pH of 7 or greater at the completion of this step.
5	Add another 50 ml of H_2O_2 and heat to 94ºC for 30 minutes. Remove from hot plate and cool for 15 minutes. This step is used to help ensure (but not guarantee) complete oxidation. If oxidation is incomplete, the NAP calculated will be a minimum value.
6	Add 1 ml of 0.016 M Cu nitrate solution and boil at 110ºC for 10 minutes.
7	Cool solution and remove solids by filtration with filter paper and thistle funnel.
8	Rinse solids in filter paper with 1M $CaCl_2$.
9	Titrate solution by burette to pH 7 with reagent-grade 0.1N NaOH. A magnetic stirrer and Teflon stir bar is used to continuously mix the solution between pH measurements.

Table 7. Procedure used to determine ANC. Steps are listed in sequential order.

Step	Procedure
1	Rock sample is crushed using jaw crusher to approximately 2 mm. Samples are not ground to avoid heating and preferential orientation of chlorite 001 crystal lattice planes.
2	Material from step 1 is sieved using a stainless steel sieve; all material less than 2 mm is saved for acid titration.
3	A representative ≈30-g split from step 2 is weighed and the starting mass recorded.
4	The 30-g sample is added to a 100-ml beaker with 30-ml deionized water and stirred; the initial pH and titration start time is recorded.
5	Sample is stirred continuously for the duration of the experiment using a mechanical mixer with a stainless steel shaft and Teflon propeller, and the starting pH is recorded. Nitrogen gas is bubbled through titrant to reduce effects of atmospheric CO_2 on pH during titration.
6	Reagent-grade 0.1N H_2SO_4 titrant is added incrementally to samples using a pH stat controller that allows pH set points to be pre-set from the starting titration pH to the ending pH 2. In this study, whole pH set-point intervals were used; for example, pH 7, 6, 5, 4, 3, and 2. The pH stat controller measures and records milliliter increments of titrant added to achieve titration set-point stability. Stability is reached when the pH stat controller detects that a pH set point is achieved and stops adding acid. Total acid added is summed for each pH set point and the cumulative total for all set points; the cumulative total is used to determine ANC for a sample. Note that titrant addition by burette is used on some samples with high ANC and the quantity added by burette is added to the total added by the pH stat controller. Completed titration duration times range from a few minutes (low ANC) to several hours (high ANC).

This calculation assumes that all of the ANC is attributable to calcite. We know that this is not the case in our study as many samples contain clinochlore, which continues to react after calcite is consumed. Some samples lack calcite and yet have measurable ANC (Yager and others, 2005).

Sequential Extraction Procedure

Sequential extractions were performed on eight volcanic rocks and one mine-waste sample. Rock samples from the previous study by Yager and others (2005) and from new samples collected in 2005 were chosen for sequential leachate analysis. Samples selected represent moderate to high ANC (9 to 123 kg/t calcium carbonate equivalent). In addition, samples were chosen that have a wide range of whole-rock and major- and trace-element concentrations (table 8). Colors used in table 8 and elsewhere throughout the report (figures 4, 8, 10, 11, and 31; and tables 11, 12, and 13) represent specific geologic units.

Volcanic rocks were prepared using the same method as described above in the sample preparation section. A < 2-mm split from each rock was obtained using a Jones splitter. One mine-waste sample was collected from the Grand Mogul (GM) mine located in upper Ross basin. The mine-waste pile was sampled using a 3-m grid-cell spacing. Surface samples were collected from each cell in 5-gal plastic buckets using a shovel. All samples were composited and mixed on-site and randomly replaced into the plastic buckets. An additional composite mixing procedure similar to the one used on-site was repeated in the lab; although during this step cobble-size clasts were excluded from further analysis. The mine waste was subsequently split using a Jones splitter and approximately 1 g of dry sample was obtained for extraction and analysis.

Duplicates of three of the samples were performed for comparison. A seven-step extraction procedure (table 9) was used to determine the metals released from specific phases and total elements liberated. A separate nine-step extraction procedure (table 10) having two pH extractions were added to determine possible metals released from chlorite species. Chlorite species were specifically targeted in sequential extraction studies because in a previous study (Yager and others, 2005) clinochlore and chamosite in propylitically altered volcanic rocks were found to have

Table 8. Major- and trace-element abundances for whole rocks selected for sequential leachate analysis.

[Elements determined by ICP–MS for samples IDY090537B and HWDY090542A (this study); all other samples determined by ICP–AES in study by Yager and others (2005). Al and Fe in weight percent; all other elements in parts per million. Colors represent specific geologic units. See table 1 for unit abbreviations; n.d., not detected]

Unit	Field sample no.	SiO_2	Mn	Fe	Cu	Zn	As	Pb
Tsj	**IDY090537B**	44.4	1,640	6.4	7.2	166	1.6	12
Tsj	**IDY0329**	61.2	2,270	3.4	17	1,100	n.d.	51
Tpa	**HDY0317**	57.5	826	5.1	25	86	n.d.	17
Tpa	**SDY0326**	58.2	834	5.0	53	91	14	29
Tb	**HWDY090542A**	58.6	1,200	5.5	67.8	90	3.5	20
Tb	**HWDY090542B**	56.9	1,450	4.8	50.4	89	1.0	15
Tb	**SDY0310**	56.5	3,420	6.4	72	266	n.d.	16
Tse	**HDY0314**	67.6	645	2.0	5	50	n.d.	34

high ANC. After each extraction step, the samples were centrifuged at 15,000 rpm for 15 min then decanted. Five hundred micro liters of concentrated ultra pure nitric acid was added to the decantate for the following fractions: (1) water soluble, (2) exchangeable, (3) carbonate, (4) pH 4, (5) pH 2, (6) amorphous Fe- and Al-hydroxides, and (7) amorphous and crystalline Mn-oxides. With the exception of the water soluble fraction, all other fractions were diluted with MiliQ, ultra-pure water, to a final volume of 50 mL. All extractions are analyzed by ICP–MS. A total digest was also performed on the nine samples and three duplicates using a four-acid digest procedure.

Rock Physical Properties (Magnetic Susceptibility)

All samples collected in 2005 and from the previous Yager and others (2005) study were analyzed for magnetic susceptibility (MS) using a Sapphire instrument. This instrument is more accurate and sensitive compared to the Bison instrument that was used in the previous 2005 study (especially at lower susceptibility values; Joseph Rosenbaum, USGS, unpub. lished data, 2007). The Sapphire instrument consists of a coil (solenoid) that is part of an alternating-current (a-c) circuit. In reporting susceptibility measurements, it is usual to indicate the magnitude of the a-c field in the coil and its frequency (600 hertz). The field amplitude in the Sapphire is about 0.1 milliTesla. The measurement coil is part of an oscillating circuit. The frequency of oscillation is measured for an empty coil and then with a sample in the coil. The difference in frequency is linearly proportional to the MS reading. For most samples (ignoring sample anisotropy), two things affect an MS reading: (1) the magnetic susceptibility of the sample and (2) the size and shape of the sample.

For analysis in the Sapphire instrument, samples are placed entirely within the solenoid and do not extend close to the ends of the coil (that is, the entire sample is in a volume of uniform field). Shape can usually be ignored. If sample A is twice the size of sample B and they are made of the same material (that is, they have the same magnetic susceptibility), then the MS reading for A will be twice as large as that for B. We record the readings without making any correction for sample volume or mass. Magnetic susceptibility readings were subsequently divided by volume (in cm^3) and reported as volume susceptibility in the centimeter-gram-second (CGS) system of units (table 11).

Results

Net Acid Production

The NAP results are reported in table 12. Box plots of NAP results are shown in figure 4. The NAP value is reported in kg/t $CaCO_3$ equivalent, and can be interpreted as the amount of $CaCO_3$ that is required to neutralize a sample to pH 7. Therefore, the higher NAP values indicate a higher acid-generating potential. Low or nondetectable NAP values are suggestive that a sample may have ANC. Of the 27 total samples analyzed, NAP values range from not detectable (14 samples) to 182 kg/t $CaCO_3$ equivalent (table 12). The mean NAP value is 26 kg/t $CaCO_3$ equivalent. We discuss NAP in relation to the abundance of sulfide mineral species in the following sections.

Table 9. Seven-step sequential extraction procedure applied to nine samples.

Phase	Description of procedure
Water soluble	1. One gram of unground sample is extracted with 25 mL of MiliQ water and agitated for 30 minutes at room temperature.
Exchangeable (Tessier and others, 1979)	2. The residue from 1 is extracted with 25 mL of sodium acetate at pH 8.2 and agitated at room temperature for 1 hour.
Carbonate (Tessier and others, 1979)	3. The residue from 2 is extracted with 25 mL sodium acetate adjusted to a pH of 5 with acetic acid and agitated for 5 hours at room temperature.
Amorphous Fe- and Al-hydroxides and amorphous and crystalline Mn-oxides (Piatak and others, 2007)	4. The residue from 3 is extracted with 25 mL 0.25M hydroxylamine hydrochloride in 0.1M HCl for 30 minutes in a 50°–54°C water bath with occasional stirring.
Crystalline Fe- and Al-oxides (Chao and Sanzolone, 1998)	5. The residue from 4 is extracted with 25 mL HCl heated in a boiling (95°C) water bath for 45 minutes with occasional shaking.
Sulfide (Chao and Sanzolone, 1977)	6. The residue from 5 is extracted by adding 0.5g $KClO_3$ and 10 mL concentrated HCl; the solution is mixed and let to stand for 30 minutes. After 30 minutes, 10 mL of MiliQ water is added, and solution is centrifuged and decanted. The residue is again extracted with 10 mL 4M HNO_3 and heated in boiling water bath for 20 minutes.
Silicates (Briggs, 2001)	7. The residue from 6 is transferred to Teflon vessels and extracted using the four-acid digest procedure.

Table 10. Nine-step sequential extraction procedure applied to nine samples.

Phase	Description of procedure
Water soluble	1. One gram of unground sample is extracted with 25 mL of MiliQ water and agitated for 30 minutes at room temperature.
Exchangeable (Tessier and others, 1979)	2. The residue from 1 is extracted with 25 mL of sodium acetate at pH 8.2 and agitated at room temperature for 1 hour.
Carbonate (Tessier and others, 1979)	3. The residue from 2 is extracted with 25 mL sodium acetate adjusted to a pH of 5 with acetic acid and agitated for 5 hours at room temperature.
Chlorite at pH 4	4. The residue from 3 is extracted with 25 mL of pH 4 HCl and agitated for 45 minutes at room temperature.
Chlorite at pH2	5. The residue form 4 is extracted with 25 mL of pH 2 HCl and agitated for 45 minutes at room temperature.
Amorphous Fe- and Al-hydroxides and amorphous and crystalline Mn-oxides (Piatak and others, 2007)	6. The residue from 5 is extracted with 25 mL 0.25M hydroxylamine hydrochloride in 0.1M HCl for 30 minutes in a 50°–54°C water bath with occasional stirring.
Crystalline Fe- and Al-oxides (Chao and Sanzolone, 1998)	7. The residue from 6 is extracted with 25 mL 4M HCl heated in a boiling (95°C) water bath for 45 minutes with occasional shaking.
Sulfide (Chao and Sanzolone, 1977)	8. The residue from 7 is extracted by adding 0.5 g $KClO_3$ and 10 mL concentrated HCl; the solution is mixed and let to stand for 30 minutes. After 30 minutes, 10 mL of MiliQ water is added, solution is centrifuged, and decanted. The residue is again extracted with 10 mL 4M HNO_3 and heated in boiling water bath for 20 minutes.
Silicates (Briggs, 2001)	9. The residue from 8 is transferred to Teflon vessels and extracted using the four-acid digest procedure.

Table 11. Volume magnetic susceptibility in the CGS system. Measurements determined by a Sapphire instrument.

[Data in this table supersedes magnetic susceptibility measurements reported in Yager and others (2005); Sapphire instrument used to make susceptibility measurements reported here is more accurate than in our previous report. Measurements provided by Ank Webbers and Joseph Rosenbaum (USGS, Denver, Colo.). See table 1 for geologic unit abbreviations; ser, sericitic; prop, propylitic; q-s-p, quartz-sericite-pyrite]

Geologic unit	Sample	Alteration type	Sapphire instrument reading (CGS)	Mass (g)	Volume (cm^3)	Volume susceptibility (CGS)
Tpa	HDY0317	Prop	3.56E-02	22.95	8.51	0.00418
Tpa	IRDY0203	Prop	5.27E-02	28.62	10.54	0.005
Tpa	SDY0326	Prop	6.50E-02	31.24	11.58	0.00562
Tpa	SDY0312	Prop	4.49E-02	31.86	11.56	0.00388
Tpa	IDY0328	Weak ser	5.00E-04	28.17	10.63	0.000047
Tpa	SDY0327	Weak ser	2.20E-04	13.48	5.12	4.31E-05
Tpa	IRDY0103	q-s-p	5.10E-05	22.15	8.55	3.64E-07
Tb	SDY0310	Prop	1.09E-03	31.41	11.57	9.41E-05
Tb	SDY0325	Prop	8.76E-04	26.99	10.18	0.000086
Tb	IRDY0403	Prop	2.60E-03	25.06	9.55	0.000272
Tb	SDY0307	Prop	5.06E-04	44.13	16.56	3.05E-05
Tb	SDY0308	Prop	7.84E-04	18.37	6.91	0.000113
Tb	SDY0309	Prop	5.45E-03	32.41	12.35	0.000441
Tb	SDY0311	Prop	1.78E-03	27.49	10.41	0.000171
Tb	HDY0313	Prop	6.27E-04	18.75	7.11	8.83E-05
Tb	SDY0306	Prop	1.93E-02	21.39	8.02	0.0024
Tb	SDY0324	Weak ser	3.69E-02	18.98	6.90	0.00534
Tb	IRDY0303	Argillic	2.94E-05	19.85	8.31	3.54E-06
Tb	HWDY090541A	Prop	2.27E-02	20.97	8.67	0.00261
Tb	HWDY090541B	Prop	1.00E-02	11.566	5.3	0.001901
Tb	HWDY090542A	Prop	1.69E-02	15.29	6.00	0.00282
Tb	HWDY090542B	Prop	1.61E-02	18.94	7.36	0.00219
Tse	HDY0314*	Prop	1.15E-03	28.83	11.23	0.000102
Tse	HDY0316	Prop	1.83E-04	31.16	12.94	1.42E-05
Tse	HDY0318	Prop	2.85E-02	27.96	10.47	0.00272
Tsemb	HDY0315	Prop	7.71E-03	29.54	11.10	0.000694
Tsemb	HWDY090543	Prop	2.80E-03	8.117	3.9	0.000717
Tse	HPDY090549	Prop	1.53E-02	60.529	30.0	0.00051
Tsj	IDY0329	Prop	3.29E-04	36.38	13.77	2.39E-05
Tsj	ODY0331	Prop	6.47E-03	22.33	8.44	0.000766
Tsj	SDY0330	Prop	4.19E-02	31.09	11.48	0.00365
Tsj	SDY090535A	Prop	1.14E-04	7.037	3.7	3.08E-05
Tsj	SDY090535B	Prop	1.63E-04	11.480	5.0	3.26E-05
Tsj	IDY090537C	Prop	1.03E-04	10.515	7.0	1.46E-05
Tsj	IDY090538G	Prop	3.29E-02	14.449	6.4	0.005179
Tsj	IDY090538E	q-s-p	6.19E-05	46.950	23.6	2.62E-06
Tsj	ODY090552B	Prop	4.87E-03	9.870	5.7	0.00085
Tsj	ODY090552C	Prop	1.83E-02	9.479	3.9	0.004669
Tsj	ODY090552D	Prop	1.06E-04	14.302	6.1	1.75E-05
Tig	HWDY0322	Prop	1.41E-02	35.20	13.08	0.00108
Tig	SDY0319	Weak ser	5.30E-02	26.67	9.71	0.00546
Tig	SDY320	Weak ser	3.02E-05	11.17	6.43	4.69E-06
Tig	SDY090532	Prop	1.65E-02	12.747	6.9	0.002413
Tig	SDY090533	Weak ser	1.02E-04	10.353	5.5	1.84E-05
Tig	SDY090534A	Prop	1.15E-01	60.70	22.29	0.00517
Tig	SDY090534B	Prop	3.21E-02	21.70	8.18	0.00393
Tig	SDY090539	Prop	9.26E-03	14.179	7.8	0.001181
Td	IDY0321	Ser	1.23E-05	36.08	15.05	1.03E-05
P€	HWDY0323	Prop	9.20E-06	18.613	7.04	1.64E-05

Sulfide-Bearing Samples

Pyrite above trace amounts is observed in 4 of the 27 samples studied (table 3). Those samples containing pyrite concentrations above trace amounts to 5 weight percent lack calcite and have NAP values that range from 13 to 182 kg/t $CaCO_3$ equivalent (table 12). Pyrite-bearing samples (SDY090533, IDY090538E, IDY090538G, and SDY090545) have the highest average NAP (80 kg/t $CaCO_3$ equivalent).

One sample (HWDY090541B) contains possible trace pyrite (table 3) in addition to abundant calcite (11 weight percent) and has no detectable NAP. The large quantity of calcite is apparently neutralizing any NAP generated during H_2O_2 reaction with trace amounts of pyrite.

nonconservative technique to estimate NAP as sulfur species are targeted for complete dissolution during boiling in H_2O_2. Thus, in this vigorous dissolution process, ferric iron could be liberated from a number of iron-bearing mineral species such as clinochlore, epidote, and hematite.

An example of the type of hydrolysis reaction that involves ferric iron is as follows:

$$4\ Fe^{3+} + 12\ H_2O \rightarrow 4\ Fe(OH)_3^- + 12\ H^+$$

Another possibility is the dissolution of finely disseminated sulfate salts that have a high surface area, readily dissolve, and thus have a high NAP. The presence of sulfate salts, while frequently abundant on surface coatings in mine waste, was not observed in rocks studied.

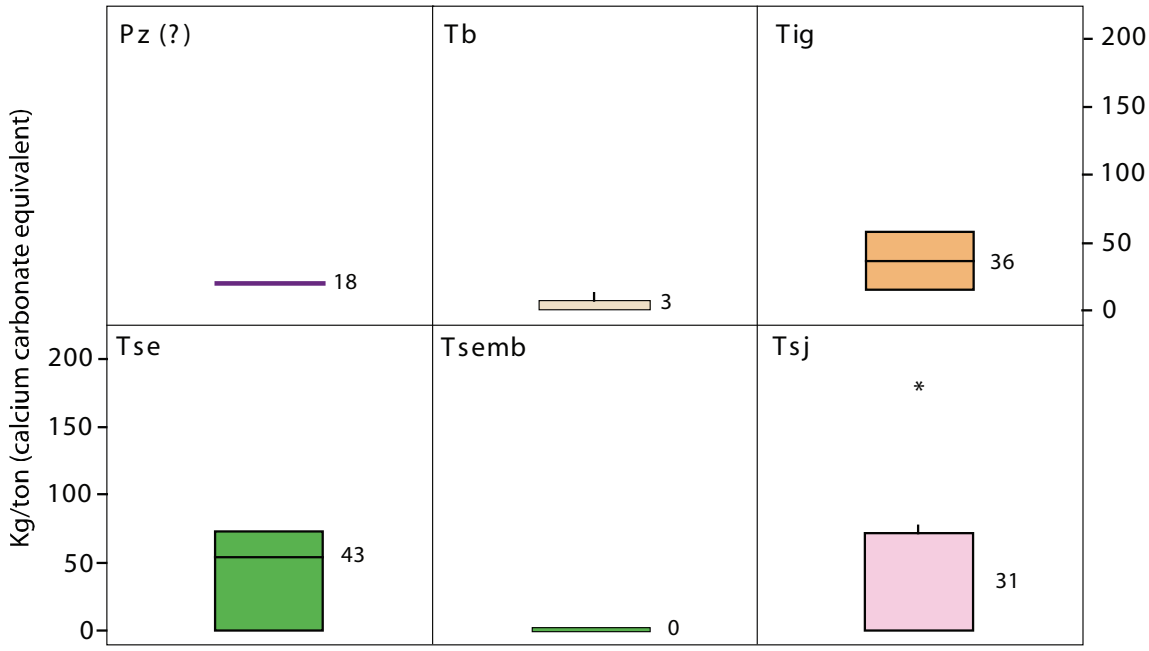

Figure 4. Boxplots of NAP results for units Pz(?), n = 1; Tb, n = 5; Tig, n = 4; Tse, n = 3; Tsemb, n = 1; and Tsj, n = 15. Mean values adjacent to box; outliers indicated by asterisk.

Nonsulfide-Bearing(?) Samples

Anomalously high NAP results were obtained for four samples (SDY090535B, SDY090536, SDY090548, and HPDY090550; table 12) that contain no detectable sulfide minerals based on X-ray diffraction analyses.

Several possible scenarios could be involved to help explain relatively high NAP determinations for samples that lack sulfide phases. The most likely scenarios involve the presence of sparse sulfide (<1 weight percent sulfide) that is not detectable based on XRD analyses, or hydrolysis reactions of ferric iron and water. Hydrolysis reactions involving ferric iron cause the water molecule to be split while also generating hydrogen ions. The Lapakko method is designed as a

Acid Neutralizing Capacity

In our previous study (Yager and others, 2005), three units had at least one sample with high ANC in acid titration tests. Unit Tse had the highest ANC in acid titration experiments of any sample studied (122 kg/t calcium carbonate equivalent). The additional units with high ANC were Tsj (44 kg/t calcium carbonate equivalent) and Tig (14 kg/t calcium carbonate equivalent). However, units Tse, Tsj, and Tig were only sparsely sampled in the previous study, thus a more statistically representative sample was needed to verify ANC rock properties for these units. Most ANC data discussed in this section is for units Tse, Tsj, Tig, and Tb. Additional samples of unit Tb were collected from a talus slope in Minnie Gulch that is accessible to

Table 12. Net acid production (NAP) results.

[Underline indicates trace amounts to 5 weight percent pyrite determined by Rietveld X-ray diffraction analysis. See table 1 for unit abbreviations; n/a indicates that after H_2O_2 digestion, the initial pH was > pH 7 and required no NaOH base for neutralization]

Unit	Field sample no.	Initial pH	Total volume NaOH (ml)	Weight (g)	Ending pH	$CaCO_3$ kg/ton
Tig	SDY090532	4.69	4.0	1.034	6.98	18
Tsj	SDY090533	2.38	40.0	1.021	7.27	182
Tig	SDY090534A	4.97	11.5	1.025	6.99	52
Tig	SDY090534B	4.82	13.0	1.028	7.00	59
Tsj	SDY090535A	<10	n/a	1.030	n/a	n/a
Tsj	SDY090535B	2.50	16.0	1.025	7.10	73
Tsj	SDY090536	2.55	17.0	1.018	7.11	78
Tsj	IDY090537A	<11	n/a	1.020	n/a	n/a
Tsj	IDY090537B	<11	n/a	1.028	n/a	n/a
Tsj	IDY090537C	<10	n/a	1.033	n/a	n/a
Tsj	IDY090538E	2.41	12.0	1.016	6.98	55
Tsj	IDY090538G	5.59	16.0	1.032	6.98	72
Tig	SDY090539	3.55	3.0	1.023	7.06	14
Pz(?)	HWDY090540	3.90	4.0	1.012	7.13	18
Tb	HWDY090541A	<10	n/a	1.018	n/a	n/a
Tb	HWDY090541B	<11	n/a	1.022	n/a	n/a
Tb	HWDY090542A	<10	n/a	1.023	n/a	n/a
Tb	HWDY090542B	<11	n/a	1.016	n/a	n/a
Tsemb	HWDY090543	<11	n/a	1.019	n/a	n/a
Tb	SDY090545	4.30	3.0	1.030	7.14	13
Tse	SDY090548	5.84	16.0	1.019	6.93	73
Tse	SDY090549	8.64	n/a	1.026	n/a	n/a
Tse	HPDY090550	5.57	12.0	1.024	6.96	54
Tsj	ODY090552A	<11	n/a	1.017	n/a	n/a
Tsj	ODY090552B	<11	n/a	1.029	n/a	n/a
Tsj	ODY090552C	<10	n/a	1.031	n/a	n/a
Tsj	ODY090553	10.92	n/a	1.018	n/a	n/a

land managers for possible use in remediation projects. Twenty-seven samples were analyzed for ANC in this study (table 13). A map showing the ANC ranking for this and the Yager and others (2005) study is shown on plate 1.

Eureka (Unit Tse) and Picayune Megabreccia (Unit Tsemb) Members

Three unit Tse samples (SDY090548, SDY090549, and HPDY090550) were collected from the southern and western parts of the San Juan caldera. Areas sampled include Deer Park trail south of Silverton, at the historical Eureka townsite, and along Picayune Gulch road. One sample of megabreccia, unit Tsemb, was sampled in Minnie Gulch.

No significant ANC was determined for unit Tse (table 13). The mean ANC calculated to reach pH 4 and pH 2 respectively, was 0.2 and 0.3 kg/t calcium carbonate equivalent.

A relatively high ANC was determined for one sample of unit Tsemb (sample HWDY090543) collected in upper Minnie Gulch southeast of Silverton (fig. 5). The ANC calculated to reach pH 4 and pH 2 respectively, was 0.8 and 26 kg/t calcium carbonate equivalent. Most of the acid added during ANC titration was below pH 4, which could be due to chlorite species reacting at lower pH; however, calcite continuing to react below pH 4 cannot be ruled out because we do not achieve equilibrium in our acid titrations.

San Juan Formation (Unit Tsj)

Eleven unit Tsj samples were analyzed for ANC. Sampling of unit Tsj was focused along the western margin of the Silverton and San Juan calderas in the following areas: near Clear Lake, north of South Fork Mineral Creek (samples ODY090552 and ODY090553) (fig. 6), near the

Table 13. Acid neutralizing capacity calculated in terms of calcium carbonate equivalent (kg/t) to reach pH values of 4 and 2 respectively, during 0.1 N H_2SO_4 titration. NAP values shown for comparison.

[n.d., no NAP detected; n.a., not analyzed. Field sample number suffix (*ca,ch*) contains calcite and or chlorite respectively; see table 1 for unit abbreviations]

Field sample no.	Unit	$CaCO_3$ equivalent units calculated in kg/t for titration to pH ≈ 4	$CaCO_3$ equivalent units calculated in kg/t for titration to pH ≈ 2	NAP
SDY090532*ch*	Tig	0.2	0.4	18
SDY090533*ch*	Tsj	n.a.	1	182
SDY090534A*ch*	Tig	n.a.	1	52
SDY090534B*ch*	Tig	0.4	0.5	59
SDY090535A*ca,ch*	Tsj	1	19	n.d.
SDY090535B*ch*	Tsj	n.a.	n.a.	73
SDY090536*ch*	Tsj	n.a.	1	78
IDY090537A*ca,ch*	Tsj	10	24	n.d.
IDY090537B*ca,ch*	Tsj	29	67	n.d.
IDY090537C*ca,ch*	Tsj	n.a.	36	n.d.
IDY090538E*ch*	Tsj	n.a.	1	55
IDY090538G*ch*	Tsj	0.2	0.5	72
SDY090539*ch*	Tig	0.5	1	14
HWDY090540*ch*	Pz(?)	n.a.	n.a.	18
HWDY090541A*ca,ch*	Tb	83	119	n.d.
HWDY090541B*ca,ch*	Tb	102	146	n.d.
HWDY090542A*ca,ch*	Tb	6	20	n.d.
HWDY090542B*ca,ch*	Tb	34	83	n.d.
HWDY090543*ca,ch*	Tsemb	0.88	26.47	n.d.
SDY090545*ch*	Tb	0.2	0.4	13
SDY090548*ch*	Tse	0.3	0.4	73
SDY090549*ch*	Tse	0.1	0.2	n.d.
HPDY090550*ch*	Tse	0.2	0.4	55
ODY090552A*ca,ch*	Tsj	10	30	n.d.
ODY090552B*ca,ch*	Tsj	n.a	n.a	n.d.
ODY090552C*ca,ch*	Tsj	n.a	n.a	n.d.
ODY090553*ca,ch*	Tsj	5.71	110.11	n.d.

Imogene mine west of highway 550 (sample SDY090535A) (fig. 7), and below the Silver Cloud mine west of Chattanooga (sample IDY090537) (fig. 6). The mean ANC calculated for all unit Tsj samples to reach pH 4 and pH 2, respectively was 9 and 29 kg/t calcium carbonate equivalent. Only five of the eleven Tsj samples analyzed were found to have high ANC (figure 8).

Burns Member (Unit Tb)

Four unit Tb samples were collected from talus in Minnie Gulch located southeast of Silverton. All unit Tb samples were found to have moderate to high ANC (figs. 9 and 10). One unit Tb sample (HWDY090541B) has the highest ANC rank of any sample studied thus far, and two other unit Tb samples (HWDY090541A and HWDY090542B) are ranked in the top 10 (plate 1).

ANC and NAP Unit Comparisons

Boxplots comparing ANC and NAP properties are shown in figure 11. These data indicate that unit Tb sampled from the Minnie Gulch talus has the highest ANC and lowest NAP in this study. Unit Tsj also has several samples with moderate to high ANC; however, this unit also tends to have a high NAP in some localities. Units Tig and Tse tend to have low ANC and high NAP. One unit Tsemb sample has a moderate ANC and low NAP suggesting that more samples are warranted to determine the overall ANC properties of this unit.

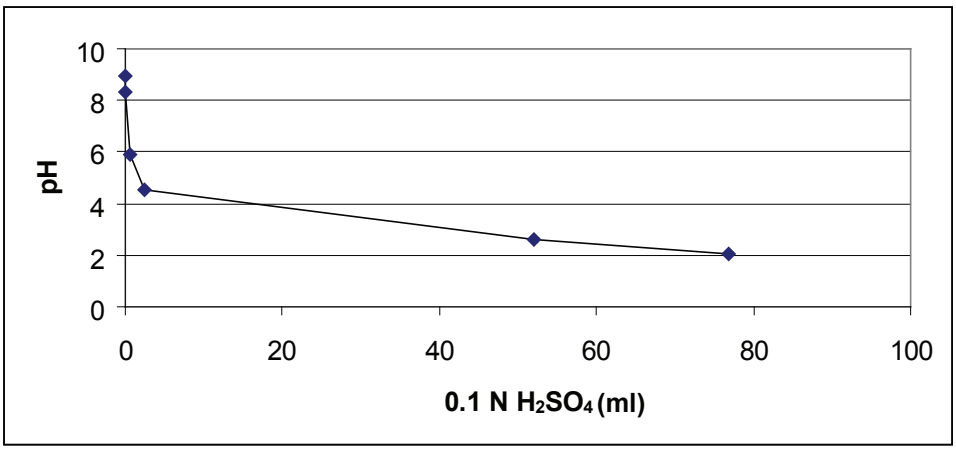

Figure 5. Acid titration curve for unit Tsemb sample HWDY090543.

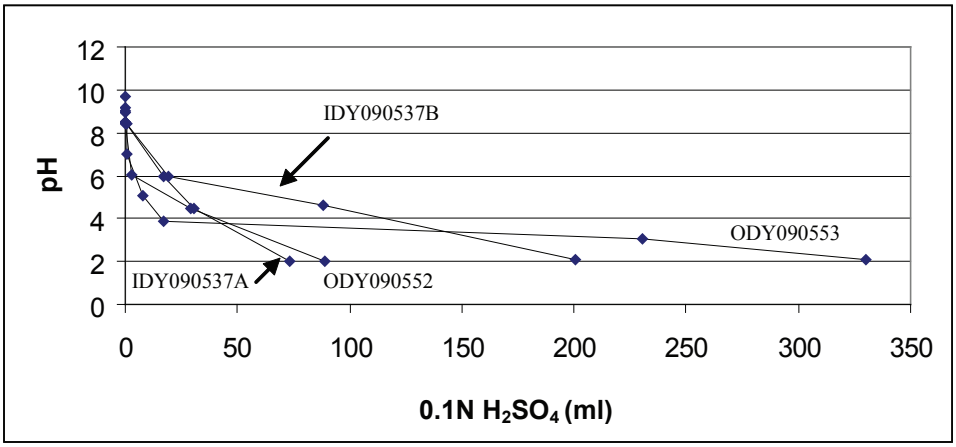

Figure 6. Acid titration curves for unit Tsj samples ODY090552, ODY090553, and IDY090537A and B.

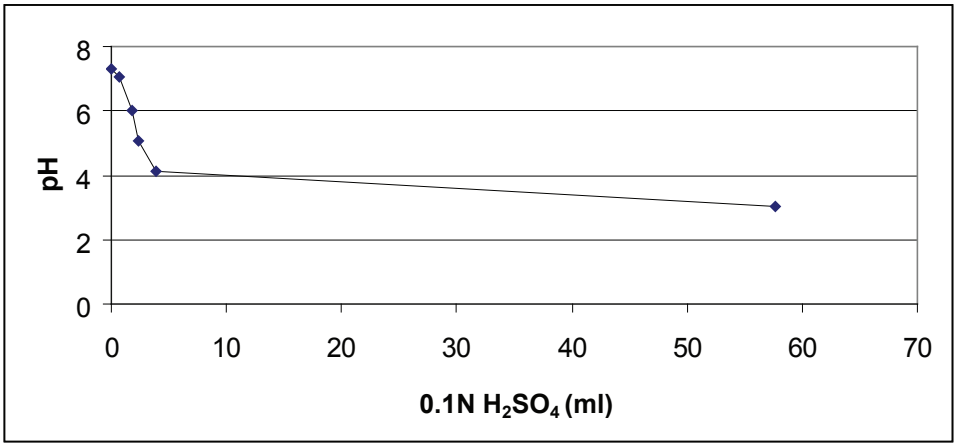

Figure 7. Acid titration curve for unit Tsj sample SDY090535A.

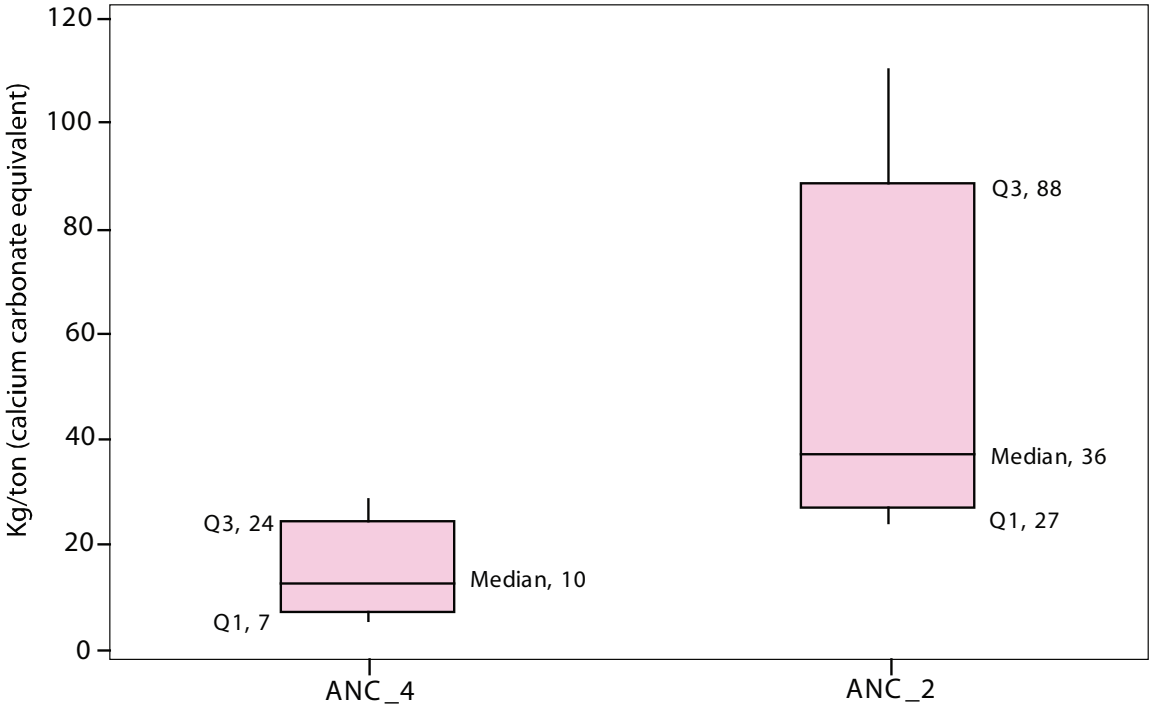

Figure 8. Boxplots of calculated ANC to reach pH 4 (ANC_4) and pH 2 (ANC_2) during acid titrations for high ANC unit Tsj samples, n = 5. Samples were collected near Clear Lake north of South Fork Mineral Creek, and west of Chattanooga adjacent to Silver Cloud mine portal. First quartile (Q1), median, and third quartile values labeled.

Sequential Leachate Results (Whole Rocks)

A suite of seven major elements (Mg, Al, P, K, Ca, Ti, and Fe) and ten trace elements (Mn, Ni, Cu, Zn, As, Sr, Mo, Cd, Ba, and Pb) were investigated as part of the sequential leaching study. These elements are of interest because of possible contaminants that could be released by ANC rocks when the materials are used in mine-waste remediation projects.

The elements released during leaching can be used to evaluate the minerals that might participate in weathering reactions. Each sequential step is designed to react with specific mineral or amorphous phases. In the following section, sequential steps are referred to as “phases.” The term “phase” in this context refers to the sequential step that has been developed to target a specific mineral species or group, such as carbonates or silicates. Major elements are discussed below in order of increasing atomic number. Note that all samples were leached using the four-acid step described in Briggs (2001) to determine totals for each element. Disparities between totals measured from the four-acid step and totals from the seven- and nine-step methods are likely caused by sample inhomogeneity, as only 2-g splits were analyzed by each method.

Magnesium

Most of the leachable magnesium is produced during dissolution of the crystalline iron and aluminum oxide phase in step six. The phase designed to react with silicates and sulfides are of secondary importance in extracting magnesium (appendix A). The highest leachable magnesium concentrations (2.51 weight percent) are observed in the most mafic, lowest silica content sample (IDY090537B) (fig. 12). This is the only basalt (44.4 weight percent SiO_2) analyzed during the sequential leachate study. In addition, samples containing the highest abundances of the Mg-bearing phase chlorite (samples IDY090537B and SDY0310) also tend to have higher leachable magnesium concentrations (see table 3 in Yager and others (2005); table 3, this study). Conversely, the less mafic, dacitic lava and rhyolitic ash-flow tuff samples (IDY0329 and HDY0314) have lower magnesium concentrations (ranging from 0.46 to 0.48 weight percent, respectively); these samples also have lower chlorite abundances.

Aluminum

The majority of leachable aluminum is concentrated in solution in the silicate phase, step nine with subsidiary amounts in the crystalline iron and aluminum oxide phase

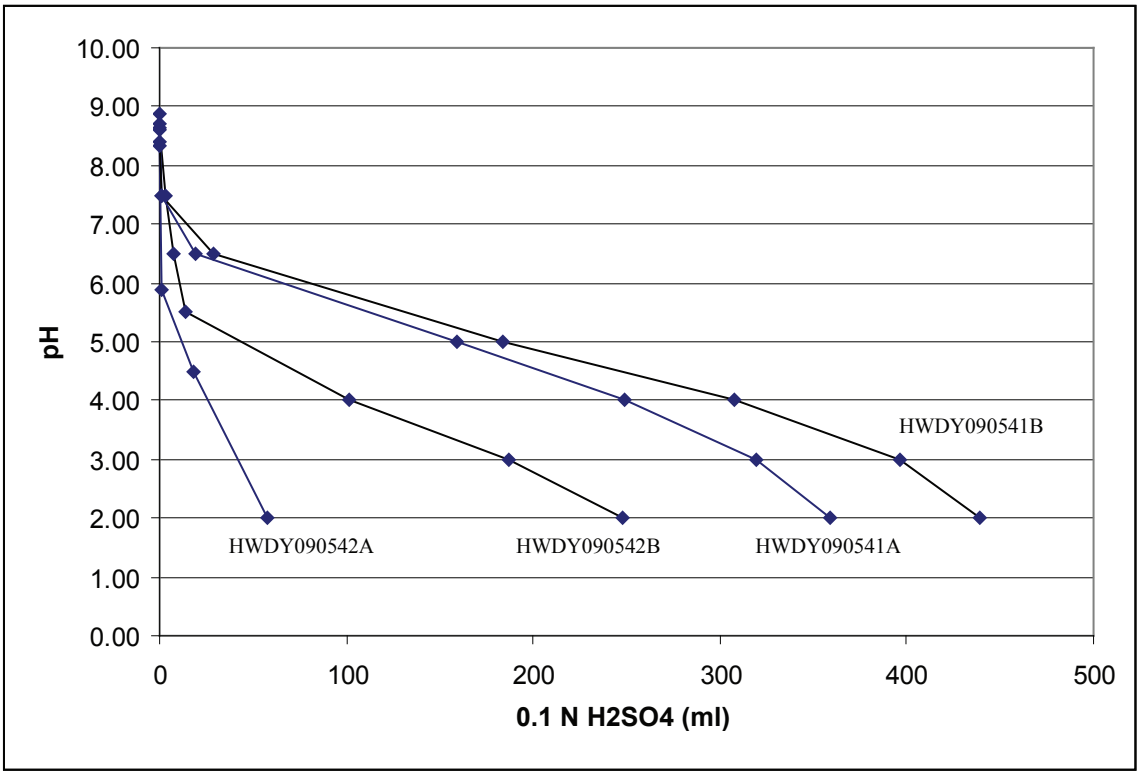

Figure 9. Acid titration curves for unit Tb samples from outcrop and talus in Minnie Gulch (sample HWDY090541A and B, outcrop; sample HWDT090542A and B, talus).

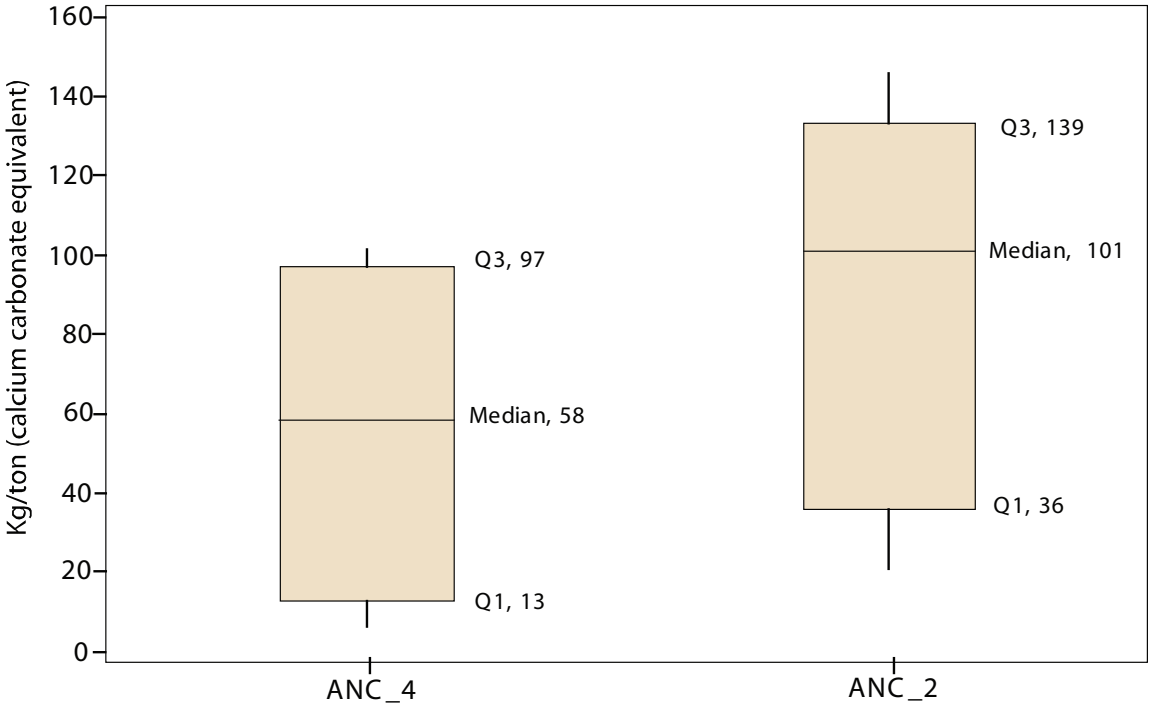

Figure 10. Boxplots of calculated ANC to reach pH 4 (ANC_4) and pH 2 (ANC_2) during acid titrations for high ANC unit Tb bedrock and talus samples in Minnie Gulch, n = 4. First quartile (Q1), median, and third quartile values labeled.

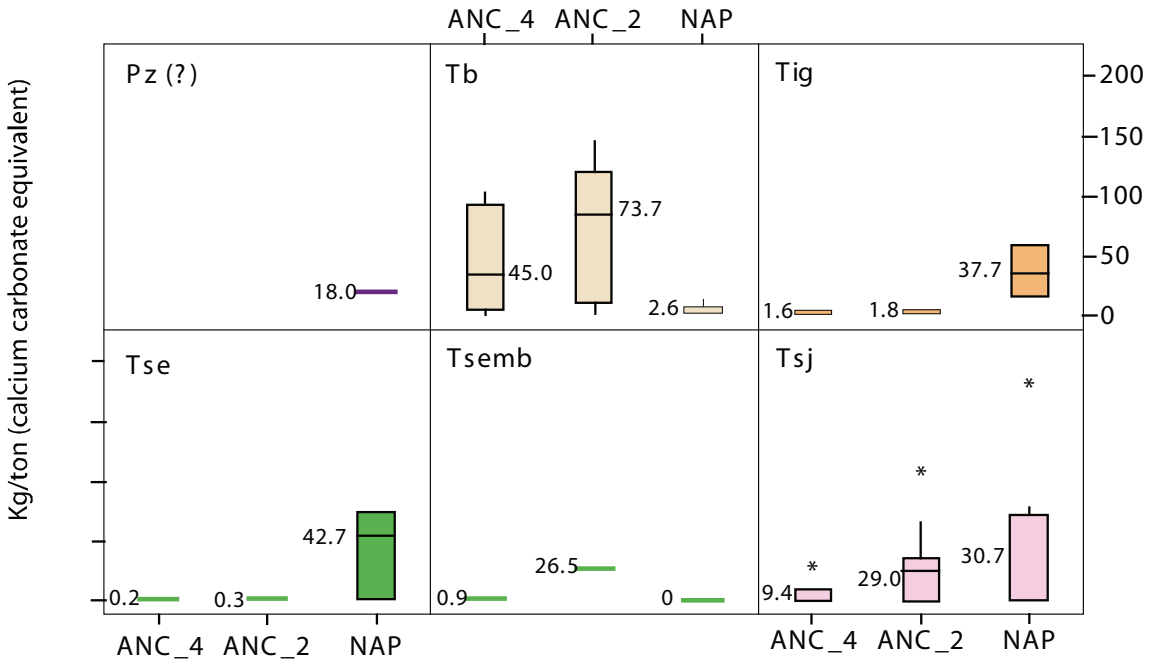

Figure 11. Boxplots of calculated ANC to reach pH 4 (ANC_4) and pH 2 (ANC_2) during acid titrations, and NAP for units Pz(?), n = 1; Tb, n = 5; Tig, n = 4; Tse, n = 3; Tsemb, n = 1; and Tsj, n = 11 (ANC) and n = 15 (NAP). Median values adjacent to box; outliers indicated by asterisk.

(fig. 13). The more mafic samples tend to have higher aluminum concentrations, with the basalt sample (IDY090537B) having the highest leachable aluminum in the silicate phase (6.32 weight percent). Lower aluminum abundances are observed in the dacitic lava and rhyolitic ash-flow tuff samples (IDY0329 and HDY0314) in the silicate phase, and range from 5.28 to 5.31 weight percent, respectively (appendix B). The probable sources for leachable aluminum are the primary mineral plagioclase and secondary illite, a potassium-aluminum-silicate mineral that is introduced during propylitic alteration and replaces primary plagioclase, potassium feldspar, and groundmass.

Potassium

Potassium in solution is concentrated in the silicate phase (fig. 14) with the greatest abundance (3.29 weight percent) observed in the rhyolitic ash-flow tuff sample (HDY0314) (appendix C). The source for potassium in the ANC rocks is primary potassium feldspar and secondary illite that is common in propylitically altered and weakly sericitized rocks, in addition to potassium in the groundmass.

Calcium

Calcium is sourced from multiple phases (fig. 15). The total leachable calcium is a result of complex reactions involving calcite introduced initially during propylitic alteration that replaced primary silicate minerals and groundmass, in addition to calcium derived from calcium-bearing aluminum silicates.

Similar to Fe, Mg, and Al, there is a trend for more mafic samples to also have higher calcium abundances, with the basalt sample (IDY090537B) having the highest calcium concentration (4.34 weight percent, four-acid leach) (appendix D). The most silicic sample (HDY0314) has the lowest total calcium (1.61 weight percent, total-sum four-acid leach).

Samples that lack or have low whole -rock calcite abundances based on x-ray diffraction analyses in the previous Yager and others (2005) study (samples SDY0310 and SDY0326) and a sample from this study (HWDY090542A) with relatively low calcite (4 weight percent calcite) also have a higher percentage of leachable calcium from the silicate phase. Other samples that have a higher percentage of calcite (ranging from 5 to 20 weight percent) have a lower proportion of calcium derived from silicates, a corresponding increase in calcium derived from the carbonate pH 5 acetic acid phase, and a larger proportion of calcium from the crystalline Fe- and Al-oxides phase (for example, samples IDY090537B, HDY0317, and IDY0329).

Other leachate phases that are involved in liberating calcium, but commonly to a lesser extent to those mentioned above, include, in relative decreasing order of abundance, (a) hydroxides and amorphous and crystalline Mn-oxides, (b) sulfide, (c) HCl pH 2, (d) exchangeable pH 8.2, and (e) HCl pH 4.

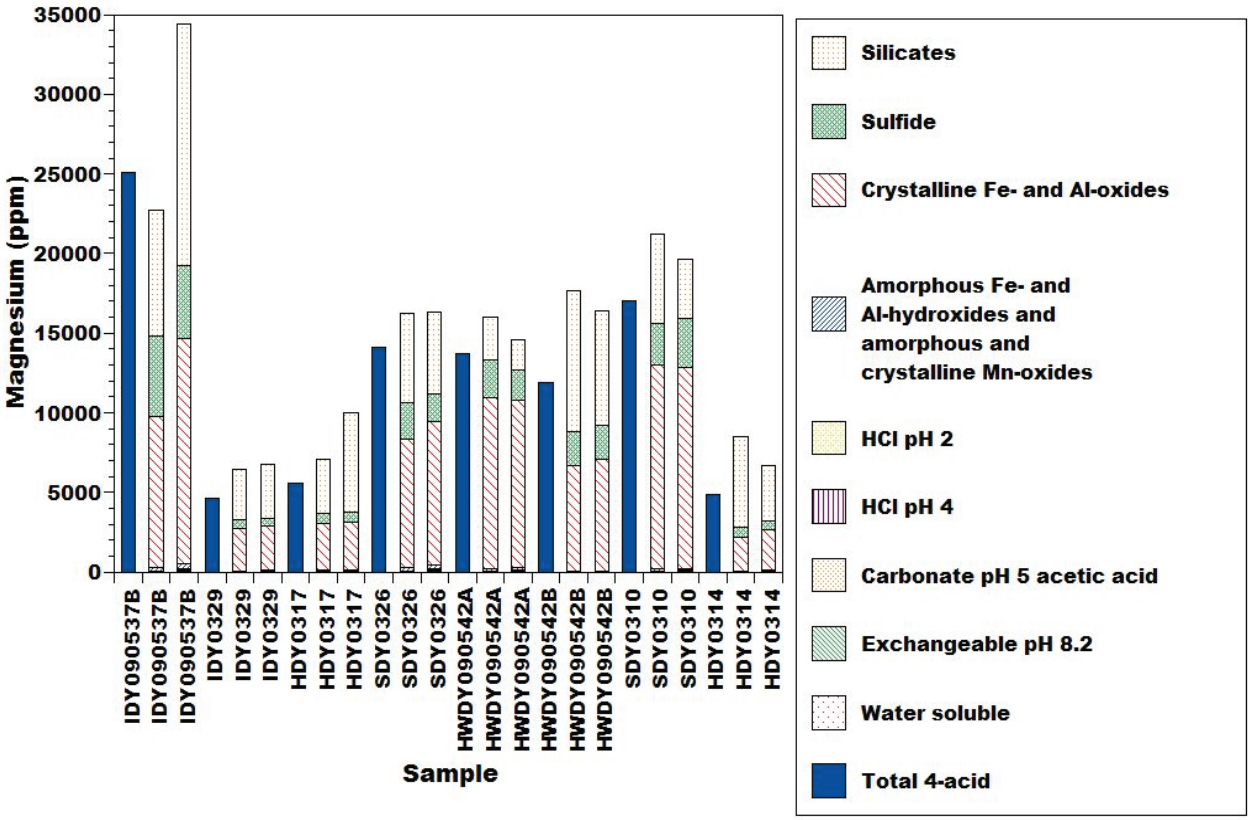

Figure 12. Histogram of whole-rock leachate results for Mg. Total digestion shown by solid blue bar; next histogram bars for each sample are for seven- and nine-step methods respectively.

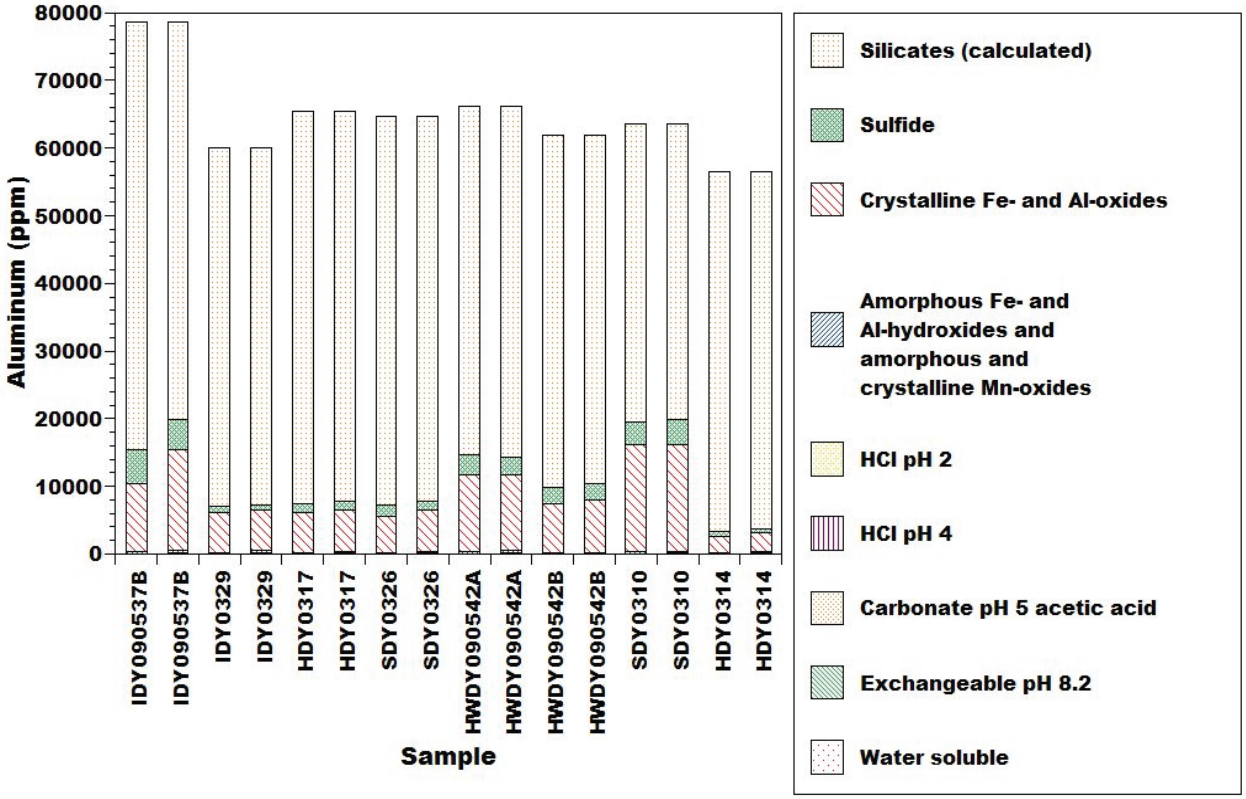

Figure 13. Histogram of whole-rock leachate results for Al. Total digestion shown by solid blue bar; next histogram bars for each sample are for seven- and nine-step methods respectively.

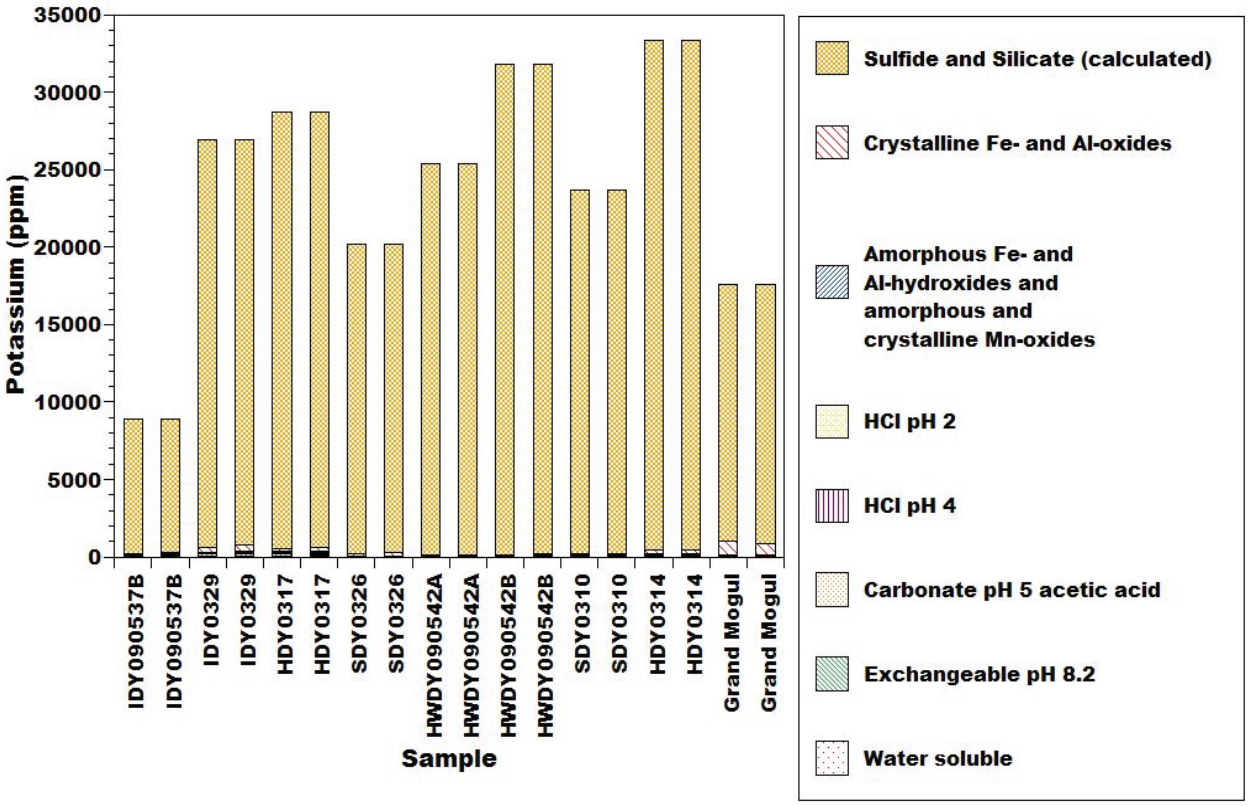

Figure 14. Histogram of whole-rock leachate results for K. Total digestion shown by solid blue bar; next histogram bars for each sample are for seven- and nine-step methods respectively.

Titanium

Titanium is mainly observed in the silicate phase (fig. 16, appendix E). This is inconsistent with the mineralogy of the rocks because the majority of titanium likely occurs as ilmenite intergrowths with magnetite (see Yager and others, 2005, their fig. 20). The higher titanium abundance in the silicate phase, however, is likely due to the refractory nature of the magnetite-ilmenite intergrowths that do not release significant titanium until the four-acid digest procedure is employed. There is an observed trend of samples having both high magnetite and titanium abundance (for example, samples HDY0317, IDY090537B, and HWDY090542A) (Yager and other, 2005; this study, table 3).

Iron

Iron has a similar trend as that observed for magnesium, with the most abundant iron present in the crystalline Fe- and Al-oxide phase, followed by the silicate and sulfide leachate phases (fig. 17; appendix F).

Small quantities of iron (<0.05 weight percent) are present in the amorphous Fe- and Al-hydroxide and amorphous and crystalline Mn-oxide phases. The majority of leachable iron is derived from the most mafic lavas (samples IDY090537B and SDY0310), which have the highest iron abundances (6.4 weight percent).

The primary minerals that are sources for leachable iron are (a) the magnesium-iron-aluminum silicates chlorite (clinochlore) formed after pyroxene, hornblende, plagioclase, and groundmass during propylitic alteration, and (b) magnetite and or titanomagnetite.

Manganese

Manganese abundance is apportioned into several leachate phases (fig. 18). The crystalline Fe- and Al-oxide phase hosts the majority of manganese. One of the rocks with the highest chlorite (clinochlore) abundances (sample SDY0310) also has the highest leachable manganese concentration (0.3 weight percent; appendix G). Four other samples (IDY090537B, IDY0329, and HWDY090542A and B) that have relatively high leachable manganese also average approximately 13 weight percent clinochlore (Yager and others, 2005, table 3; table 3, this study). This finding is consistent with the manganese being derived from chlorite, as manganese substitutes for iron in the chlorite crystal lattice (Halferdahl, 1961). Other leachate phases in which manganese occurs, listed in relative order of abundance, include the

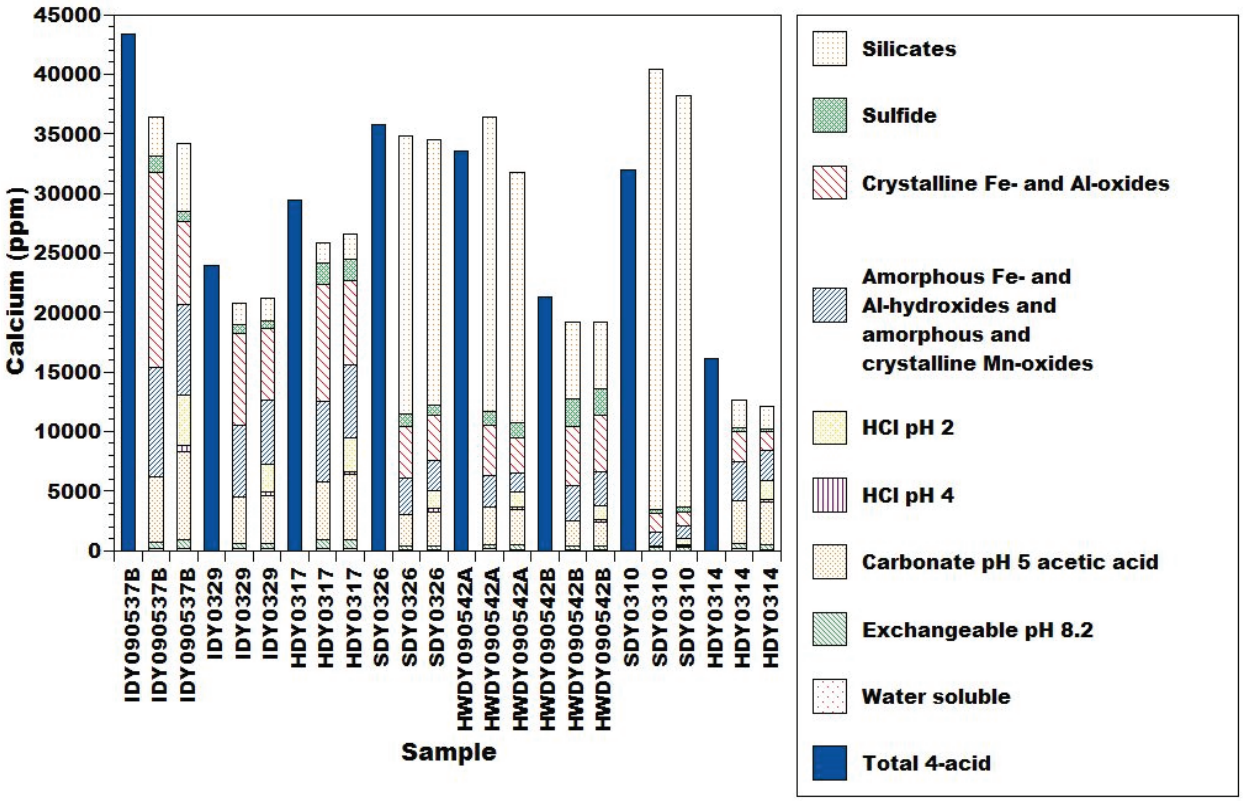

Figure 15. Histogram of whole-rock leachate results for Ca. Total digestion shown by solid blue bar; next histogram bars for each sample are for seven- and nine-step methods respectively.

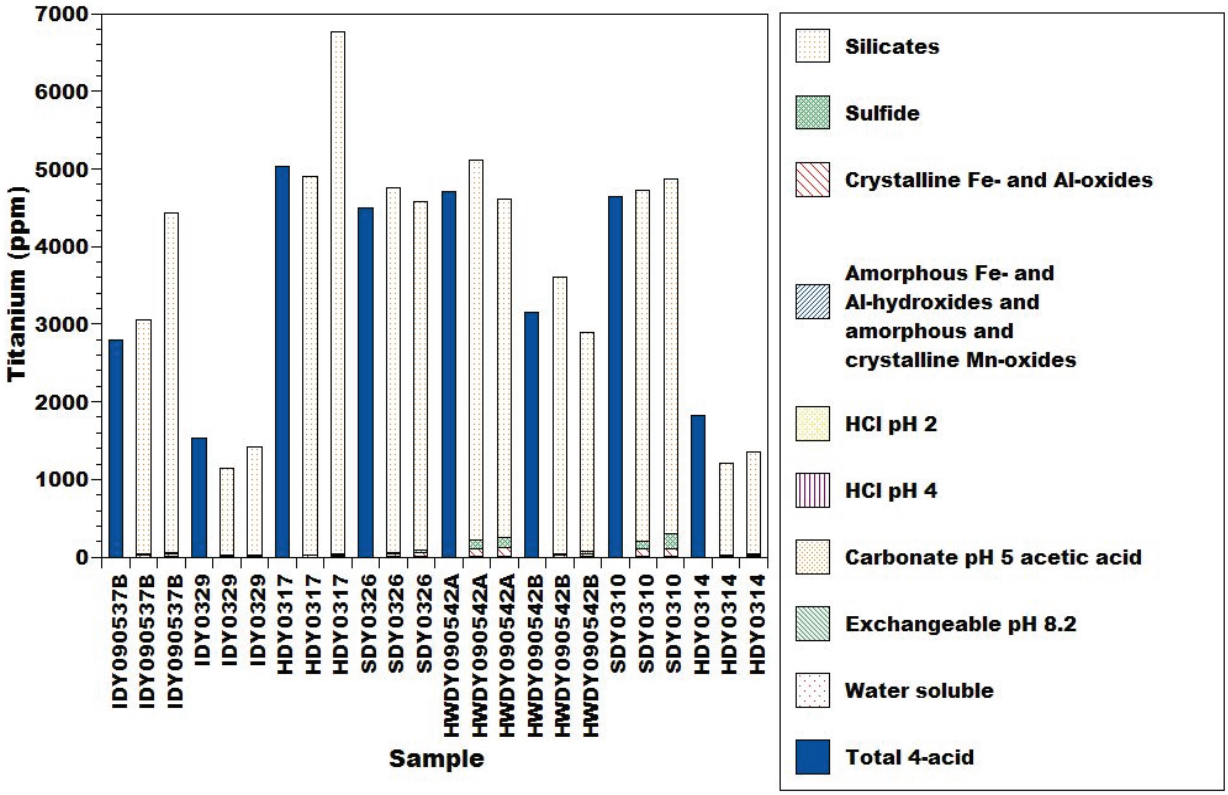

Figure 16. Histogram of whole-rock leachate results for Ti. Total digestion shown by solid blue bar; next histogram bars for each sample are for seven- and nine-step methods respectively.

following: silicate; hydroxide, amorphous, and crystalline Mn-oxides; and sulfide leachate phases. Note that in some instances, manganese in the sulfide phase predominates over the hydroxide, amorphous, and crystalline Mn-oxide phase (for example, andesite lava sample SDY0310). Several samples indicate relatively small quantities of manganese being sourced from Mn-bearing carbonates (samples IDY090537B, IDY0329, HDY0317, SDY090326, HWDY090542A and B, and HDY0314). No Mn-bearing carbonates, however, were identified in X-ray diffraction analysis.

Nickel

Nickel concentrations are highest in the crystalline Fe- and Al-oxide phases. The silicate and sulfide phases are of secondary importance (fig. 19; appendix H). Minor amounts of nickel are leached during the hydroxide, amorphous, and crystalline Mn-oxides phase, which are all part of one leachate step (tables 9 and 10, steps 4 and 6, respectively); which represents one leachate step. The lavas of the Burns Member of the Silverton Volcanics are relatively high in leachable nickel when compared to San Juan Formation and Eureka Member of the Sapinero Mesa Tuff samples. The highest nickel concentrations are observed in the Burns Member andesite lava sample (SDY0310). This could be due to the presence of trace quantities (<1 weight percent) of chalcopyrite ($CuFeS_2$) in this sample (Yager and others, 2005). Nickel is a transition metal with a 2^+ charge and similar ionic radius that may substitute for copper in chalcopyrite. Unit Tpa sample SDY0326 also has elevated Ni concentrations compared to the other unit Tpa sample HDY0317.

Copper

Copper is derived from several leachate phases indicating that this element is mobile at multiple acidic pH intervals. The sample with the highest copper concentration (0.0054 weight percent, appendix 1I) is SDY0310, which was found to contain trace chalcopyrite in the study by Yager and others (2005). Unit Tpa sample SDY0326 also has elevated Cu concentrations compared to the other unit Tpa sample HDY0317. The leachate phases that produce the most copper, while highly sample dependent, include silicate, sulfide, and crystalline Fe- and Al-hydroxide and crystalline Mn-oxide phases (fig. 20; appendix I).

Zinc

The crystalline Fe- and Al-oxide, and the amorphous Fe- and Al-hydroxide, and amorphous and crystalline Mn-oxide phases, are host to the majority of zinc (fig. 21; appendix J).

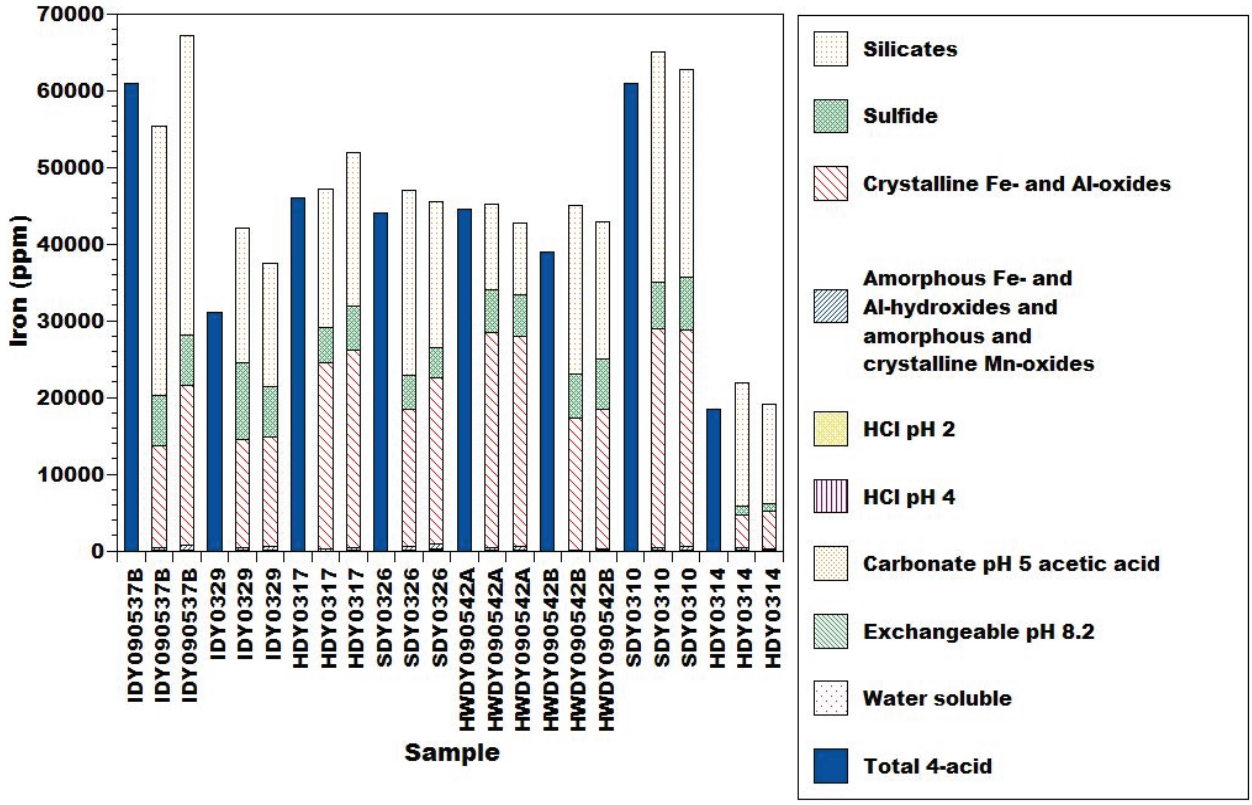

Figure 17. Histogram of whole-rock leachate results for Fe. Total digestion shown by solid blue bar; next histogram bars for each sample are for seven- and nine-step methods respectively.

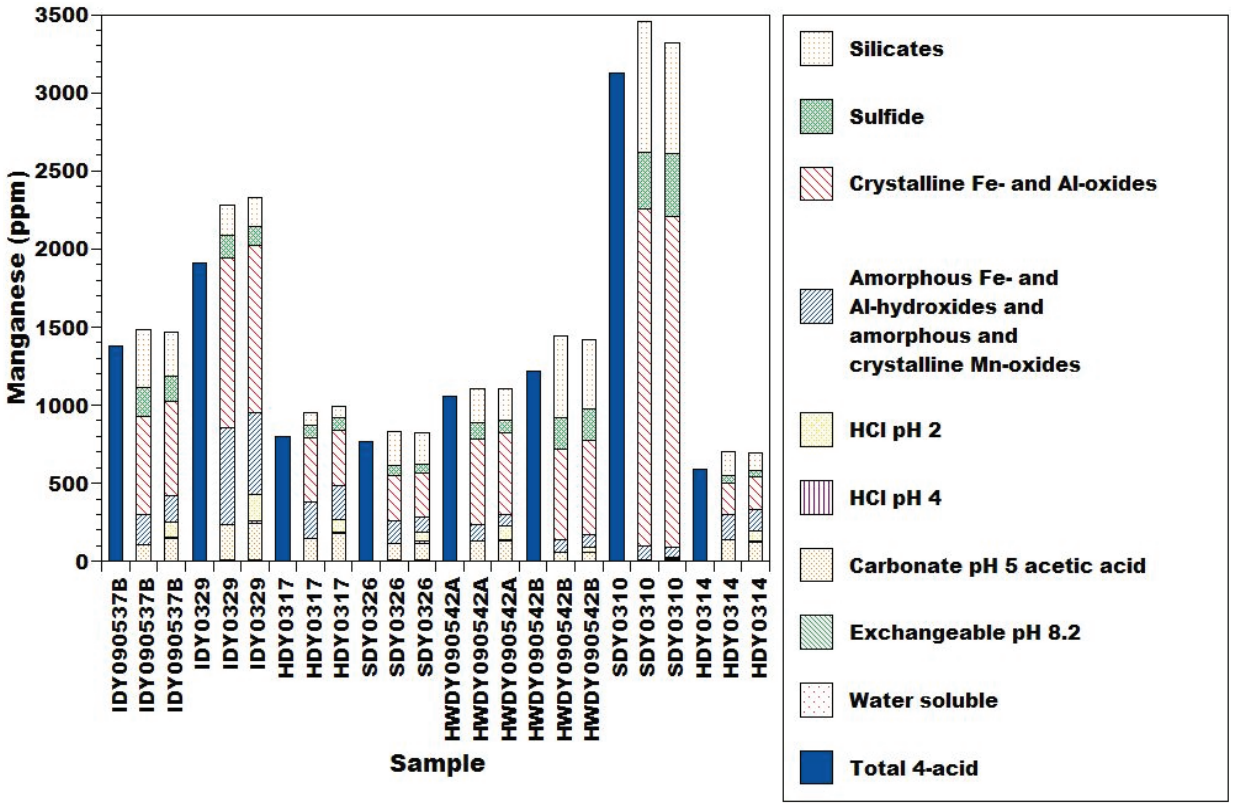

Figure 18. Histogram of whole-rock leachate results for Mn. Total digestion shown by solid blue bar; next histogram bars for each sample are for seven- and nine-step methods respectively.

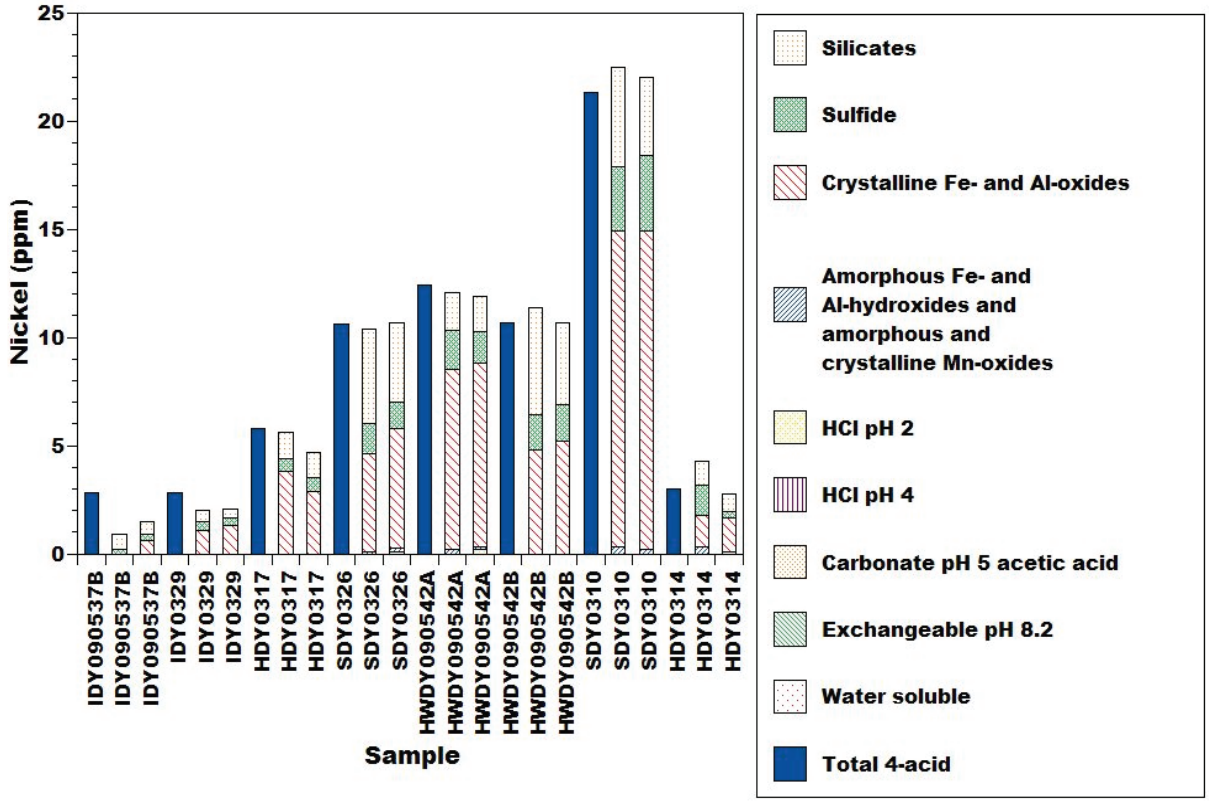

Figure 19. Histogram of whole-rock leachate results for Ni. Total digestion shown by solid blue bar; next histogram bars for each sample are for seven- and nine-step methods respectively.

The silicate and sulfide phases are of secondary importance in most samples. Unit Tsj sample IDY0329 has the highest leachable zinc concentrations (between 0.14 and 0.15 weight percent) and a correspondingly high whole -rock zinc concentration (0.1 weight percent, table 8).

Arsenic

Arsenic tends to be concentrated in solution in the silicate and sulfide phases (fig. 22; appendix K). The crystalline Fe- and Al-oxide and the amorphous Fe- and Al-hydroxide and amorphous and crystalline Mn-oxide phases are of secondary arsenic abundance. The sample with the highest leachable arsenic (IDY0326) is exposed near the relatively high arsenic-acid-sulfate mineralized system centered near Red Mountain Pass and on Anvil Mountain.

Strontium

The majority of strontium leached was produced in the silicate phase (fig. 23; appendix L). This is consistent with strontium being leached from plagioclase and epidote. Strontium commonly substitutes for calcium in plagioclase and epidote. An additional source for leachable strontium could be from calcite; although, strontium was not detected in calcite by SEM analysis (Sharon Diehl, written commun., 2007). The highest leachable strontium was observed in the basalt sample IDY090537B.

Molybdenum

Molybdenum concentrations are low and mostly in the silicate phase (fig. 24; appendix M). This is possibly due to the molybdenum being leached from stockwork micro-veinlets that are commonly associated with granitoid intrusions along the southern margins of the Silverton caldera (Ringrose, 1982).

Cadmium

As with zinc and lead, the highest cadmium is observed from sample IDY0329 (fig. 25; appendix N) and is derived principally from the amorphous Fe- and Al-hydroxide and amorphous and crystalline Mn-oxide phase. The carbonate pH 5 acetic acid phase and crystalline Fe- and Al-oxide phases were also important leachate phases for sample IDY0329. Most other samples, with the exception of sample SDY0310, have relatively low cadmium abundances.

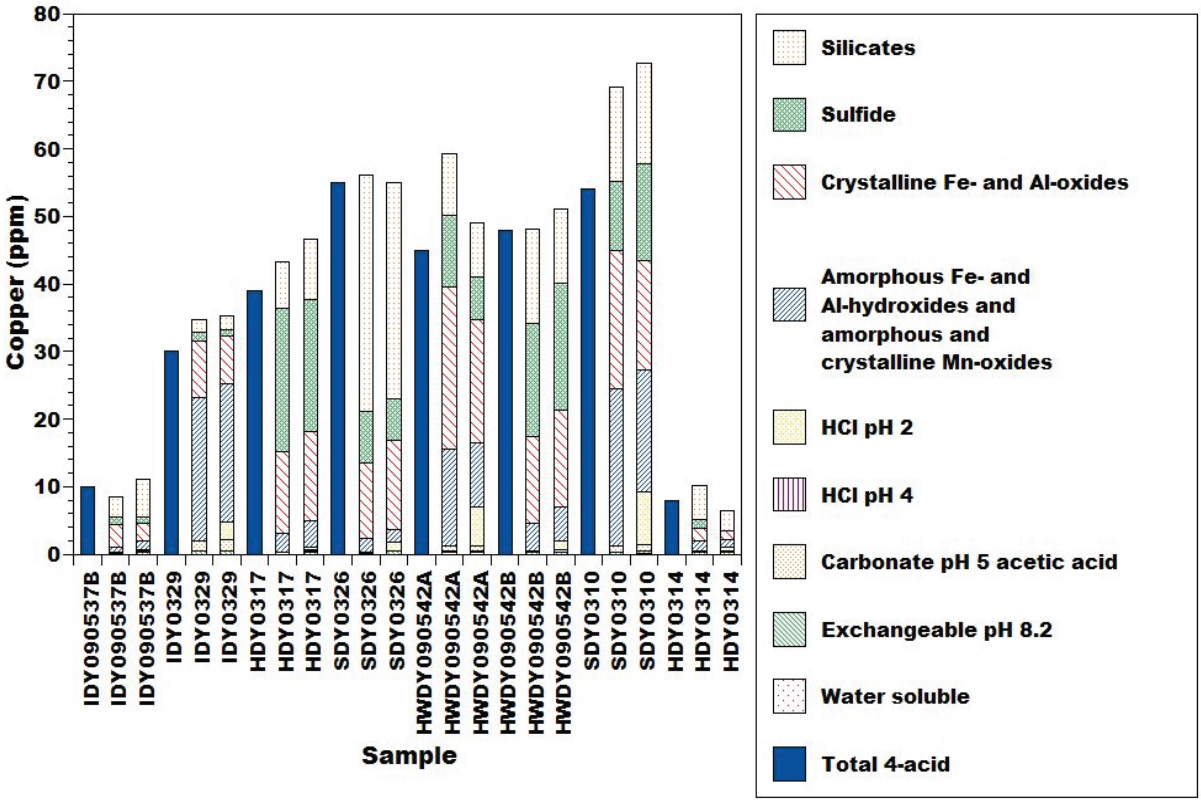

Figure 20. Histogram of whole-rock leachate results for Cu. Total digestion shown by solid blue bar; next histogram bars for each sample are for seven- and nine-step methods respectively.

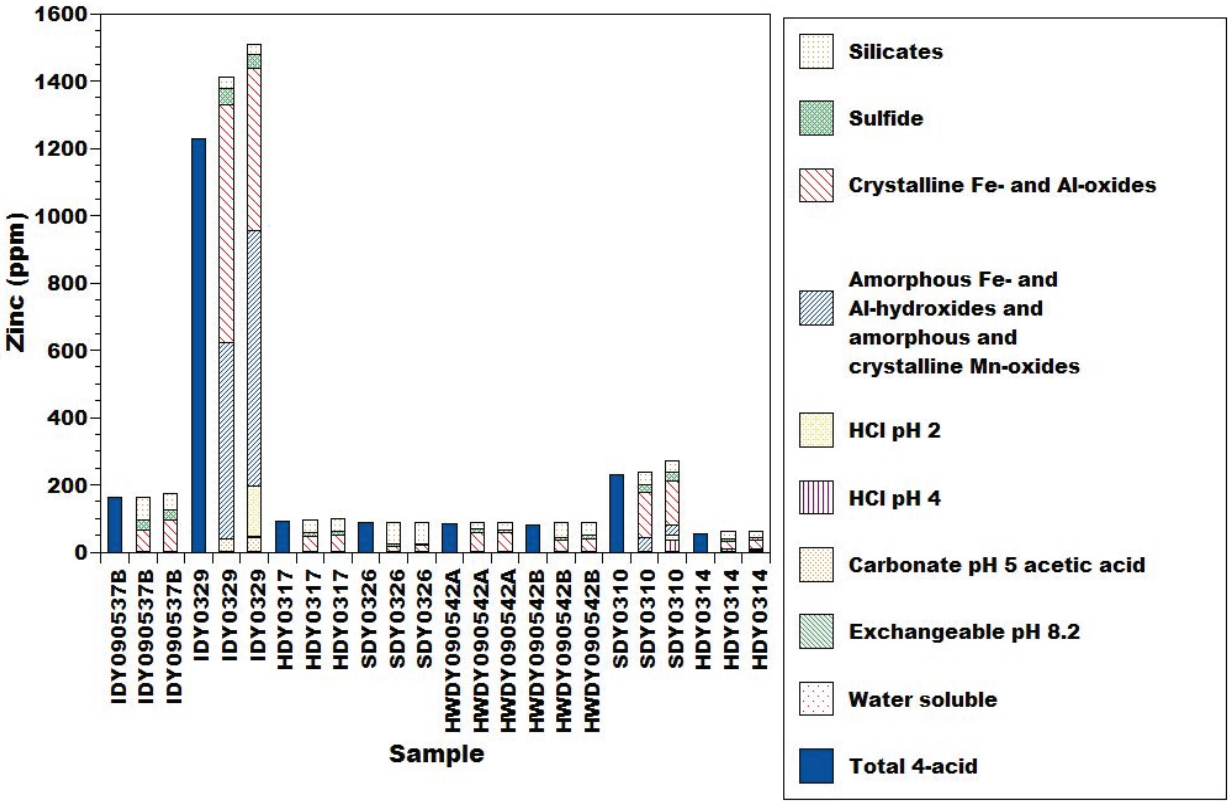

Figure 21. Histogram of whole-rock leachate results for Zn. Total digestion shown by solid blue bar; next histogram bars for each sample are for seven- and nine-step methods respectively.

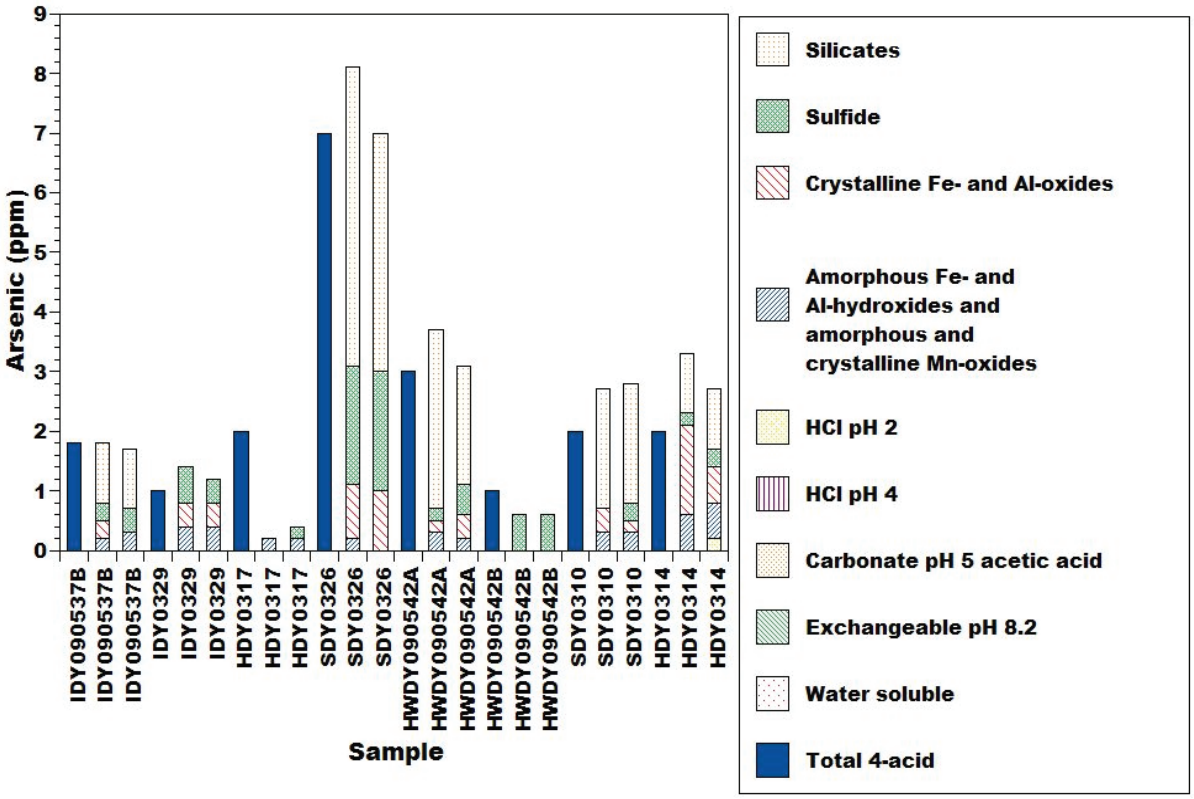

Figure 22. Histogram of whole-rock leachate results for As. Total digestion shown by solid blue bar; next histogram bars for each sample are for seven- and nine-step methods respectively.

Barium

Barium is mostly in the silicate phase (fig. 26; appendix O). This is consistent with barium being derived from plagioclase as barium substitutes for calcium in plagioclase. More complex leachate histograms are observed for samples IDY0329 and HDY0317. In the case of sample IDY0329, barite was detected in SEM analyses (Sharon Diehl, written commun., 2007), which helps explain barite dissolution at higher pH phases. Barite was not identified in sample HDY0317, so it is unclear what is causing the more complex Ba leachate histogram for this sample.

Lead

The phases producing leachable lead are highly variable, with no clear trend being consistently observed between samples (fig. 27; appendix P). Sample IDY0329 produced the highest total lead (between 70 and 80 µg/l) and has a high pyrite abundance (3 weight percent) (Yager and others, 2005, their table 3). No other sulfide minerals were observed in SEM analyses that could be used to identify the source of the lead. However, sample IDY0329 does have a high illite concentration (27 weight percent) (Yager and others, 2005, their table 3), and it is possible that there has been lead substitution for potassium in the illite lattice. More work is needed to determine the mineral residence of lead. Whole-rock concentrations are high (51 ppm) in sample IDY0329 compared with other samples, and leachable lead is approximately proportional with whole-rock lead abundances.

Sequential Leachate Results (Grand Mogul Mine Waste)

Magnesium

The magnesium abundance, concentrated mainly in the silicate phase, is low when compared with ANC volcanic rocks that are host to the mineral deposits (fig. 28; appendix A). The lower magnesium concentrations, along with lower abundances of other major elements (P, Ca, and Ti), are a result of dilution of these elements by ore and gangue material in the mine waste.

Aluminum

Aluminum is concentrated mainly in the silicate phase, and its abundance is four times greater (3.2 weight percent, > 32,000 µg/l) in the mine waste compared to the highest aluminum concentrations observed in ANC volcanic rocks (fig. 29; appendix B). The likely source of aluminum is illite

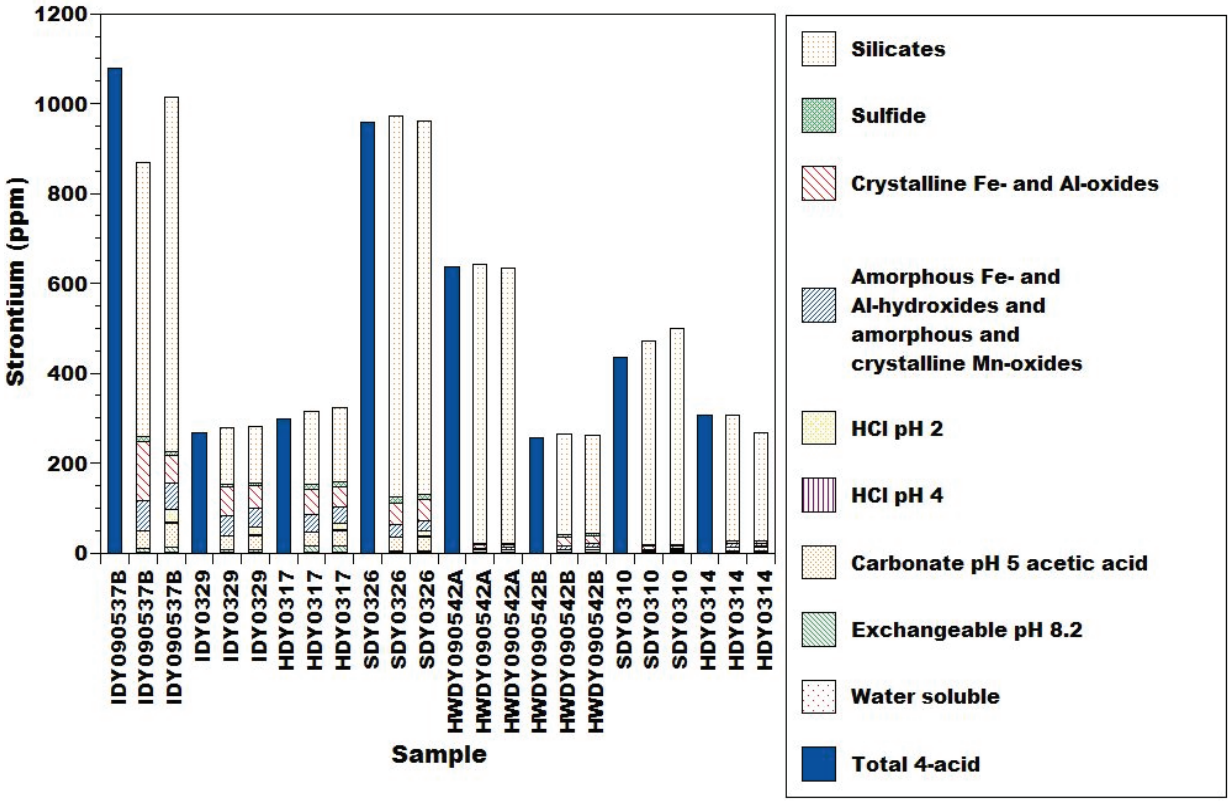

Figure 23. Histogram of whole-rock leachate results for Sr. Total digestion shown by solid blue bar; next histogram bars for each sample are for seven- and nine-step methods respectively.

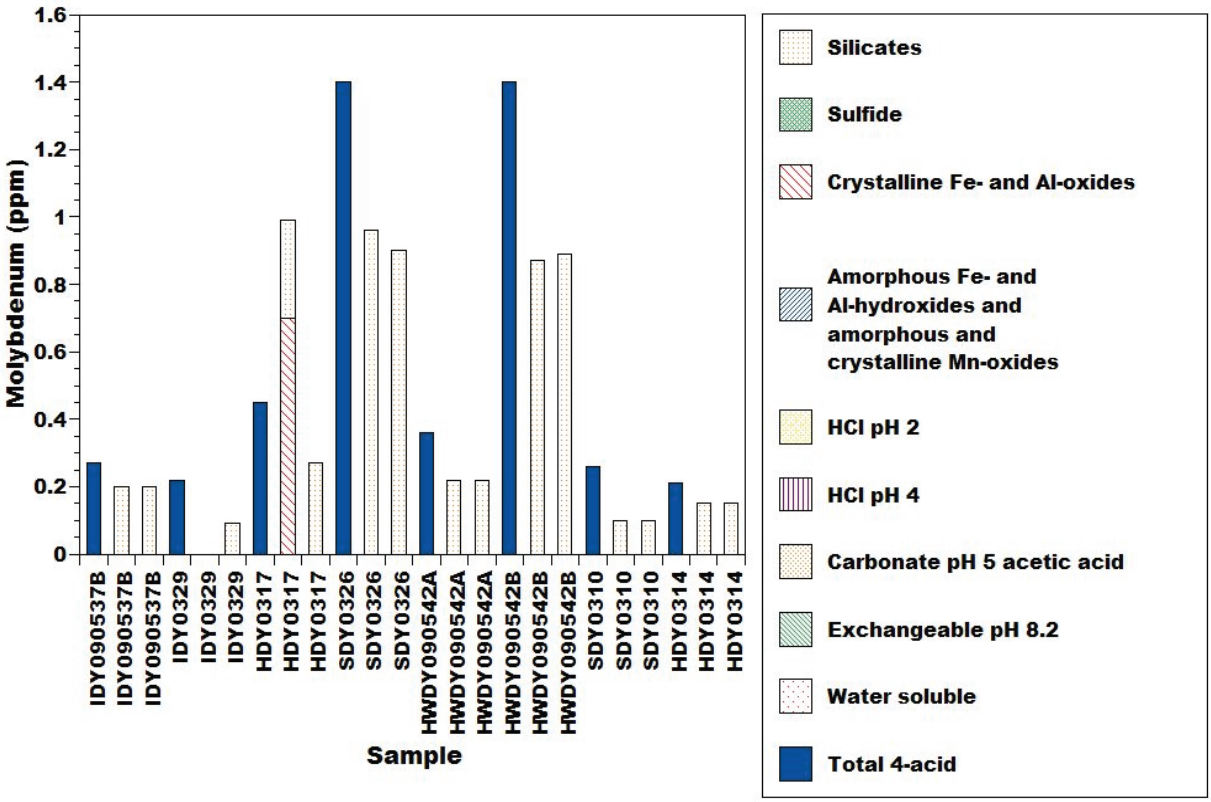

Figure 24. Histogram of whole-rock leachate results for Mo. Total digestion shown by solid blue bar; next histogram bars for each sample are for seven- and nine-step methods respectively.

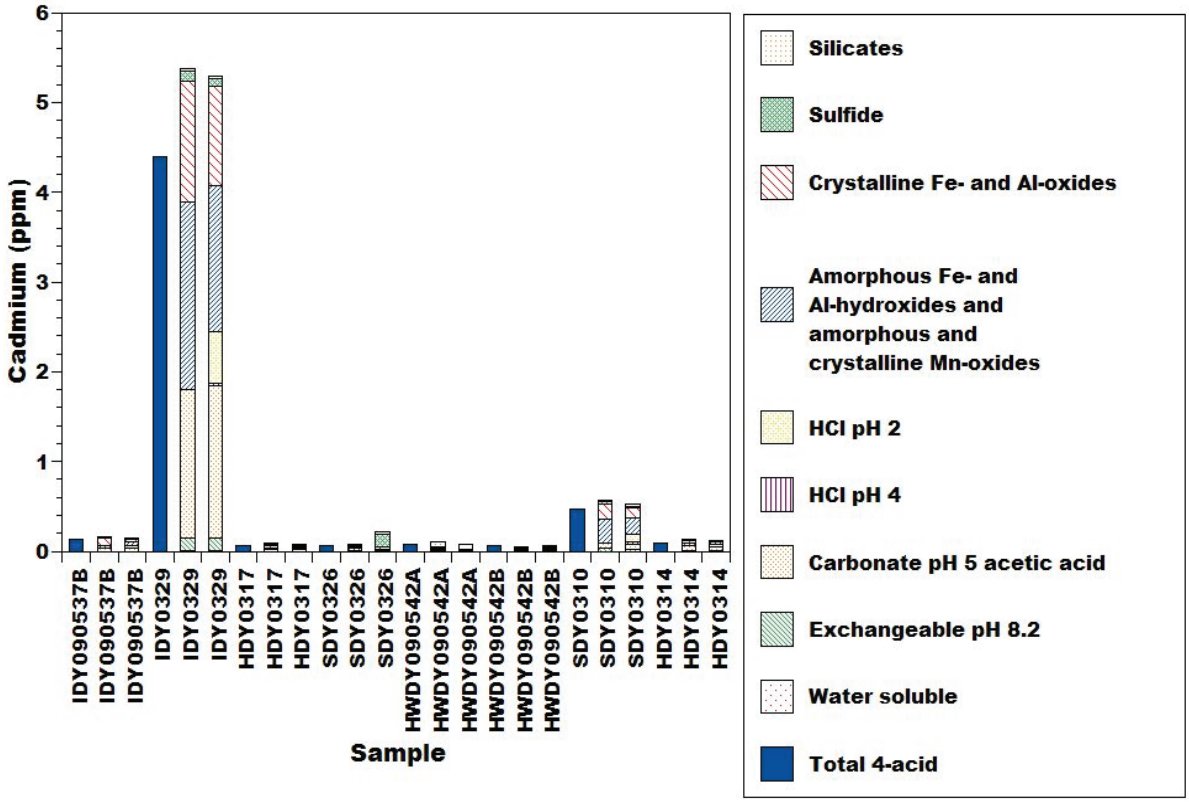

Figure 25. Histogram of whole-rock leachate results for Cd. Total digestion shown by solid blue bar; next histogram bars for each sample are for seven- and nine-step methods respectively.

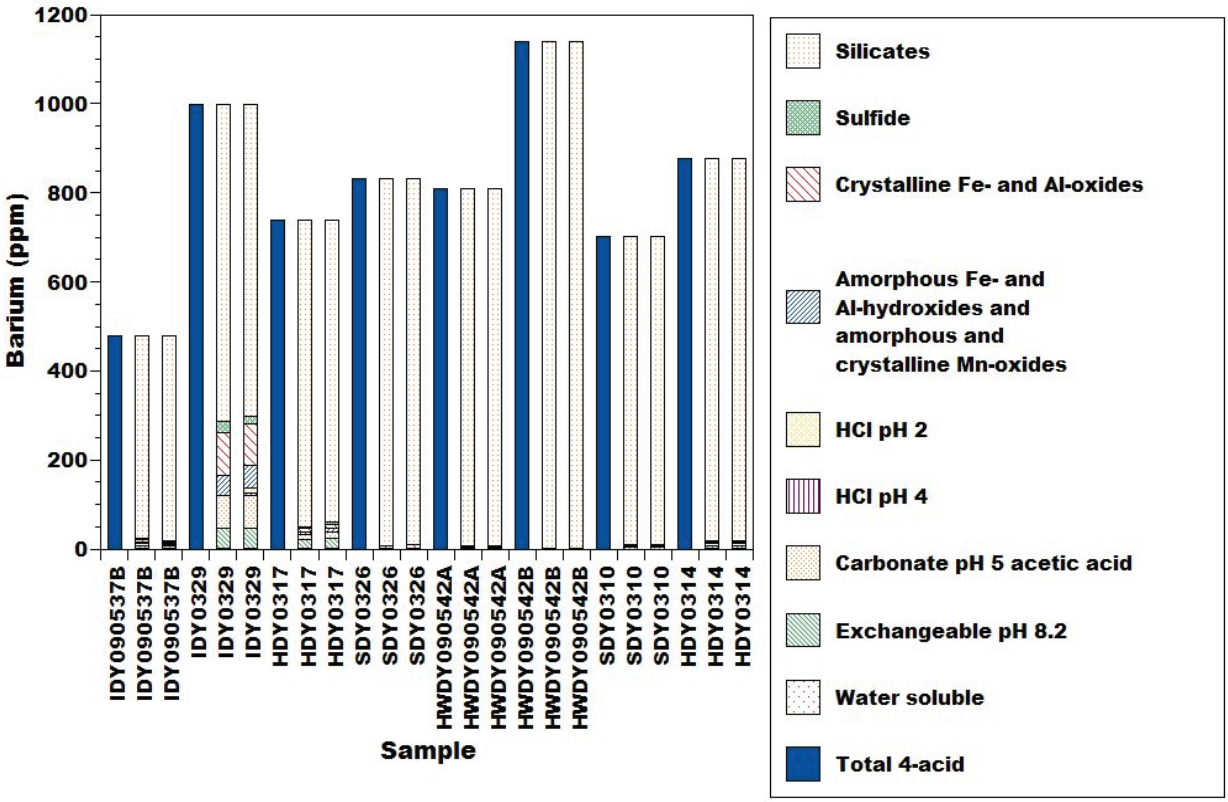

Figure 26. Histogram of whole-rock leachate results for Ba. Total digestion shown by solid blue bar; next histogram bars for each sample are for seven- and nine-step methods respectively.

(K-Al-Si-OH) that is prevalent in quartz-sericite-pyrite alteration in upper Ross basin. Another possible aluminum source is chlorite that is weathering from ANC rocks that are commingled with ore and gangue material. Since the magnesium concentration is depressed in mine waste compared with ANC rocks, the principal source for aluminum is likely illite.

Calcium

Calcium is mainly concentrated in the silicate phase in addition to the crystalline Fe- and Al-oxide phase (fig. 28; appendix D). Calcium abundances are four times lower in mine-waste material compared to the ANC mineral deposit host rocks. As with magnesium, this is a result of acid leaching of primary silicate minerals and dilution by calcium-poor gangue and ore.

Titanium

Titanium is almost exclusively concentrated in the silicate phase (fig. 28; appendix E) and is nearly seven times lower in abundance in mine-waste material compared with ANC rocks. The lower titanium abundance is a result of the titanium host (intergrown magnetite-ilmenite) being destroyed along the quartz-sericite-pyrite veins during hydrothermal alteration.

Iron

Iron displays more heterogeneity compared with other major elements and is concentrated primarily in the silicate, sulfide, crystalline Fe- and Al-oxide, and amorphous Fe- and Al-hydroxide and amorphous and crystalline Mn-oxide phase (fig. 29; appendix F). The mine waste has three times the quantity of leachable iron in the amorphous Fe- and crystalline Mn-oxide phase (0.15 weight percent) compared with ANC rocks (about 0.05 weight percent), even though the host ANC rocks have as much as 6 to 7 weight percent total leachable iron. This suggests that the mine waste and derived leachate may be the primary source of iron in iron flocculent.

Manganese

Manganese is concentrated mainly in the silicate and sulfide phases (fig. 28; appendix G). The abundance of manganese in mine waste is mostly lower (0.05 to about 0.1 weight percent) compared with ANC rocks (> 0.05 to nearly 0.35 weight percent) (fig. 18). This suggests that manganese has been diluted by quartz-sericite-pyrite altered rocks that are commingled with ANC rocks in the mine waste.

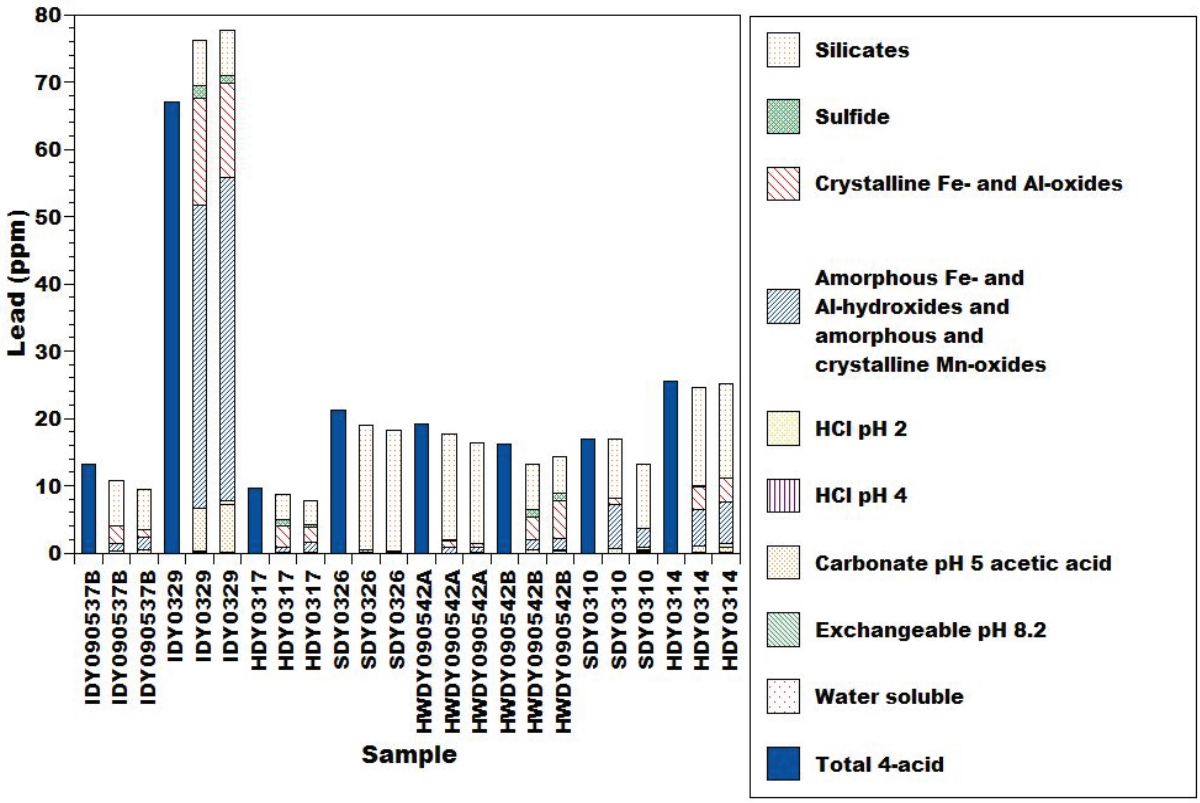

Figure 27. Histogram of whole-rock leachate results for Pb. Total digestion shown by solid blue bar; next histogram bars for each sample are for seven- and nine-step methods respectively.

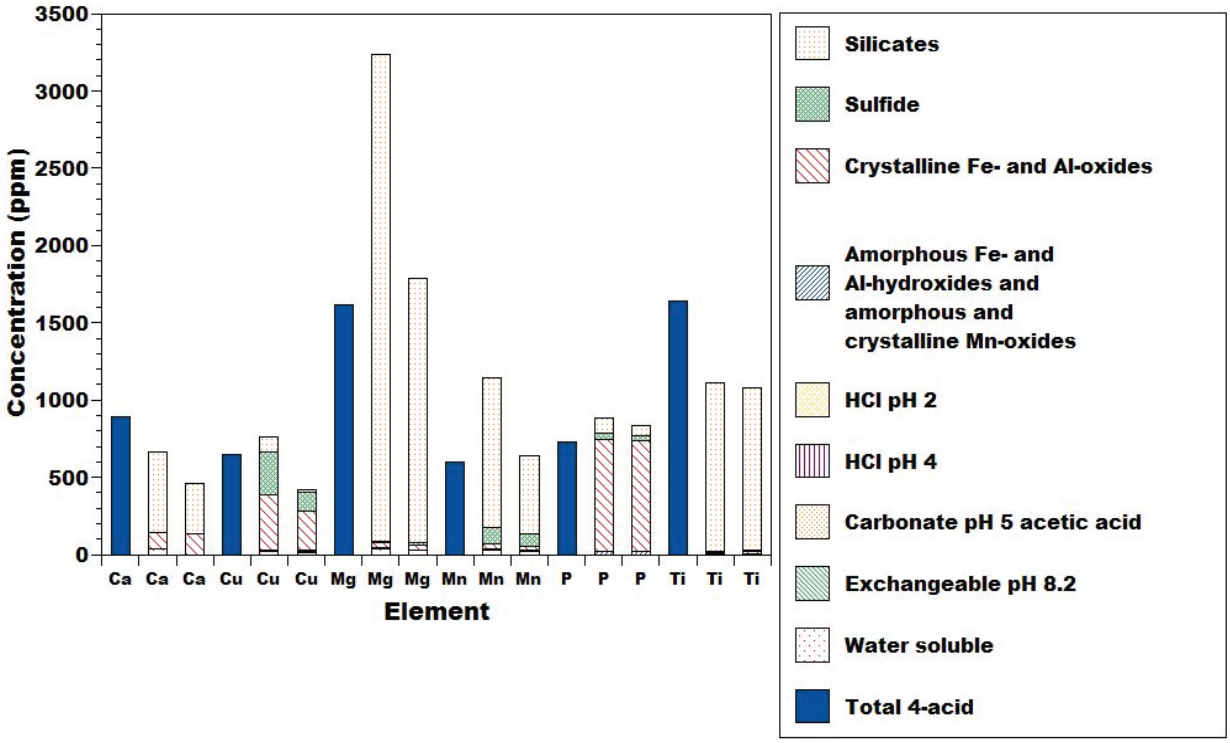

Figure 28. Histogram of Grand Mogul mine waste leachate results for Ca, Cu, Mg, Mn, P, and Ti. Total digestion shown by solid blue bar; next histogram bars for each element are for seven- and nine-step methods respectively.

Nickel

Nickel was not observed in mine-waste leachate indicating this is not a metal of concern from a remediation standpoint at the GM mine-waste pile.

Copper

Leachable copper concentrations are elevated in GM mine waste (0.05 weight percent) compared with ANC rocks (<0.008 to about 0.001 weight percent) (figs. 28 and 20, respectively; appendix I). Most copper is concentrated in the sulfide and crystalline Fe- and Al-oxide phases with small abundances being concentrated in the silicate phase. Chalcopyrite is the likely source of leachable copper in the mine waste.

Zinc

Zinc concentrations are highly elevated in the mine waste (> 1.5 weight percent) (fig. 29; appendix J). Zinc is primarily concentrated in the sulfide phase with the mineral sphalerite (ZnS) being the source of zinc. The other two leachate phases where zinc was concentrated are the silicate and crystalline Fe- and Al-oxide phase.

Arsenic

Arsenic abundances are higher by a factor of 6 to 25 in GM mine waste compared with ANC rocks. Arsenic concentration in mine-waste leachate is about 0.005 weight percent (fig. 30); arsenic leachate abundances in ANC rocks range from about 0.0001 to 0.0008 weight percent (fig. 22; appendix K). The sulfide and crystalline Fe- and Al-oxide phases is host to most of the arsenic. The source mineral for arsenic is not known.

Strontium

Strontium concentrations in the GM mine waste overlap those observed in ANC rock leachate and range from about 0.025 to nearly 0.05 weight percent (fig. 30; appendix L). The distribution of strontium is heterogeneous and is observed in multiple leachate fractions, but is principally concentrated in the crystalline Fe- and Al-oxide phases.

Molybdenum

Molybdenum abundances are higher by a factor of 50 to 100 in GM mine waste compared with ANC rocks. Molybdenum concentration in GM mine waste is about 0.005 weight percent and is primarily concentrated in crystalline Fe- and Al-oxide and sulfide phases (fig. 30; appendix M).

Cadmium

Cadmium is also concentrated by a factor of 10 to 100 times in GM mine waste compared with ANC rocks. Cadmium concentration in GM mine waste is about 0.005 to 0.009 weight percent. The crystalline Fe- and Al-oxide and sulfide phases are host to most of the cadmium (fig. 30; appendix N).

Barium

Similar to strontium, barium abundances overlap those observed in ANC rocks. Barium concentration in GM mine waste is about 0.0250 weight percent and is primarily concentrated in silicate and crystalline Fe- and Al-oxide phases (fig. 30; appendix O).

Lead

Lead is concentrated by a factor of 100 to 1,000 in GM mine waste compared to ANC rocks. Lead attains a concentration of 1 weight percent in GM mine waste and is concentrated primarily in the crystalline Fe- and Al-oxide and sulfide phases; although a significant proportion is also observed in the hydroxides and amorphous and crystalline Mn-oxide phase (fig. 29; appendix P).

Rock Physical Properties (Magnetic Susceptibility)

A box plot of volume susceptibility is shown in figure 31. The highest median value was observed in unit Tpa; the lowest median value was identified in unit Tb. Units Tsj and Tse have similar susceptibility values that are relatively low compared to the other units. Unit Tig has a moderate magnetic susceptibility. Unit Tsemb also has a relatively moderate susceptibility; however, only two samples are represented.

Summary

ANC and NAP

Burns Member (Unit Tb) and Picayune Megabreccia Member (Unit Tsemb)

In this study, two units (Tb and Tsemb) were identified as having moderate to high ANC and no NAP. One Tb sample (HWDY090541B) has the highest ANC of any sample studied. Unit Tb in the previous study (Yager and others, 2005) did not have a high ANC (notably sample SDY0310, with some exceptions), and most of those unit Tb samples were collected within the core of the Silverton caldera.

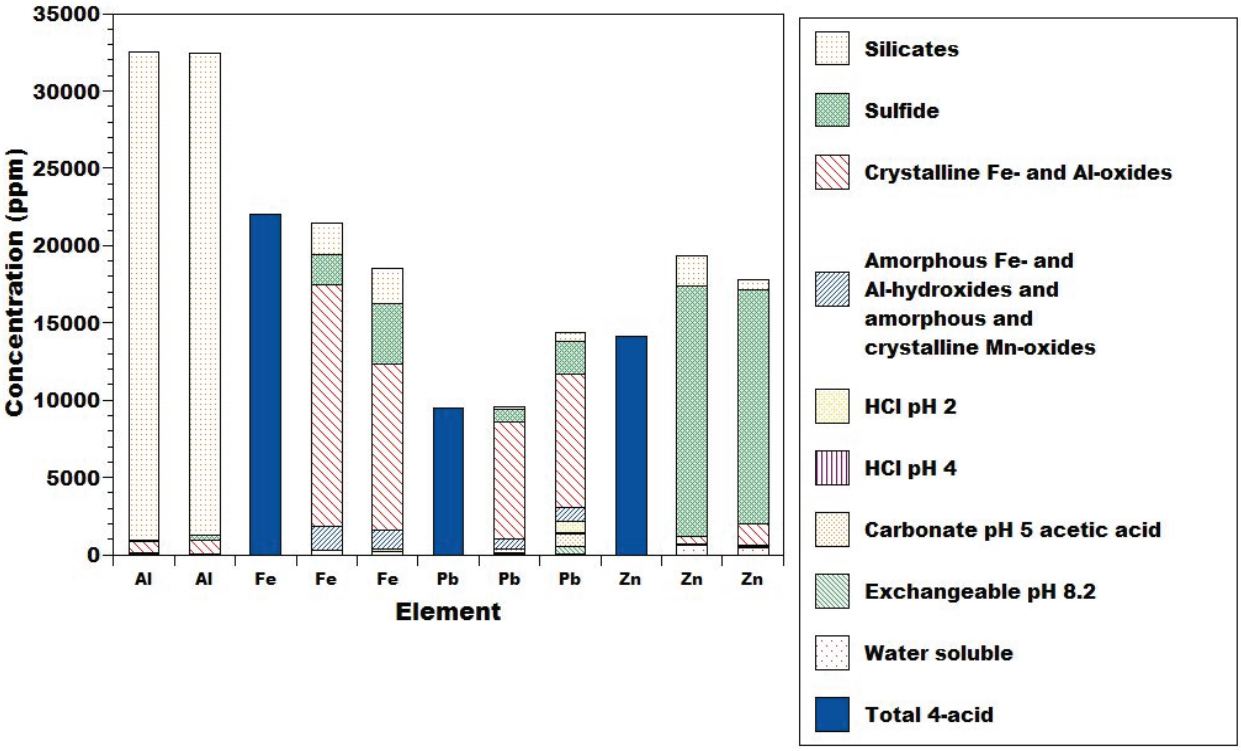

Figure 29. Histogram of Grand Mogul mine waste leachate results for Al, Fe, Pb, and Zn. Total digestion shown by solid blue bar; next histogram bars for each element are for seven- and nine-step methods respectively.

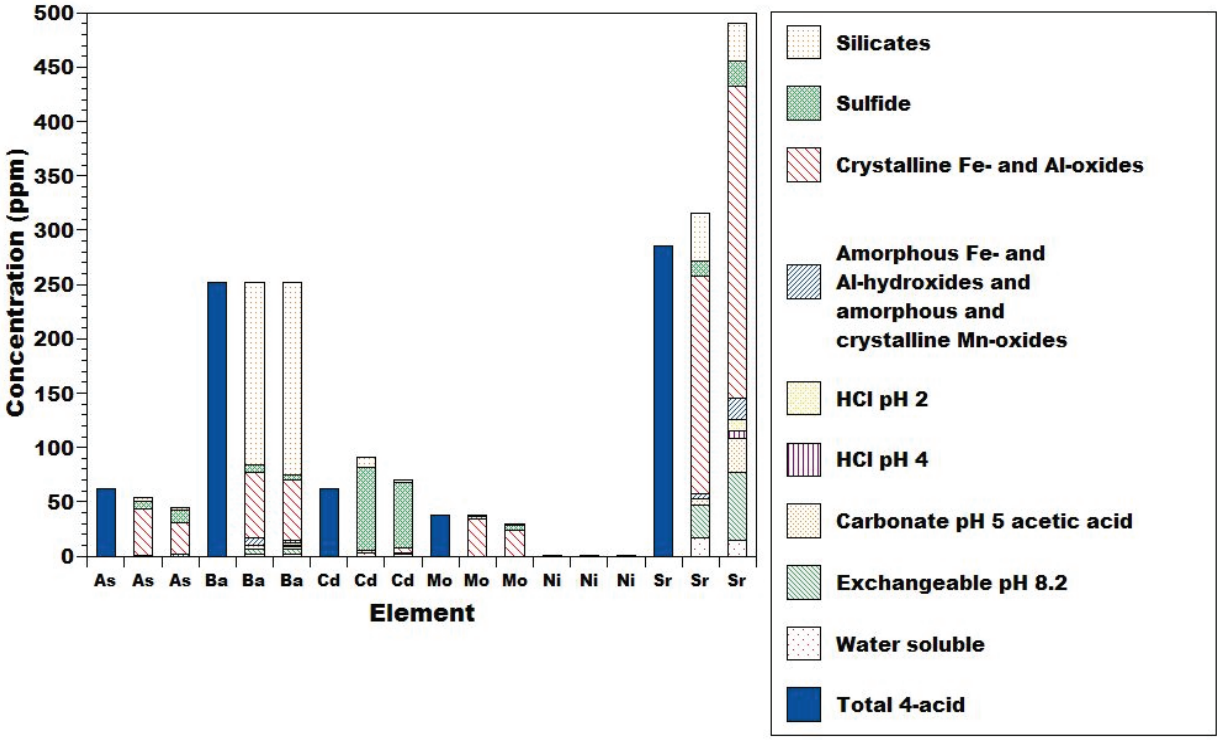

Figure 30. Histogram of Grand Mogul mine waste leachate results for As, Ba, Cd, Mo, Ni, and Sr. Total digestion shown by solid blue bar; next histogram bars for each element are for seven- and nine-step methods respectively.

San Juan Formation (Unit Tsj)

Unit Tsj lavas and volcaniclastic sedimentary rocks were thought to have a potentially high ANC based on sparse samples collected during the Yager and others (2005) study. The median ANC for 11 unit Tsj samples studied is relatively high (29 kg/t calcium carbonate equivalent); however, the median NAP for this sample suite is also high (30 kg/t calcium carbonate equivalent).

Sultan Mountain Stock (Unit Tig)

Unit Tig was found to have minimal ANC and moderate NAP. Sparse fir trees, grasses, and other vegetation are observed on the North Star mine waste pile west of Silverton, which is composed of Tig clasts. This is an indication that the minimal ANC that unit Tig does supply at the North Star mine waste, could be neutralizing some acidity and aiding vegetation growth at the North Star Mmine site.

Sequential Leachate Studies (Whole Rocks)

Major Elements

Major-element constituents produced during four-acid total digestion and from the silicate and crystalline Fe- and Al-oxide sequential phases are consistent with the original whole-rock compositions. Mafic rocks such as basalt sample IDY090537B and andesite sample SDY0310 produced high Mg, Fe, and Ca. More silicic samples, for example HDY0314, had lower ferromagnesian and higher potassium concentrations.

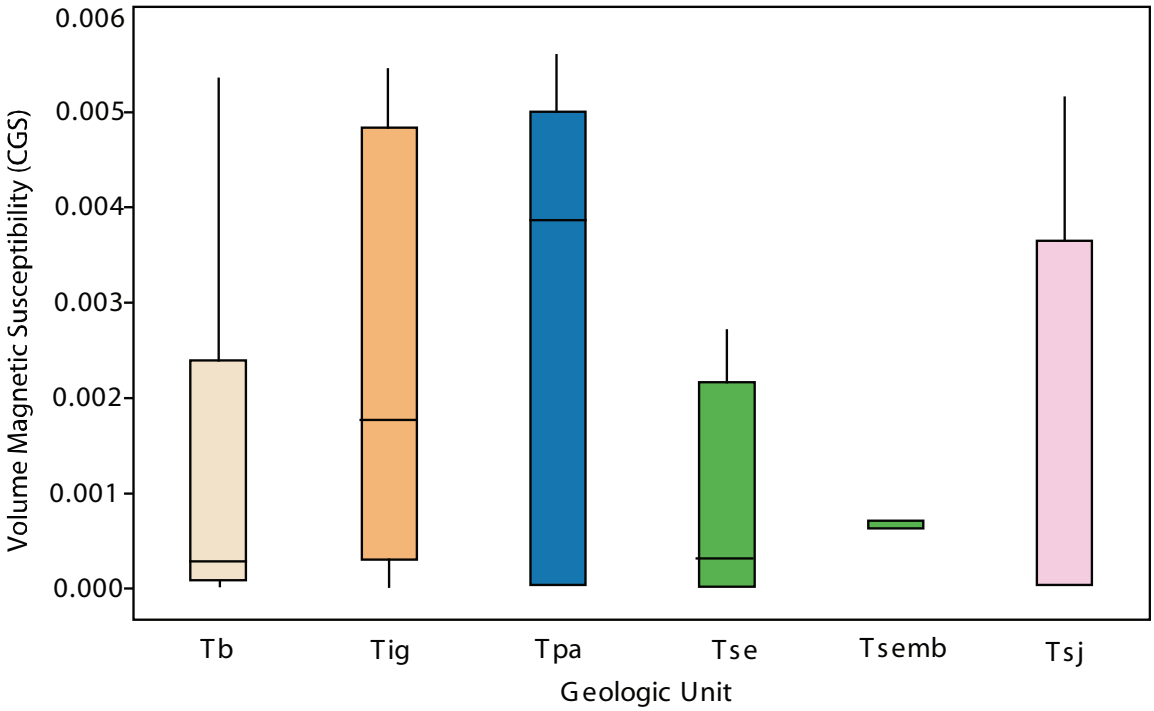

Figure 31. Boxplots of volume magnetic susceptibility for units Tb, n = 15; Tig, n = 8; Tpa, n = 7; Tse, n = 4; Tsemb, n = 2; Tsj, n = 11. Median value is represented by horizontal line in each box.

Mineralogic Control on Leachate Compositions

Silicate mineralogy strongly controls leachate compositions for some elements. For example, strontium commonly substitutes for calcium in plagioclase due to similar ionic radius and charge. The mafic to intermediate composition samples IDY090537B and SDY0326 have high plagioclase abundances and high calcium and strontium abundances. Chlorite (clinochlore) abundances also influence the total magnesium abundance. Unit Tb lavas (samples SDY0310 and HWDY090542A and B) have several weight-percent chlorite and correspondingly high total magnesium leachate concentrations. Titanium leachate abundance appears to be influenced by magnetite concentration. High magnetite and titanium abundances in samples IDY090537B, HWDY090542A and B, and HDY0317 are possibly due to dissolution of intergrown ilmenite in the magnetite crystal lattice (Yager and others, 2005, figure 20).

Trace-Element Leachate Abundances

San Juan Formation (Unit Tsj)

Whole rocks with the highest whole-rock trace-element abundances, for example unit Tsj sample IDY0329, have high total sequential leachate abundances for the elements Zn, Cd, Pb, and Mn. While pyrite is the only sulfide detected thus far in sample IDY0329 (3 weight percent pyrite, from XRD) other sulfides could be present in trace quantities that are responsible for the relatively high trace-element concentrations.

Burns Member (Unit Tb)

Unit Tb sample SDY0310 also has high Mn, Ni, Cu, Zn, and Cd abundances. This sample has trace quantities of both pyrite and chalcopyrite (Yager and others, 2005). Unit Tb samples HWDY090542A and B have moderately elevated leachate concentrations of Cu and Ni, and low to moderate Mo.

Pyroxene Andesite Member (Unit Tpa)

One sample (SDY0326) of unit Tpa has relatively high As and Mo. More work is needed to determine the source of As in this sample.

Mine-Waste-Leachate Compositions

The Grand Mogul mine waste was subjected to the four-acid total-digestion and the seven- and nine-step sequential-leaching methods for comparison with whole-rock sequential-leachate data. Several trace elements are elevated in mine waste compared to the volcanic rocks: Cu (1 order of magnitude), Zn (1 order of magnitude), As (1 order of magnitude), Mo (1.5 to 2 orders of magnitude), Cd (1 to 2 orders of magnitude), Pb (2 to 3 orders of magnitude). Iron is also elevated in the mine-waste amorphous Fe- and crystalline Mn-oxide phase compared to volcanic rocks. Elevated iron in the amorphous-leachate phase may shed light on the primary source of iron flocculent when water, mine waste, and ANC rocks interact. These data suggest that mine waste may be the principal source of amorphous iron floc; however more data is needed to answer this question.

Magnetic Susceptibility and Corresponding ANC, NAP, and Leachate Rock Properties

Pyroxene Andesite Member (Unit Tpa)

New magnetic susceptibility measurements made during this study indicate that unit Tpa has the highest median magnetic susceptibility of all igneous units. Unit Tpa also has corresponding high ANC and low to no NAP. In addition, whole-rock-leachate analyses for unit Tpa sample HDY0317 have the lowest trace contaminant abundances.

Burns Member (Unit Tb)

Unit Tb (talus) has a high magnetic susceptibility compared to Tb samples studied previously (Yager and others, 2005) and low NAP. Talus of unit Tb also has relatively high Cu, Mo, and Ni leachate abundances and a relatively low median magnetic susceptibility.

Eureka Member (Unit Tse)

Sample HDY0314 of unit Tse has moderate magnetic susceptibility, high ANC, and low NAP, and has corresponding low trace-contaminant abundances, with the possible exception of As (3 ppm), in sequential leachate studies.

Sultan Mountain Stock (Unit Tig)

Unit Tig has a relatively moderate magnetic susceptibility, low ANC, and high NAP. Field observations of mine-waste piles where unit Tig clasts compose a significant part of the pile indicate that fir trees, willows, grasses, and other plants can be established, and thus, the NAP properties of this unit are not too adverse to prevent some acid tolerant plant growth. The total organic carbon content (0.7 weight percent) of mine waste with high proportions of unit Tig clasts is an indicator that this unit can weather to provide at least some chemical properties beneficial for soil development and plant growth. This is in contrast to unreclaimed, high NAP mine waste (for example, Grand Mogul mine) that has nearly 0 weight percent total organic carbon and no established vegetation (Yager and others, 2007).

San Juan Formation (Unit Tsj)

One unit Tsj sample (IDY090537B) has high ANC, no NAP, and moderate magnetic susceptibility. Sample IDY090537B also has low trace contaminants in leachate analyses. Other unit Tsj samples studied for ANC and NAP in this and previous studies suggest that in some places this unit has properties that may be favorable for remediation projects.

Conclusions

We have augmented sampling of units that were sparsely sampled in our previous study (Yager and others, 2005). Units Tsj, Tig, Tse, and Tsemb were targeted for additional sampling because one or more samples in the previous study had high ANC. In addition, talus from unit Tb was sampled in the present study.

Results of this study suggest that unit Tsj can in some places provide high ANC, low NAP, and low leachable trace contaminants. Due to the variable magnetic susceptibility and ANC of unit Tsj, each outcrop targeted for potential use in remediation would need to be studied for environmental rock properties ANC and NAP.

Unit Tig was found to have low ANC and moderate NAP. No sequential leachate analyses were done on this unit. Fir trees, willows, shrubs, grasses, and other plants were observed growing on mine waste composed largely of unit Tig clasts. This is an indicator that the NAP properties of this unit are not too adverse to prevent some acid-tolerant plant growth.

Unit Tse has a low ANC and low to moderate NAP in several places. Unit Tsemb and unit Tse near the San Juan caldera margin appear to have higher ANC, low NAP, and low leachable trace contaminants (one sample).

Unit Tb talus in Minnie Gulch, also near the Silverton caldera margin, was found to have the highest ANC of any sample studied. The talus also has low to moderate sequential leachate abundances for trace contaminants Cu, Ni, As, and Mo suggesting this material could be favorable for use in mine-waste remediation projects.

This study suggests that proximity to caldera margins may control the high ANC of some units (Tsj, Tse, and Tsemb). Caldera structural margins could have functioned as permeable conduits during propylitic alteration that focused fluids that enhanced formation of high ANC rocks in some areas.

Acknowledgments

Joe Rosenbaum's expertise and guidance in updating the magnetic susceptibility data is greatly appreciated. Reviews by Sharon Diehl and Philip Hageman improved this report. Ank Webbers provided technical support. Thanks to Alison Burchell for scientific discussions. Discussions with William Simon (Animas River Stakeholders Group) are appreciated. Stephanie Odell, San Juan Forest Abandoned Mine Lands Coordinator; Rob Robinson, BLM, Lakewood, Colo., under U.S. Bureau of Land Management interagency agreement number 1422CAI060047; and the U.S. Geological Survey Mineral Resources Program supported our research.

References Cited

Barker, Fred, 1969, Precambrian geology of the Needle Mountains, southwestern Colorado: U.S. Geological Survey Professional Paper 644-A, p. A1–A35.

Bejnar, Waldemere, 1957, Lithologic control of ore deposits in the southwestern San Juan Mountains, *in* Kottlowski, F.E., and Baldwin, Brewster, eds., Guidebook of southwestern San Juan Mountains, Colorado: New Mexico Geological Society 8th Annual Field Conference Guidebook, p. 162–173.

Blair, R.W., Jr., Yager, D.B., and Church, S.E., 2002, Surficial geologic maps along the riparian zone of the Animas River and its headwater tributaries, Silverton to Durango, Colorado, with upper Animas River watershed gradient profiles: U.S. Geological Survey Digital Data Series 071, 1 CD-ROM.

Blowes, D.W., Ptacek, C.J., and Jurjovic, Jasna, 2003, Mill tailings: hydrogeology and geochemistry: Mineralogical Association of Canada Short Course Series, v. 31, p. 95–116.

Bove, D.J., Hon, Ken, Budding, K.E., Slack, J.F., Snee, L.W., and Yeoman, R.A., 2001, Geochronology and geology of late Oligocene through Miocene volcanism and mineralization in the western San Juan Mountains, Colorado: U.S. Geological Survey Professional Paper 1642, 30 p.

Bove, D.J., Mast, M.A., Dalton, J.B., Wright, W.G., and Yager, D.B., 2007, Major styles of mineralization and hydrothermal alteration and related solid- and aqueous-phase geochemical signatures, chap. E3 *of* Church, S.E., von Guerard, Paul, and Finger, S.E., eds., Integrated investigations of environmental effects of historical mining in the Animas River watershed, San Juan County, Colorado: U.S. Geological Survey Professional Paper 1651, p. 161–230.

Bove, D.J., Yager, D.B., Mast, M.A., and Dalton, J.B., 2007, Alteration map showing major faults and veins and associated water-quality signatures of the Animas River watershed headwaters near Silverton, Colorado: U.S. Geological Survey Scientific Investigations Map 2976, 18-p. pamphlet, 1 pl., scale 1:24,000.

Briggs, P.H., 2001, The determination of forty elements in geological and botanical samples by inductively coupled plasma–atomic emission spectrometry, *in* Taggart, J., ed., Analytical methods for chemical analysis of geologic and other materials: U.S. Geological Survey Open-File Report 02-223, p. G-3.

Burbank, W.S., 1960, Pre-ore propylitization, Silverton caldera, Colorado, *in* Geological Survey Research 1960: U.S. Geological Survey Professional Paper 400-B, p. B12–B13.

Casadevall, Thomas, and Ohmoto, H., 1977, Sunnyside mine, Eureka mining district, San Juan County, Colorado—Geochemistry of gold and base metal ore deposition in a volcanic environment: Economic Geology, v. 92, p. 1,285–1,320.

Chapin, C.E., and Cather, S.M., 1994, Tectonic setting of the axial basins of the northern and central Rio Grande rift: Geological Society of America Special Paper 291, p. 5–25.

Chao, T.T., and Sanzolone, R.F., 1977, Chemical dissolution of sulfide minerals: U.S. Geological Survey Journal of Research, v. 5, no. 4, p. 409–412.

Chao, T.T., and Sanzolone, R.F., 1998, Fractionation of soil selenium by partial dissolution: Soil Science Society of America Journal, v. 53, no. 2, p. 385–392.

Davis, J.A., and Kent, D.B., 1990, Surface complexation modeling in aqueous geochemistry, *in* Hochella, M.F., Jr., and White, A.F., eds., Mineral-water interface geochemistry: Mineralogical Society of America Reviews in Mineralogy, v. 23, p.177–260.

Desborough, G.A., and Driscoll, R.L., 1998, Mineralogical characteristics and acid-neutralizing potential of drill core samples from eight sites considered from metal-mine related waste repositories in northern Jefferson, Powell, and Lewis and Clark Counties, Montana: U.S. Geological Survey Open-File Report 98-0790, 6 p.

Desborough, G.A., and Yager, D.B., 2000, Acid-neutralizing potential of igneous bedrocks in the Animas River headwaters, San Juan County, Colorado: U.S. Geological Survey Open-File Report 00-0165, 14 p.

Halferdahl, L.B., 1961, Chloritoid: Its composition, X-ray and optical properties, stability and occurrence: Journal of Petrology, no. 2 , p. 49–135.

Hutchison, I.P.G., and Ellison, R.D., eds., 1992, Mine waste management: a resource for mining industry professionals, regulators and consulting engineers: Boca Raton:, Florida, Lewis Publishers, Inc., 672 p.

Jambor, J.L., 2003, Mine-waste mineralogy and mineralogical perspectives of acid-base accounting, *in* Jambor, J.L., Blowes, D.W., and Ritchie, A.I.M., eds., Environmental aspects of mine wastes: Mineralogical Association of Canada Short Course Series, v. 31, p. 117–145.

Jambor, J.L., Dutrizac, J.E., Groat, L.A., and Raudsepp, Mati, 2002, Static tests of neutralization potentials of silicate and aluminosilicate minerals: Environmental Geology, v. 43, p. 1–17.

Lanphere, M.A., 1988, High resolution $^{40}Ar/^{39}Ar$ chronology of Oligocene volcanic rocks, San Juan Mountains, Colorado: Geochimica et Cosmochimica Acta, v. 52, p. 1,425–1,434.

Lapakko, Kim, and Lawrence, R.W., 1993, Modification of the net acid production (NAP) test: Proceedings of the Seventeenth Annual British Columbia Mine Reclamation Symposium, Port Hardy, British Columbia, 1993, p. 145–159.

Lipman, P.W., 1976, Geologic map of the Lake City caldera area, western San Juan Mountains, southwestern Colorado: U.S. Geological Survey Miscellaneous Investigation Series Map I-962, scale 1:48,000.

Lipman, P.W., Dungan, Michael, Bachmann, Olivier, 1997, Comagmatic granophyric granite in the Fish Canyon Tuff, Colorado—Implications for magma-chamber processes during a large ash-flow eruption: Geology, v. 25, p. 915–918.

Lipman, P.W., Steven, T.A., Luedke, R.G., and Burbank, W.S., 1973, Revised volcanic history of the San Juan, Uncompahgre, Silverton, and Lake City calderas in the western San Juan Mountains, Colorado: U.S. Geological Survey Journal of Research, v. 1, p. 627–642.

Luedke, R.G., and Burbank, W.S., 2000, Geologic map of the Silverton and Howardsville quadrangles, southwestern Colorado: U.S. Geological Survey Geologic Investigation Series Map I-2681, scale 1:24,000.

McCafferty, A.E., Yager, D.B., Horton, R.J., and Diehl, S.F., 2006, Magnetic properties, acid neutralization capacity, and net acid production of rocks in the Animas River watershed, Silverton, Colorado: Environmental and Engineering Geophysical Society, 2006 Symposium on the Application of Geophysics to Engineering and Environmental Problems, 10 p.

Piatak, N.M., Seal, R.R., II, Sanzolone, R.F., Lamothe, P.J., Brown, Z.A., and Adams, M., 2007, Sequential extraction results and mineralogy of mine waste and stream sediments associated with metal mines in Vermont, Maine, and New Zealand: U.S. Geological Survey Open-File Report 2007-1063, 34 p.

Raudsepp, Mati, and Pani, Elisabetta, 2003, Application of Rietveld analysis to environmental mineralogy: Mineralogical Association of Canada Short Course Series, v. 31, p. 165–180.

Raudsepp, Mati, Pani, Elisabetta, and Dipple, G.M., 1999, Measuring mineral abundance in skarn I: the Rietveld method using X-ray powder diffraction data: Canadian Mineralogist, v. 37, p. 1–15.

Ringrose, C.R., 1982, Geology, geochemistry, and stable isotope studies of a porphyry-style hydrothermal system, west Silverton district, San Juan Mountains, Colorado: Aberdeen, Scotland, University of Aberdeen, Ph. D. dissertation, 257 p., 19 pls.

Salmon, U.S., and Malmström, M.E., 2004, Geochemical processes in mill tailings deposits: modeling of groundwater composition: Applied Geochemistry, v. 19, p. 1–17.

Shaw, Shannon, Wels, Christoph, Robertson, Andy, and Lorinczi, Geyza, 2002, Physical and geochemical characterization of mine rock piles at the Questa mine, New Mexico, *in* Tailings and mine waste 2002: Proceedings of the Ninth International Conference on Tailings and Mine Waste, Fort Collins, Colo., USA, 27–30 January 2002, p. 447–458.

Steven, T.A., Hon, Ken, and Lanphere, M.A., 1995, Neogene geomorphic evolution of central San Juan Mountains near Creede, Colorado: Miscellaneous Investigation Series Map I-2504, scale 1:100,000.

Steven, T.A., and Lipman, P.W., 1976, Calderas of the San Juan volcanic field, southwestern Colorado: U.S. Geological Survey Professional Paper 958, 35 p.

Steven, T.A., Schmitt, L.J., Jr., Sheridan, M.J., Williams, F.E., Gair, J.E., and Klemic, H., 1969, Mineral resources of the San Juan primitive area, Colorado: U.S. Geological Survey Bulletin 1261-F, 187 p.

Tessier, A., Campbell, P.G.C., and Bisson, M., 1979, Sequential extraction procedure for the speciation of particulate trace metals: Analytical Chemistry, v. 51, no. 7, p. 844–851.

Yager D.B., and Bove, D.J., 2002, Generalized geologic map of part of the upper Animas River watershed and vicinity, Silverton, Colorado: U.S. Geological Survey Miscellaneous Field Studies Map MF-2377, scale 1:48,000.

Yager, D.B., and Bove, D.J., 2007, Geologic framework, chap. E1 *of* Church, S.E., von Guerard, Paul, and Finger, S.E., eds., Integrated investigations of environmental effects of historical mining in the Animas River watershed, San Juan County, Colorado: U.S. Geological Survey Professional Paper 1651, p. 107–140.

Yager, D.B., Burchell, Alison, Robinson, Rob, Odell, Stephanie, Dick, R.P., Johnson, C.A., Hidinger, Jack, and Rathke, David, 2007, Natural terrestrial sequestration potential of high plains prairie to subalpine forest and mined-lands soils derived from weathering of Tertiary volcanics: Eos, Transactions of the American Geophysical Union, Fall Meeting, Suppl., Abstract, B23D-1,588.

Yager, D.B., McCafferty, A.E., Stanton, M.R., Diehl, S.F., Driscoll, R.L., Fey, D.L., and Sutley, S.J., 2005, Net acid production, acid neutralizing capacity, and associated geophysical, mineralogical, and geochemical characteristics of Animas River watershed rocks near Silverton, Colorado: U.S. Geological Survey Open-File Report 2005-1433, 75 p.

Young, R.A., 1993, The Rietveld method: New York, Oxford University Press, International Union Crystallography, 298 p.

Appendix A. Sequential leachate results for magnesium.

[Magnesium (ppm); BDL, below detection limit (<2 ppm); total, seven-step, and nine-step leachate reported for each sample]

Sample	Total four-acid	Water soluble	Exchangeable pH 8.2	Carbonate pH 5 acetic acid	HCl pH 4	HCl pH 2	Amorphous Fe- and Al-hydroxides and amorphous and crystalline Mn-oxides	Crystalline Fe- and Al-oxides	Sulfide	Silicates
IDY090537B	25,100									
IDY090537B		13	16	41			203	9,460	5,120	7,830
IDY090537B		18	20	56	25	79	294	14,200	4,550	15,200
IDY0329	4,590									
IDY0329		4	6	13			39	2,675	526	3,175
IDY0329		4	6	13	4	12	54	2,815	418	3,465
HDY0317	5,580									
HDY0317		5	15	20			67	2,920	645	3,390
HDY0317		5	15	22	6	25	75	2,970	667	6,180
SDY0326	14,100									
SDY0326		7	10	45			248	8,040	2,280	5,580
SDY0326		7	9	47	24	123	213	9,040	1,720	5,150
HWDY090542A	13,700									
HWDY090542A		14	14	18			148	10,750	2,340	2,720
HWDY090542A		10	11	20	15	56	170	10,500	1,920	1,895
HWDY090542B	11,900									
HWDY090542B		3	5	9			32	6,610	2,130	8,880
HWDY090542B		3	5	9	6	11	36	6,980	2,190	7,150
SDY0310	17,000									
SDY0310		7	26	8			137	12,800	2,670	5,590
SDY0310		8	24	11	6	38	143	12,600	3,060	3,770
HDY0314	4,850									
HDY0314		9	8	13			41	2,085	665	5,690
HDY0314		5	8	12	4	18	40	2,560	569	3,465
Grand Mogul	1,620									
Grand Mogul		38	5	BDL			BDL	33	9	3,150
Grand Mogul		27	5	BDL	BDL	BDL	BDL	30	18	1,710

Appendix B. Sequential leachate results for aluminum.

[Aluminum (ppm); detection limit (<0.4 ppm); total, seven-step, and nine-step leachate reported for each sample]

Sample	Total four-acid	Water soluble	Exchangeable pH 8.2	Carbonate pH 5 acetic acid	HCl pH 4	HCl pH 2	Amorphous Fe- and Al-hydroxides and amorphous and crystalline Mn-oxides	Crystalline Fe- and Al-oxides	Sulfide	Silicates (calculated)
IDY090537B	78,600									
IDY090537B		21.9	6.9	3.9			250	10,200.0	4,840	63,277
IDY090537B		38.1	12.8	17.0	40.8	59.4	455	14,800.0	4,490	58,686
IDY0329	60,000									
IDY0329		22.2	12.1	7.3			214	5,900.0	968	52,875
IDY0329		26.1	7.9	11.9	13.4	22.0	376	6,015.0	817	52,709
HDY0317	65,400									
HDY0317		24.4	6.4	3.2			206	5,910.0	1,260	57,990
HDY0317		32.0	10.7	12.6	18.0	52.6	272	6,030.0	1,440	57,532
SDY0326	64,600									
SDY0326		6.7	1.9	0.6			157	5,400.0	1,700	57,333
SDY0326		6.8	1.8	1.6	1.9	90.8	162	6,160.0	1,340	56,835
HWDY090542A	66,200									
HWDY090542A		20.0	6.7	4.5			337	11,300.0	3,020	51,511
HWDY090542A		14.9	4.3	5.0	15.1	134.0	351	11,200.0	2,600	51,875
HWDY090542B	61,900									
HWDY090542B		5.9	0.9	2.6			74	7,350.0	2,390	52,076
HWDY090542B		4.6	1.2	2.0	4.3	29.1	74	7,810.0	2,420	51,554
SDY0310	63,600									
SDY0310		14.0	3.7	2.4			336	15,800.0	3,290	44,153
SDY0310		16.2	2.0	6.6	2.8	96.9	319	15,700.0	3,790	43,666
HDY0314	56,450									
HDY0314		35.3	4.9	4.9			198	2,415.0	680	53,111
HDY0314		13.5	3.4	4.6	7.2	77.8	185	2,815.0	616	52,727
Grand Mogul	32,500									
Grand Mogul		67.0	11.7	8.2			51	710.0	116	31,536
Grand Mogul		50.4	2.0	3.2	4.6	23.7	46	845.0	302	31,222

Appendix C. Sequential leachate results for potassium.

[Potassium (ppm); BDL, below detection limit (<6 ppm); total, seven-step, and nine-step leachate reported for each sample]

Sample	Total four-acid	Water soluble	Exchangeable pH 8.2	Carbonate pH 5 acetic acid	HCl pH 4	HCl pH 2	Amorphous Fe- and Al-hydroxides and amorphous and crystalline Mn-oxides	Crystalline Fe- and Al-oxides	Sulfide and silicate (calculated)
IDY090537B	8,880								
IDY090537B		31	57	30			30	85	8,648
IDY090537B		40	49	33	9	18	30	99	8,604
IDY0329	26,950								
IDY0329		77	107	71			68	322	26,305
IDY0329		78	104	80	15	39	90	339	26,205
HDY0317	28,700								
HDY0317		49	141	70			72	234	28,134
HDY0317		53	112	69	17	32	66	290	28,061
SDY0326	20,200								
SDY0326		9	17	14			26	152	19,982
SDY0326		9	10	22	6	16	13	215	19,909
HWDY090542A	25,400								
HWDY090542A		18	19	10			25	39	25,289
HWDY090542A		17	11	13	5	14	17	42	25,281
HWDY090542B	31,800								
HWDY090542B		20	27	27			26	59	31,640
HWDY090542B		21	18	23	10	8	13	84	31,624
SDY0310	23,700								
SDY0310		27	48	25			27	86	23,487
SDY0310		25	31	36	14	18	16	83	23,477
HDY0314	33,350								
HDY0314		51	70	41			66	210	32,913
HDY0314		35	58	43	12	32	48	234	32,888
Grand Mogul	17,600								
Grand Mogul		BDL	17	38			46	897	16,602
Grand Mogul		BDL	BDL	31	6	14	40	746	16,763

Appendix D. Sequential leachate results for calcium.

[Calcium (ppm); BDL, below detection limit (<40 ppm); total, seven-step, and nine-step leachate reported for each sample]

Sample	Total four-acid	Water soluble	Exchangeable pH 8.2	Carbonate pH 5 acetic acid	HCl pH 4	HCl pH 2	Amorphous Fe- and Al-hydroxides and amorphous and crystalline Mn-oxides	Crystalline Fe- and Al-oxides	Sulfide	Silicates
IDY090537B	43,400									
IDY090537B		149	516	5,560			9,120	16,400	1,340	3,330
IDY090537B		205	692	7,440	449	4,250	7,640	6,950	817	5,730
IDY0329	23,900									
IDY0329		137	403	3,945			6,005	7,765	690	1,830
IDY0329		122	413	4,035	331	2,385	5,370	6,005	633	1,890
HDY0317	29,400									
HDY0317		139	729	4,880			6,760	9,820	1,780	1,720
HDY0317		147	773	5,500	235	2,770	6,200	7,000	1,880	2,040
SDY0326	35,800									
SDY0326		108	283	2,630			3,090	4,320	1,090	23,300
SDY0326		99	273	2,900	252	1,480	2,520	3,810	923	22,200
HWDY090542A	33,550									
HWDY090542A		119	394	3,095			2,670	4,210	1,240	24,650
HWDY090542A		111	404	2,890	238	1,250	1,650	2,960	1,220	21,000
HWDY090542B	21,300									
HWDY090542B		93	263	2,140			2,950	5,000	2,300	6,480
HWDY090542B		69	281	2,030	196	1,220	2,860	4,710	2,220	5,560
SDY0310	32,000									
SDY0310		BDL	232	151			1,130	1,610	344	36,900
SDY0310		BDL	226	188	45	554	1,020	1,190	427	34,600
HDY0314	16,100									
HDY0314		126	414	3,645			3,295	2,515	284	2,405
HDY0314		104	418	3,535	269	1,510	2,520	1,615	234	1,900
Grand Mogul	891									
Grand Mogul		38	BDL	BDL			BDL	101	BDL	525
Grand Mogul		BDL	BDL	BDL	BDL	BDL	BDL	135	BDL	323

Appendix E. Sequential leachate results for titanium.

[Titanium (ppm); BDL, below detection limit (<0.1 ppm); total, seven-step, and nine-step leachate reported for each sample]

Sample	Total four-acid	Water soluble	Exchangeable pH 8.2	Carbonate pH 5 acetic acid	HCl pH 4	HCl pH 2	Amorphous Fe- and Al-hydroxides and amorphous and crystalline Mn-oxides	Crystalline Fe- and Al-oxides	Sulfide	Silicates
IDY090537B	2,790									
IDY090537B		0.2	BDL	BDL			0.3	26.2	11.7	3,020
IDY090537B		0.4	BDL	BDL	1.9	BDL	1.1	40.0	19.4	4,370
IDY0329	1,530									
IDY0329		0.2	0.1	BDL			0.5	14.1	5.6	1,125
IDY0329		0.3	BDL	0.2	0.1	0.1	1.2	15.0	4.6	1,393
HDY0317	5,030									
HDY0317		0.2	BDL	BDL			0.4	19.9	8.6	4,870
HDY0317		0.4	BDL	BDL	0.2	0.3	1.1	24.8	13.8	6,720
SDY0326	4,500									
SDY0326		BDL	BDL	BDL			1.3	39.0	19.2	4,700
SDY0326		0.2	BDL	BDL	BDL	0.2	3.1	57.1	22.9	4,500
HWDY090542A	4,705									
HWDY090542A		0.4	0.3	0.2			1.3	104.9	108.4	4,900
HWDY090542A		0.4	0.1	BDL	0.7	0.2	2.6	121.5	127.5	4,360
HWDY090542B	3,150									
HWDY090542B		BDL	BDL	BDL			0.4	19.5	23.3	3,570
HWDY090542B		0.6	BDL	BDL	BDL	BDL	0.8	32.4	35.6	2,820
SDY0310	4,640									
SDY0310		0.5	0.1	BDL			1.2	97.7	104.0	4,520
SDY0310		0.7	BDL	BDL	BDL	BDL	1.8	107.0	198.0	4,560
HDY0314	1,825									
HDY0314		0.4	BDL	BDL			0.6	20.5	10.0	1,175
HDY0314		0.1	BDL	BDL	BDL	BDL	1.2	30.0	13.7	1,311
Grand Mogul	1,640									
Grand Mogul		0.2	BDL	BDL			1.0	13.9	2.7	1,090
Grand Mogul		0.2	BDL	BDL	BDL	0.3	1.4	16.4	9.6	1,050

Appendix F. Sequential leachate results for iron.

[Iron (ppm); BDL, below detection limit (<10 ppm); total, seven-step, and nine-step leachate reported for each sample]

Sample	Total four-acid	Water soluble	Exchangeable pH 8.2	Carbonate pH 5 acetic acid	HCl pH 4	HCl pH 2	Amorphous Fe- and Al-hydroxides and amorphous and crystalline Mn-oxides	Crystalline Fe- and Al-oxides	Sulfide	Silicates
IDY090537B	61,000									
IDY090537B		16	BDL	BDL			332	13,400	6,520	35,000
IDY090537B		21	BDL	13	30	74	546	20,900	6,530	39,000
IDY0329	31,000									
IDY0329		16	BDL	BDL			366	14,150	9,985	17,500
IDY0329		15	BDL	BDL	8	17	530	14,250	6,630	16,000
HDY0317	46,000									
HDY0317		BDL	BDL	BDL			300	24,200	4,650	18,000
HDY0317		10	BDL	BDL	11	65	400	25,600	5,860	20,000
SDY0326	44,000									
SDY0326		BDL	BDL	16			577	17,800	4,550	24,000
SDY0326		BDL	BDL	22	BDL	234	659	21,600	3,970	19,000
HWDY090542A	44,500									
HWDY090542A		22	BDL	BDL			450	28,000	5,630	11,000
HWDY090542A		15	BDL	BDL	28	101	518	27,300	5,370	9,400
HWDY090542B	39,000									
HWDY090542B		BDL	BDL	BDL			147	17,200	5,660	22,000
HWDY090542B		BDL	BDL	BDL	BDL	38	164	18,300	6,430	18,000
SDY0310	61,000									
SDY0310		13	BDL	BDL			462	28,400	6,080	30,000
SDY0310		15	BDL	BDL	BDL	81	454	28,200	6,940	27,000
HDY0314	18,500									
HDY0314		15	BDL	BDL			423	4,315	1,139	16,000
HDY0314		BDL	BDL	BDL	BDL	45	239	4,850	952	13,000
Grand Mogul	22,000									
Grand Mogul		283	25	15			1,550	15,600	1,920	2,100
Grand Mogul		199	BDL	BDL	21	142	1,270	10,700	3,900	2,300

Appendix G. Sequential leachate results for manganese.

[Manganese (ppm); detection limit <0.04 ppm; total, seven-step, and nine-step leachate reported for each sample]

Sample	Total four-acid	Water soluble	Exchangeable pH 8.2	Carbonate pH 5 acetic acid	HCl pH 4	HCl pH 2	Amorphous Fe- and Al-hydroxides and amorphous and crystalline Mn-oxides	Crystalline Fe- and Al-oxides	Sulfide	Silicates
IDY090537B	1,380									
IDY090537B		0.60	1.90	105.00			196.00	622.00	185.00	374.0
IDY090537B		0.80	3.70	146.00	3.70	94.60	168.00	606.00	162.00	282.0
IDY0329	1,910									
IDY0329		1.80	5.25	230.00			620.50	1,085.00	143.50	198.5
IDY0329		1.45	5.55	236.50	12.85	175.50	524.00	1,070.00	118.10	187.0
HDY0317	797									
HDY0317		0.30	3.40	142.00			232.00	414.00	76.30	82.0
HDY0317		0.40	4.80	174.00	5.30	82.90	220.00	349.00	80.20	76.9
SDY0326	766									
SDY0326		0.30	8.50	108.00			143.00	286.00	69.20	214.0
SDY0326		0.30	7.60	108.00	11.20	60.10	95.20	286.00	55.40	198.0
HWDY090542A	1,060									
HWDY090542A		0.70	4.30	124.50			102.50	553.00	102.05	218.0
HWDY090542A		0.45	4.55	128.50	9.15	82.35	74.55	521.00	85.45	196.0
HWDY090542B	1,220									
HWDY090542B		0.40	5.20	54.70			77.50	585.00	194.00	530.0
HWDY090542B		0.20	5.00	50.30	4.10	33.10	78.20	603.00	201.00	442.0
SDY0310	3,130									
SDY0310		0.80	2.20	10.10			84.00	2,160.00	366.00	831.0
SDY0310		1.00	1.90	10.20	2.50	14.50	57.70	2,120.00	403.00	707.0
HDY0314	592									
HDY0314		1.35	4.25	136.50			158.00	201.50	45.45	153.0
HDY0314		0.40	4.20	122.00	7.60	64.15	134.00	208.00	39.20	117.5
Grand Mogul	600									
Grand Mogul		28.10	1.40	0.90			5.30	29.90	107.00	975.0
Grand Mogul		21.30	4.00	1.70	0.40	0.70	1.00	27.70	75.70	508.0

Appendix H. Sequential leachate results for nickel.

[Nickel (ppm); BDL, below detection limit (<0.08 ppm); total, seven-step, and nine-step leachate reported for each sample]

Sample	Total four-acid	Water soluble	Exchangeable pH 8.2	Carbonate pH 5 acetic acid	HCl pH 4	HCl pH 2	Amorphous Fe- and Al-hydroxides and amorphous and crystalline Mn-oxides	Crystalline Fe- and Al-oxides	Sulfide	Silicates
IDY090537B	2.8									
IDY090537B		BDL	BDL	BDL			BDL	BDL	0.20	0.70
IDY090537B		BDL	BDL	BDL	BDL	BDL	BDL	0.60	0.30	0.60
IDY0329	2.8									
IDY0329		BDL	BDL	BDL			BDL	1.05	0.45	0.5
IDY0329		BDL	BDL	BDL	BDL	BDL	BDL	1.30	0.35	0.4
HDY0317	5.8									
HDY0317		BDL	BDL	BDL			BDL	3.80	0.60	1.2
HDY0317		BDL	BDL	BDL	BDL	BDL	BDL	2.90	0.60	1.2
SDY0326	10.6									
SDY0326		BDL	BDL	BDL			0.10	4.50	1.40	4.4
SDY0326		BDL	BDL	BDL	BDL	0.09	0.20	5.50	1.20	3.7
HWDY090542A	12.4									
HWDY090542A		BDL	BDL	BDL			0.20	8.35	1.80	1.7
HWDY090542A		BDL	BDL	BDL	BDL	0.20	0.14	8.45	1.50	1.6
HWDY090542B	10.7									
HWDY090542B		BDL	BDL	BDL			BDL	4.80	1.60	5.0
HWDY090542B		BDL	BDL	BDL	BDL	BDL	BDL	5.20	1.70	3.8
SDY0310	21.3									
SDY0310		BDL	BDL	BDL			0.30	14.60	3.00	4.6
SDY0310		BDL	BDL	BDL	BDL	BDL	0.20	14.70	3.50	3.6
HDY0314	3.0									
HDY0314		BDL	BDL	BDL			0.35	1.45	1.40	1.1
HDY0314		BDL	BDL	BDL	BDL	0.09	BDL	1.55	0.30	0.8
Grand Mogul	0.4									
Grand Mogul		0.20	BDL	BDL			BDL	0.30	0.10	BDL
Grand Mogul		BDL	BDL	BDL	0.20	BDL	BDL	0.09	BDL	0.4

Appendix I. Sequential leachate results for copper.

[Copper (ppm); BDL, below detection limit (<0.1 ppm); total, seven-step, and nine-step leachate reported for each sample]

Sample	Total four-acid	Water soluble	Exchangeable pH 8.2	Carbonate pH 5 acetic acid	HCl pH 4	HCl pH 2	Amorphous Fe- and Al-hydroxides and amorphous and crystalline Mn-oxides	Crystalline Fe- and Al-oxides	Sulfide	Silicates
IDY090537B	10									
IDY090537B		BDL	0.1	0.2			0.8	3.3	1.1	3.0
IDY090537B		BDL	0.3	0.1	BDL	0.3	1.3	2.5	1.0	5.5
IDY0329	30									
IDY0329		BDL	0.4	1.6			21.1	8.4	1.3	2
IDY0329		BDL	0.5	1.7		2.5	20.6	7.0	0.9	2
HDY0317	39									
HDY0317		BDL	BDL	0.3			2.7	12.2	21.1	7
HDY0317		BDL	0.2	0.3	0.1	0.4	4.0	13.2	19.4	9
SDY0326	55									
SDY0326		BDL	0.1	0.2			2.0	11.2	7.6	35
SDY0326		BDL	0.4	0.1	BDL	1.2	1.9	13.2	6.2	32
HWDY090542A	45									
HWDY090542A		0.2	0.3	0.8			14.2	24.0	10.7	9
HWDY090542A		0.2	0.3	0.8	BDL	5.6	9.6	18.2	6.3	8
HWDY090542B	48									
HWDY090542B		BDL	0.2	0.3			4.0	13.0	16.6	14
HWDY090542B		BDL	0.2	0.4	BDL	1.4	5.0	14.3	18.8	11
SDY0310	54									
SDY0310		BDL	0.3	1.0			23.1	20.6	10.2	14
SDY0310		0.1	0.3	1.0	BDL	7.8	18.1	16.2	14.2	15
HDY0314	8									
HDY0314		BDL	0.2	0.3			1.5	1.8	1.4	5
HDY0314		BDL	0.2	0.3	BDL	0.6	1.0	1.3	0.1	3
Grand Mogul	650									
Grand Mogul		18.1	0.9	0.6			9.2	355.0	283.0	93
Grand Mogul		13.4	0.5	0.4	0.5	4.3	7.6	251.0	125.0	18

Appendix J. Sequential leachate results for zinc.

[Zinc (ppm); BDL, below detection limit (<0.1 ppm); total, seven-step, and nine-step leachate reported for each sample]

Sample	Total four - acid	Water soluble	Exchangeable pH 8.2	Carbonate pH 5 acetic acid	HCl pH 4	HCl pH 2	Amorphous Fe- and Al-hydroxides and amorphous and crystalline Mn-oxides	Crystalline Fe- and Al-oxides	Sulfide	Silicates
IDY090537B	161									
IDY090537B		BDL	BDL	BDL			2.0	62.1	30.8	68.7
IDY090537B		0.1	BDL	BDL	0.2	0.7	2.0	92.6	28.8	50.2
IDY0329	1,230									
IDY0329		1.6	BDL	38.9			584.0	703.5	51.2	31
IDY0329		1.5	BDL	42.9	1.5	150.0	760.0	483.5	39.6	30
HDY0317	91									
HDY0317		BDL	BDL	BDL			1.0	46.9	9.7	37
HDY0317		BDL	BDL	BDL	2.1	0.4	1.0	46.8	10.7	39
SDY0326	88									
SDY0326		BDL	BDL	BDL			1.0	17.0	5.3	64
SDY0326		BDL	BDL	BDL	BDL	0.4	0.6	20.1	4.7	64
HWDY090542A	86									
HWDY090542A		BDL	BDL	BDL			1.5	55.3	11.7	19
HWDY090542A		BDL	BDL	BDL	0.2	0.7	1.5	54.8	9.6	20
HWDY090542B	79									
HWDY090542B		BDL	BDL	BDL			0.4	33.6	10.7	44
HWDY090542B		BDL	BDL	BDL	0.1	0.2	3.4	35.7	11.2	38
SDY0310	230									
SDY0310		BDL	BDL	2.0			40.5	134.0	23.9	37
SDY0310		0.2	BDL	2.0	33.2	16.5	29.4	131.0	27.1	32
HDY0314	56									
HDY0314		0.2	BDL	1.0			8.7	21.8	6.0	25
HDY0314		BDL	BDL	0.9	BDL	4.3	4.3	26.7	5.5	22
Grand Mogul	14,000									
Grand Mogul		638.0	10.3	28.9			49.8	463.0	16,000.0	1,930
Grand Mogul		460.0	35.3	39.5	7.7	33.7	33.5	1,410.0	15,100.0	697

Appendix K. Sequential leachate results for arsenic.

[Arsenic (ppm); BDL, below detection limit (<0.2 ppm); total, seven-step, and nine-step leachate reported for each sample]

Sample	Total four-acid	Water soluble	Exchangeable pH 8.2	Carbonate pH 5 acetic acid	HCl pH 4	HCl pH 2	Amorphous Fe- and Al-hydroxides and amorphous and crystalline Mn-oxides	Crystalline Fe- and Al-oxides	Sulfide	Silicates
IDY090537B	1.8									
IDY090537B		BDL	BDL	BDL			0.2	0.3	0.3	1.0
IDY090537B		BDL	BDL	BDL	BDL	BDL	0.3	BDL	0.4	1.0
IDY0329	1									
IDY0329		BDL	BDL	BDL			0.4	0.4	0.6	BDL
IDY0329		BDL	BDL	BDL	BDL	BDL	0.4	0.4	0.4	BDL
HDY0317	2									
HDY0317		BDL	BDL	BDL			0.2	BDL	BDL	BDL
HDY0317		BDL	BDL	BDL	BDL	BDL	0.2	BDL	0.2	BDL
SDY0326	7									
SDY0326		BDL	BDL	BDL			0.2	0.9	2.0	5
SDY0326		BDL	BDL	BDL	BDL	BDL	BDL	1.0	2.0	4
HWDY090542A	3									
HWDY090542A		BDL	BDL	BDL			0.3	0.2	0.2	3
HWDY090542A		BDL	BDL	BDL	BDL	BDL	0.2	0.4	0.5	2
HWDY090542B	1									
HWDY090542B		BDL	BDL	BDL			BDL	BDL	0.6	BDL
HWDY090542B		BDL	BDL	BDL	BDL	BDL	BDL	BDL	0.6	BDL
SDY0310	2									
SDY0310		BDL	BDL	BDL			0.3	0.4	BDL	2
SDY0310		BDL	BDL	BDL	BDL	BDL	0.3	0.2	0.3	2
HDY0314	2									
HDY0314		BDL	BDL	BDL			0.6	1.5	0.2	1
HDY0314		BDL	BDL	BDL	BDL	0.2	0.6	0.6	0.3	1
Grand Mogul	62									
Grand Mogul		BDL	BDL	BDL			1.0	42.1	7.2	4
Grand Mogul		BDL	BDL	BDL	BDL	BDL	2.0	28.6	11.6	3

Appendix L. Sequential leachate results for strontium.

[Strontium (ppm); detection limit <0.1 ppm; total, seven-step, and nine-step leachate reported for each sample]

Sample	Total four-acid	Water soluble	Exchangeable pH 8.2	Carbonate pH 5 acetic acid	HCl pH 4	HCl pH 2	Amorphous Fe- and Al-hydroxides and amorphous and crystalline Mn-oxides	Crystalline Fe- and Al-oxides	Sulfide	Silicates
IDY090537B	1,080									
IDY090537B		1.6	8.8	38.9			66.2	133.0	11.6	609.0
IDY090537B		2.2	10.8	53.2	3.1	28.1	59.0	60.6	7.7	789.0
IDY0329	268.5									
IDY0329		1.4	6.7	29.9			45.3	64.0	6.7	124.0
IDY0329		1.2	6.9	30.6	2.8	17.2	40.8	50.1	5.9	126.5
HDY0317	298.0									
HDY0317		1.4	14.4	29.7			38.6	57.3	10.8	163.0
HDY0317		1.5	15.0	33.7	1.6	14.3	36.4	43.5	11.5	166.0
SDY0326	958.0									
SDY0326		0.8	4.1	29.0			29.0	46.8	13.8	848.0
SDY0326		0.8	4.1	29.4	2.4	12.0	23.8	45.7	12.1	831.0
HWDY090542A	636.0									
HWDY090542A		0.3	2.0	4.0			4.4	8.0	2.3	621.0
HWDY090542A		0.3	2.0	3.9	0.3	1.8	3.2	6.6	2.4	612.0
HWDY090542B	256.0									
HWDY090542B		0.2	1.3	6.5			8.7	17.1	7.7	223.0
HWDY090542B		0.2	1.4	6.3	0.6	3.2	8.3	16.6	7.5	218.0
SDY0310	436.0									
SDY0310		0.1	2.6	1.0			4.3	7.8	2.0	453.0
SDY0310		0.1	2.6	1.3	0.3	1.8	4.1	6.6	2.8	480.0
HDY0314	306.5									
HDY0314		0.6	3.1	8.6			7.6	7.2	1.0	279.0
HDY0314		0.5	3.3	7.9	0.6	3.1	5.7	4.8	0.8	240.0
Grand Mogul	285.0									
Grand Mogul		17.4	29.2	6.0			4.9	200.0	13.9	44.0
Grand Mogul		14.9	62.3	30.8	7.5	10.0	20.1	287.0	23.2	34.0

Appendix M. Sequential leachate results for molybdenum.

[Molybdenum (ppm); BDL, below detection limit (<0.4 ppm); total, seven-step, and nine-step leachate reported for each sample]

Sample	Total four-acid	Water soluble	Exchangeable pH 8.2	Carbonate pH 5 acetic acid	HCl pH 4	HCl pH 2	Amorphous Fe- and Al-hydroxides and amorphous and crystalline Mn-oxides	Crystalline Fe- and Al-oxides	Sulfide	Silicates
IDY090537B	0.27									
IDY090537B		BDL	BDL	BDL			BDL	BDL	BDL	0.2
IDY090537B		BDL	BDL	BDL	BDL	BDL	BDL	BDL	BDL	0.2
IDY0329	0.22									
IDY0329		BDL	BDL	BDL			BDL	BDL	BDL	BDL
IDY0329		BDL	BDL	BDL	BDL	BDL	BDL	BDL	BDL	0.09
HDY0317	0.45									
HDY0317		BDL	BDL	BDL			BDL	0.7	BDL	0.29
HDY0317		BDL	BDL	BDL	BDL	BDL	BDL	BDL	BDL	0.27
SDY0326	1.40									
SDY0326		BDL	BDL	BDL			BDL	BDL	BDL	0.96
SDY0326		BDL	BDL	BDL	BDL	BDL	BDL	BDL	BDL	0.90
HWDY090542A	0.36									
HWDY090542A		BDL	BDL	BDL			BDL	BDL	BDL	0.22
HWDY090542A		BDL	BDL	BDL	BDL	BDL	BDL	BDL	BDL	0.22
HWDY090542B	1.40									
HWDY090542B		BDL	BDL	BDL			BDL	BDL	BDL	0.87
HWDY090542B		BDL	BDL	BDL	BDL	BDL	BDL	BDL	BDL	0.89
SDY0310	0.26									
SDY0310		BDL	BDL	BDL			BDL	BDL	BDL	0.10
SDY0310		BDL	BDL	BDL	BDL	BDL	BDL	BDL	BDL	0.10
HDY0314	0.21									
HDY0314		BDL	BDL	BDL			BDL	BDL	BDL	0.15
HDY0314		BDL	BDL	BDL	BDL	BDL	BDL	BDL	BDL	0.15
Grand Mogul	37.40									
Grand Mogul		BDL	BDL	BDL			BDL	33.7	2.3	1.20
Grand Mogul		BDL	BDL	BDL	BDL	BDL	BDL	24.0	4.1	1.10

Appendix N. Sequential leachate results for cadmium.

[Cadmium (ppm); BDL, below detection limit (<0.004 ppm); total, seven-step, and nine-step leachate reported for each sample]

Sample	Total four-acid	Water soluble	Exchangeable pH 8.2	Carbonate pH 5 acetic acid	HCl pH 4	HCl pH 2	Amorphous Fe- and Al-hydroxides and amorphous and crystalline Mn-oxides	Crystalline Fe- and Al-oxides	Sulfide	Silicates
IDY090537B	0.140									
IDY090537B		BDL	BDL	0.030			0.040	0.080	0.010	0.009
IDY090537B		BDL	BDL	0.040	BDL	0.020	0.040	0.040	0.010	BDL
IDY0329	4.400									
IDY0329		0.008	0.135	1.660			2.085	1.345	0.120	0.025
IDY0329		0.007	0.135	1.705	0.030	0.565	1.625	1.110	0.090	0.020
HDY0317	0.070									
HDY0317		BDL	BDL	0.020			0.020	0.030	0.008	0.020
HDY0317		BDL	BDL	0.020	BDL	0.009	0.020	0.020	0.008	BDL
SDY0326	0.060									
SDY0326		BDL	BDL	0.010			0.020	0.020	0.009	0.020
SDY0326		BDL	BDL	0.010	BDL	0.006	0.009	0.020	0.150	0.020
HWDY090542A	0.080									
HWDY090542A		BDL	0.004	0.013			0.009	0.015	0.007	0.060
HWDY090542A		BDL	BDL	0.004	BDL	BDL	0.005	0.010	0.005	0.060
HWDY090542B	0.060									
HWDY090542B		BDL	BDL	0.007			0.009	0.020	0.010	0.010
HWDY090542B		BDL	BDL	0.008	BDL	0.004	0.009	0.020	0.010	0.010
SDY0310	0.470									
SDY0310		BDL	0.030	0.060			0.270	0.170	0.020	0.020
SDY0310		BDL	0.020	0.060	0.020	0.090	0.180	0.120	0.010	0.020
HDY0314	0.095									
HDY0314		BDL	0.007	0.050			0.040	0.020	0.004	0.012
HDY0314		BDL	0.008	0.045	BDL	0.020	0.030	0.020	0.003	BDL
Grand Mogul	61.900									
Grand Mogul		2.920	0.260	0.100			0.090	1.870	76.900	9.000
Grand Mogul		2.090	0.430	0.140	0.020	0.050	0.080	5.070	59.600	3.000

Appendix O. Sequential leachate results for barium.

[Barium (ppm); BDL, below detection limit (<0.04 ppm); total, seven-step, and nine-step leachate reported for each sample]

Sample	Total four-acid	Water soluble	Exchangeable pH 8.2	Carbonate pH 5 acetic acid	HCl pH 4	HCl pH 2	Amorphous Fe- and Al-hydroxides and amorphous and crystalline Mn-oxides	Crystalline Fe- and Al-oxides	Sulfide	Silicates
IDY090537B	480.0									
IDY090537B		0.21	6.31	5.19			3.44	6.35	1.97	456.53
IDY090537B		0.40	6.13	3.07	0.35	0.69	2.47	3.46	1.30	462.13
IDY0329	998.0									
IDY0329		2.94	44.95	72.40			45.45	96.65	24.55	711.07
IDY0329		2.30	43.85	74.45	3.84	12.15	50.35	95.20	17.35	698.52
HDY0317	740.0									
HDY0317		0.41	21.40	10.60			6.38	6.95	2.86	691.40
HDY0317		0.49	22.90	13.90	0.47	1.00	8.53	9.14	4.74	678.83
SDY0326	833.0									
SDY0326		0.05	0.59	0.54			0.87	4.27	2.22	824.46
SDY0326		0.06	0.58	0.85	0.06	0.55	0.66	6.30	2.16	821.78
HWDY090542A	810.5									
HWDY090542A		0.10	2.17	1.23			1.48	1.54	0.30	803.69
HWDY090542A		0.10	2.13	1.30	0.10	0.70	0.89	1.37	0.44	802.90
HWDY090542B	1,140.0									
HWDY090542B		BDL	0.45	0.36			0.55	0.80	0.48	1,137.36
HWDY090542B		BDL	0.44	0.40	0.09	0.20	0.46	0.83	0.46	1,137.12
SDY0310	701.0									
SDY0310		0.10	4.79	1.74			2.18	1.41	0.39	690.39
SDY0310		0.10	4.61	1.92	0.20	0.68	1.23	1.23	0.43	690.60
HDY0314	876.0									
HDY0314		0.37	6.76	4.56			3.43	2.97	0.69	857.23
HDY0314		0.20	6.95	4.45	0.23	1.23	2.93	2.82	0.83	856.39
Grand Mogul	252.0									
Grand Mogul		1.94	4.17	4.23			7.03	59.70	7.07	167.86
Grand Mogul		1.40	4.65	2.94	0.51	2.19	3.22	54.80	5.09	177.20

Appendix P. Sequential leachate results for lead.

[Lead (ppm); BDL, below detection limit (<0.01 ppm); total, seven-step, and nine-step leachate reported for each sample]

Sample	Total four-acid	Water soluble	Exchangeable pH 8.2	Carbonate pH 5 acetic acid	HCl pH 4	HCl pH 2	Amorphous Fe- and Al-hydroxides and amorphous and crystalline Mn-oxides	Crystalline Fe- and Al-oxides	Sulfide	Silicates
IDY090537B	13.1									
IDY090537B		BDL	BDL	0.20			1.20	2.60	0.08	6.61
IDY090537B		BDL	BDL	0.40	BDL	0.04	2.00	0.99	BDL	6.08
IDY0329	67.0									
IDY0329		0.15	0.08	6.40			45.10	15.80	1.95	6.7
IDY0329		0.10	0.07	7.00	0.07	0.53	48.00	14.00	1.23	6.6
HDY0317	9.6									
HDY0317		BDL	BDL	0.10			0.83	3.10	0.88	3.8
HDY0317		BDL	BDL	0.10	0.02	BDL	1.40	2.40	0.30	3.5
SDY0326	21.3									
SDY0326		BDL	BDL	0.02			0.50	BDL	BDL	18.5
SDY0326		BDL	BDL	BDL	BDL	0.06	0.20	BDL	BDL	18.0
HWDY090542A	19.2									
HWDY090542A		BDL	BDL	BDL			0.77	0.94	0.18	15.7
HWDY090542A		0.01	BDL	0.02	0.01	0.12	0.71	0.45	0.01	15.0
HWDY090542B	16.2									
HWDY090542B		BDL	BDL	0.56			1.40	3.30	1.20	6.7
HWDY090542B		BDL	BDL	0.20	BDL	0.20	1.70	5.60	1.20	5.5
SDY0310	17.0									
SDY0310		0.01	BDL	0.65			6.50	1.00	BDL	8.8
SDY0310		0.02	BDL	0.20	0.30	0.40	2.80	BDL	BDL	9.5
HDY0314	25.5									
HDY0314		0.11	BDL	1.01			5.25	3.40	0.21	14.6
HDY0314		0.06	BDL	0.81	0.01	0.51	6.20	3.50	0.08	14.0
Grand Mogul	9,480.0									
Grand Mogul		25.00	108.00	208.00			712.00	7,580.00	739.00	169.0
Grand Mogul		35.10	489.00	828.00	60.50	738.00	934.00	8,630.00	2,050.00	582.0

Publishing support provided by:
Denver Publishing Service Center, Denver, Colorado
Manuscript approved for publication, April 23, 2008

USGS

Yager and others—**Geochemical Characteristics of Animas River Watershed Rocks, Colorado**—U.S. Geological Survey Scientific Investigations Report 2008–5063

ISBN 978-141132164-9

Printed on recycled paper